

Conceptual Design of a Fixed-Wing Crop Dusting Unmanned Aerial Vehicle

A project present to
The Faculty of the Department of Aerospace Engineering
San Jose State University

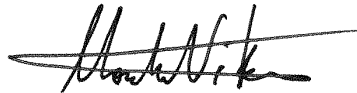
in partial fulfillment of the requirements for the degree
Master of Science in Aerospace Engineering

By

Kelvin Young

May, 2016

approved by



Dr. Nikos Mourtos
Faculty Advisor



© 2016

Kevin Young

ALL RIGHTS RESERVED

The Designated Project Advisor(s) Approves the Thesis Titled

CONCEPTUAL DESIGN OF A FIXED-WING CROP DUSTING UNMANNED AERIAL
VEHICLE

by

Kevin Young

APPROVED FOR THE DEPARTMENT OF AEROSPACE ENGINEERING
SAN JOSÉ STATE UNIVERSITY

May 2016

Dr. Nikos Mourtos

Department of Aerospace Engineering

Advisor

ABSTRACT

CONCEPTUAL DESIGN OF A FIXED-WING CROP DUSTING UNMANNED AERIAL
VEHICLE

by Kevin Young

This master's project studies the conceptual design of a fixed-wing crop dusting unmanned aerial vehicle (UAV) capable of carrying 50 gallons of pesticide. This UAV will be used to apply pesticide to crops only, and will not be designed to apply pesticide to forested areas. The maximum cruise speed was limited to 45 mph, with an aerial application airspeed of 40 mph, and a takeoff distance of 500 ft. on a dirt runway. The initial gross takeoff weight and wingspan were found to be 1450.0 lb. and 44.8 ft. respectively. The conventional tail design was selected due to the simplicity and low weight. An electrostatic aerial applicator was selected due to the minimized drift and pesticide usage. The quadricycle landing gear arrangement was selected to improve stability on dirt runways. The aircraft was found to not generate enough lift during cruise, requiring a redesign around increasing maximum cruise speed to 90 mph. The redesign fulfilled all requirements. Cost analysis showed the potential for this aircraft to be cheaper than a manned crop duster. Trade studies showed the minimum cruise speed could not be lowered much passed 75 mph, as the aircraft would not generate enough lift.

ACKNOWLEDGEMENTS

I would like to thank all of the people who provided assistance and encouragement while working on this project.

First, I would like to thank Professor Nikos Mourtos for his guidance through out this paper and my time at San Jose State University. He was always provided help and support whenever needed during my graduate research. His willingness to meet with me before I

decided on attending San Jose State showed me he was passionate and cared about his students.

Second, I would like to thank Professor Gonzalo Mendoza for his recommendations on potential topics for this paper. I would also like to thank him for his passion and knowledge during Advanced Aircraft Design. Every interaction with him felt insightful and furthered my passion for aircraft design.

Third, I would like to thank Professor Kamran Turkoglu for his assistance when writing this paper, and his willingness to meet with and help his students.

Finally, I would like to thank my family and friends for all of their support and encouragement through out my academic career and my life. Jenny, you were the one who helped me work through what topic I wanted to work on, and help provide information on pesticides. Dad, you were always there to offer me words of encouragement and were a great father and role model. Mom, you were the one that encouraged me to pursue my Master's degree, and have always been the one that pushed me to achieve more and never settle.

To receive a Master's degree from San Jose State University is a great honor, but to be the first person in my family to receive a Master's degree is a greater honor. This honor would not mean nearly as much without those who have supported me. Again, thank you everyone who encouraged and supported me through out my academic career and my lifetime.

TABLE OF CONTENTS

LIST OF FIGURES.....	
LIST OF TABLES.....	
NOMENCLATURE.....	XIII
1. INTRODUCTION.....	
1.1 MOTIVATION.....	1
1.2 OBJECTIVE.....	1
2. LITERATURE REVIEW.....	
2.1 HISTORY OF CROP DUSTING.....	2
2.2 CROP DUSTING STUDIES.....	5
2.3 MARKET ANALYSIS & RESEARCH.....	14
3. MISSION SPECIFICATIONS.....	
3.1 MISSION REQUIREMENTS.....	18
3.2 GENERAL FLIGHT.....	19
3.3 PAYLOAD.....	19
3.4 FLIGHT SPEED.....	19
3.5 ENDURANCE.....	20
3.6 TAKEOFF AND LANDING.....	20
3.7 CREW.....	20
3.8 MISSION PROFILE.....	20
4. INITIAL CONFIGURATION.....	
4.1 DESIGN TAKEOFF WEIGHT.....	21
4.2 INITIAL WING CONFIGURATION.....	24
4.3 INITIAL TAIL CONFIGURATION.....	24
5. INITIAL SIZING.....	
5.1 THRUST-TO-WEIGHT RATIO.....	25
5.2 WING LOADING.....	27
5.3 REFINED INITIAL WEIGHT SIZING.....	32
5.4 FUSELAGE AND WING SIZING.....	34
5.5 TAIL SIZING.....	34
5.6 CONTROL SURFACE SIZING.....	36
6. INITIAL LAYOUT.....	
6.1 PROPULSION AND FUEL SYSTEM.....	37
6.2 PESTICIDE DISPERSAL METHOD.....	40
6.3 AVIONICS.....	41
6.4 FLIGHT CONTROL SYSTEM.....	41
6.5 ELECTRONICS.....	42
6.6 WETTED AREAS.....	43
6.7 CONFIGURATION.....	43
6.8 CENTER OF GRAVITY ANALYSIS.....	46
7. LANDING GEAR.....	

7.1 LANDING GEAR ARRANGEMENT.....	49
7.2 TIRE SIZING.....	49
7.3 GEAR SIZING AND RETRACTION.....	52
8. AERODYNAMIC ANALYSIS.....	
8.1 LIFT-CURVE SLOPE.....	53
8.2 PARASITIC DRAG.....	54
8.3 INDUCED DRAG.....	56
8.4 DRAG POLAR.....	58
9. PROPULSION ANALYSIS.....	
10. STRUCTURE ANALYSIS.....	
11. WEIGHT ANALYSIS.....	
11.1 WEIGHT CALCULATIONS.....	62
11.2 IMPROVED CENTER OF GRAVITY ANALYSIS.....	65
12. STABILITY AND CONTROL ANALYSIS.....	
12.1 STABILITY CONSTANTS.....	67
12.2 POWER-OFF NEUTRAL POINT.....	68
12.3 TRIM ANALYSIS.....	70
12.4 SURFACE SIZING.....	71
13. PERFORMANCE AND FLIGHT MECHANICS.....	
13.1 STEADY LEVEL FLIGHT.....	74
13.2 STEADY CLIMB AND DESCENDING.....	77
13.3 GLIDING FLIGHT.....	78
13.4 TAKEOFF ANALYSIS.....	79
13.5 LANDING ANALYSIS.....	81
14. DESIGN REVIEW.....	
15. REDESIGN INITIAL SIZING.....	
15.1 THRUST-TO-WEIGHT RATIO.....	82
15.2 WING LOADING.....	82
15.3 WEIGHT ESTIMATION.....	83
15.4 INITIAL SIZING.....	84
15.5 PROPULSION AND FUEL SYSTEM.....	85
15.6 WETTED AREAS.....	86
15.7 C.G. ANALYSIS.....	86
15.8 LANDING GEAR.....	88
16. REDESIGN ANALYSIS.....	
16.1 AERODYNAMICS.....	88
16.2 PROPULSION.....	90
16.3 STABILITY AND CONTROL ANALYSIS.....	90
16.4 PERFORMANCE.....	92
17. COST ANALYSIS.....	
18. TRADE STUDIES.....	
19. FEASIBILITY VS. PRACTICALITY.....	

20. CONCLUSION.....100

REFERENCES.....101

APPENDICES.....104

 APPENDIX A – FAA REGULATIONS.....104

 APPENDIX B – YAMAHA EXEMPTIONS.....107

 APPENDIX C – AGDRIFT STUDY.....124

 APPENDIX D – XFOIL RESULTS.....130

 APPENDIX E – REFINED WEIGHT ESTIMATE TABLE.....132

 APPENDIX F – AIRCRAFT C.G.....133

 APPENDIX G – REDESIGN AIRCRAFT C.G.....135

 APPENDIX H – CAD MODEL.....136

 APPENDIX I – MATLAB CODE.....138

 APPENDIX J – HAND CALCULATIONS.....148

LIST OF FIGURES

FIGURE 1. MISSION PROFILE.....	21
FIGURE 2. TOP VIEW (MM).....	44
FIGURE 3. SIDE VIEW (MM).....	44
FIGURE 4. WING-FUSELAGE CROSS SECTION (MM).....	45
FIGURE 5. C.G. LOCATION RESULTING FROM FUSELAGE LENGTH CHANGES.....	47
FIGURE 6. WEIGHT VARIANCE DUE TO C.G. LOCATION.....	47
FIGURE 7. LANDING GEAR DIMENSIONS.....	50
FIGURE 8. GROUND EFFECTS ON LIFT-DUE-TO-DRAG FACTOR.....	57
FIGURE 9. LIFT COEFFICIENT CURVE.....	58
FIGURE 10. DRAG POLAR.....	59
FIGURE 11. TRIM PLOT.....	71
FIGURE 12. DRAG POLAR COMPARISON.....	89
FIGURE 13. REDESIGN TRIM PLOT.....	91
FIGURE 14. EFFECT OF ASPECT RATIO ON WEIGHT.....	97
FIGURE 15. TIER 3 AGDRIFT INTERFACE.....	124
FIGURE 16. TIER 3 AGDRIFT AIRCRAFT INTERFACE.....	125
FIGURE 17. TIER 3 AGDRIFT SPRAY INTERFACE.....	126
FIGURE 18. APPLICATION EFFICIENCY VS AIRSPEED.....	126
FIGURE 19. APPLICATION EFFICIENCY VS AIRSPEED, 40 TO 60 MPH.....	127
FIGURE 20. DOWNWIND DRIFT VS AIRSPEED.....	128
FIGURE 21. AIRBORNE DRIFT VS AIRSPEED.....	128
FIGURE 22. AIR TRACTOR VARIABLE RATE APPLICATION EFFICIENCY.....	129
FIGURE 23. AG HUSKY VARIABLE RATE APPLICATION EFFICIENCY.....	129
FIGURE 24. NACA 4415 XFOIL RESULTS.....	130
FIGURE 25. EPPLER 1210 XFOIL RESULTS.....	130
FIGURE 26. USA 40B XFOIL RESULTS.....	131
FIGURE 27. CAD MODEL OF UAV.....	136
FIGURE 28. FRONT VIEW OF UAV.....	136
FIGURE 29. TOP VIEW OF UAV.....	137
FIGURE 30. SIDE VIEW OF UAV.....	137

LIST OF TABLES

TABLE 1. BASIC SPECIFICATIONS OF MANNED CROP DUSTERS.....	
TABLE 2. BASIC SPECIFICATIONS OF UAV CROP DUSTERS.....	
TABLE 3. ESTIMATED GROSS TAKEOFF WEIGHT.....	
TABLE 4. FLIGHT SPEEDS.....	
TABLE 5. WING LOADINGS.....	
TABLE 6. AIRFOIL COMPARISON.....	
TABLE 7. REFINED SEGMENT FUEL WEIGHTS.....	
TABLE 8. REFINED WEIGHT ESTIMATE (LB.).....	
TABLE 9. INITIAL TAIL SIZING.....	
TABLE 10. ENGINE COMPARISON.....	
TABLE 11. ENGINE AND PROPELLER ANALYSIS.....	
TABLE 12. CONVENTIONAL SPRAY METHOD ³²	
TABLE 13. ULTRA-LOW VOLUME SPRAY METHOD ³²	
TABLE 14. ELECTROSTATIC SPRAY METHOD ³²	
TABLE 15. WETTED AREA AND INTERNAL VOLUME.....	
TABLE 16. COMPONENT SIZES.....	
TABLE 17. AIRCRAFT C.G. CALCULATION.....	
TABLE 18. FORE AND AFT C.G.....	
TABLE 19. SKIN FRICTION.....	
TABLE 20. PARASITIC DRAG.....	
TABLE 21. PROPULSION ANALYSIS AT 40 MPH.....	
TABLE 22. COMPONENT WEIGHT.....	
TABLE 23. COMPARISON COMPONENT WEIGHT.....	
TABLE 24. COMPONENT WEIGHT AND C.G. LOCATIONS.....	
TABLE 25. NEW DESIGN WEIGHT AND C.G. LOCATION.....	
TABLE 26. CHANGES IN DESIGN.....	
TABLE 27. THRUST-TO-WEIGHT RATIO.....	
TABLE 28. WING LOADING.....	
TABLE 29. VELOCITIES.....	
TABLE 30. WEIGHT ESTIMATE.....	
TABLE 31. INITIAL SIZING.....	
TABLE 32. PROPELLER SIZING.....	
TABLE 33. WETTED AREAS.....	
TABLE 34. C.G. ANALYSIS.....	
TABLE 35. AIRCRAFT CHANGES DUE TO ENGINE ALTERATION.....	
TABLE 36. LANDING GEAR.....	
TABLE 37. REDESIGN AERODYNAMICS.....	
TABLE 38. PROPULSION COMPARISON.....	
TABLE 39. STABILITY AND CONTROL ANALYSIS.....	
TABLE 40. CONTROL SURFACE SIZING.....	
TABLE 41. PERFORMANCE COMPARISON.....	
TABLE 42. HOURS ANALYSIS.....	
TABLE 43. COST ANALYSIS.....	
TABLE 44. MAXIMUM CRUISE WING LOADING-ASPECT RATIO TRADE STUDY.....	
TABLE 45. MAXIMUM CRUISE WING LOADING-POWER-TO-WEIGHT TRADE STUDY.....	
TABLE 46. MINIMUM CRUISE VELOCITY WING AREA TRADE STUDY.....	
TABLE 47. FORE AND AFT C.G. ROTAX ENGINE.....	133
TABLE 48. FORE AND AFT C.G. LYCOMING ENGINE.....	133
TABLE 49. FORE AND AFT C.G. LYCOMING ENGINE, NEW MOMENT ARM.....	134
TABLE 50. FORE AND AFT C.G. LYCOMING O-235-F.....	135

NOMENCLATURE

AR = Aspect Ratio

AR_{HT}	=	Horizontal Tail Aspect Ratio
AR_{VT}	=	Vertical Tail Aspect Ratio
$A_{cooling}$	=	Engine cooling area
A_{exit}	=	Engine cooling area exit
A_{inlet}	=	Engine cooling area inlet
A_p	=	Tire footprint area
A_{side}	=	Side of fuselage area
A_{top}	=	Top of fuselage area
a_{cg}	=	Aft C.G.
B	=	Distance between tires
b	=	Span
bhp	=	brake horsepower
b_{VT}	=	Vertical Tail Span
b_w	=	Wingspan
C	=	Specific fuel consumption
c	=	chord
C_D	=	Drag Coefficient
C_{D_0}	=	Zero-lift drag coefficient
C_L	=	Lift Coefficient
C_{L_h}	=	Horizontal Tail Lift Coefficient
$C_{D_{min_{sink}}}$	=	Minimum sink Lift Coefficient
$C_{L_{max}}$	=	Maximum wing lift coefficient
$C_{L_{min_p}}$	=	Minimum Power Lift Coefficient
$C_{L_{min_{sink}}}$	=	Minimum Sink Lift Coefficient
$C_{L_{min_t}}$	=	Minimum Thrust Lift Coefficient

$C_{L_{Stall}}$	=	Stall Lift Coefficient
C_{L_i}	=	Takeoff lift coefficient
$C_{L_{total}}$	=	Total lift coefficient
$C_{L_{\alpha}}$	=	Lift-Curve Slope
$C_{L_{\alpha_h}}$	=	Horizontal Tail Lift-Curve Slope
$C_{L_{\alpha_v}}$	=	Vertical Tail Lift-Curve Slope
C_P	=	Power coefficient
C_S	=	Speed-power coefficient
C_T	=	Thrust coefficient
$C_{l_{max}}$	=	Maximum airfoil lift coefficient
$C_{l_{\beta}}$	=	Static Lateral Stability
$C_{l_{\beta_{planform}}}$	=	Static Lateral Stability due to Planform
$C_{l_{\beta_{\Delta}}}$	=	Static Lateral Stability due to Delta
$C_{l_{\beta_{\theta}}}$	=	Static Lateral Stability due to Dihedral
$C_{l_{\beta_{vt}}}$	=	Static Lateral Stability of Vertical Tail
$C_{l_{\beta_{wf}}}$	=	Static Lateral Stability of Wing Fuselage
$C_{l_{\beta_{wing}}}$	=	Static Lateral Stability of Wing
C_{m_g}	=	Total Pitching Moment
C_{m_w}	=	Wing Pitching Moment
$C_{m_{\alpha}}$	=	Static Pitch Stability

$C_{m_{\alpha_{fus}}}$	=	Fuselage Static Pitch Stability
$C_{n_{\beta}}$	=	Static Directional Stability
$C_{n_{\beta_{yaw}}}$	=	Yawing Moment due to Sideslip
$C_{n_{\beta_{vt}}}$	=	Static Directional Stability Vertical Tail
$C_{n_{\beta_{wing}}}$	=	Static Directional Stability Wing
C_r	=	Planform Characteristic
c_{HT}	=	Horizontal Tail volume coefficient
c_f	=	Skin friction
c_{f_e}	=	Equivalent skin friction
c_{root}	=	Root chord
c_{tip}	=	Tip chord
c_{VT}	=	Vertical Tail volume coefficient
$C(y)$	=	Trapezoidal Chord
$C(y)_{elliptical}$	=	Elliptical Chord
\bar{C}	=	Mean aerodynamic chord
\bar{C}_w	=	Wing mean aerodynamic chord
D	=	Drag
d	=	diameter
D_C	=	Climb Distance
D_G	=	Ground Distance
D_R	=	Rotational Distance
D_{TO}	=	Takeoff Distance
D_{TR}	=	Transition Horizontal Distance
D_{I_n}	=	Dynamic braking load nose

D_{min_p}	=	Minimum Power Drag
D_{min_T}	=	Minimum Thrust Drag
$d_{landing}$	=	Landing distance
d_p	=	Propeller diameter
$(D/q)_{misc}$	=	Miscellaneous engine drag
e	=	Oswald Efficiency
F	=	Fuselage lift factor
f	=	Fuselage form
F_g	=	Number of Gallons of Fuel
FF	=	Form Factor
FF_{fuse}	=	Fuselage Form Factor
G	=	Climb gradient
g	=	Gravity
H	=	Distance between center of gravity and ground
h	=	Fuselage Height
hp	=	Horsepower
$h_{obstacle}$	=	Obstacle Height
h_{qc}	=	Horizontal Tail Quarter Chord
h_{TR}	=	Transition Height
J	=	Advance ratio
K	=	Drag due to lift factor
k	=	Skin roughness value
K_A	=	Ground Roll Parameter
K_P	=	Propeller blade factor
K_T	=	Ground Roll Parameter
K_f	=	Plain flap lift increment empirical correction
K_{fuse}	=	Empirical Pitching Moment
$K_{effective}$	=	Effective drag due to lift factor

$KE_{braking}$	=	Kinetic energy dissipated by brakes
L	=	Lift
l	=	Length
L_{HT}	=	Horizontal tail moment arm
L_{VT}	=	Vertical tail moment arm
L_m	=	Extended Length of Main Landing Gear
l_f	=	Fuselage Length
l_t	=	Tail Moment Arm
M	=	Mach
m	=	Downwash Vertical Parameter
M_a	=	Distance between aft center of gravity and main tire
M_f	=	Distance between fore center of gravity and main tire
m_a	=	mechanical advantage
n	=	Rotations per minute
N_a	=	Distance between aft center of gravity and nose tire
N_e	=	Load Factor
N_{en}	=	Number of Engines
N_{gear}	=	Gear loading factor
N_l	=	Ultimate Landing Load Factor
n_{rs}	=	rotation speed
N_t	=	Number of Fuel Tanks
N_z	=	Ultimate Load Factor
P	=	Power
P_t	=	Tire pressure
q	=	Dynamic pressure
q_{climb}	=	Cruise dynamic pressure
q_{cruise}	=	Cruise dynamic pressure
R	=	Range
r	=	Downwash Horizontal Parameter

R_T	=	Transition Arc Radius
R_r	=	Rolling Radius
Re	=	Reynolds number
\Re_{cutoff}	=	Cutoff Reynolds number
S	=	Area
SM	=	Static Margin
S_a	=	Shock absorber stroke
S_{exp}	=	Exposed Area
$S_{exp_{tail}}$	=	Exposed tail area
$S_{exp_{wing}}$	=	Exposed wing area
S_{HT}	=	Horizontal Tail Area
S_L	=	Maximum static load
S_{L_n}	=	Maximum static load nose
S_{l_n}	=	Minimum static load
S_{ref}	=	Reference area
S_{ref_w}	=	Wing reference area
S_t	=	Tire stroke
S_{VT}	=	Vertical Tail Area
S_w	=	Wing area
S_{wet}	=	Wetted Area
$S_{wet_{fuse}}$	=	Fuselage wetted area
$S_{wet_{tail}}$	=	Tail wetted area
$S_{wet_{wing}}$	=	Wing wetted area
S'_{vs}	=	Vertical Tail Area to Centerline of Fuselage
T	=	Thrust

T_{climb}	=	Climb thrust
T_{cruise}	=	Cruise thrust
T_d	=	Tire diameter
T_{ff}	=	Forward thrust
t_{HR}	=	Horizontal Tail Maximum Root Thickness
T_s	=	Static thrust
$T_{takeoff}$	=	Takeoff thrust
T_w	=	Tire width
t	=	thickness
t_{VR}	=	Vertical Tail Maximum Root Thickness
V	=	Velocity
V_{app}	=	Approach velocity
V_{climb}	=	Climb velocity
V_e	=	Equivalent Velocity
V_f	=	Final Velocity
V_i	=	Initial Velocity
V_{max}	=	Maximum aircraft velocity
V_{min_p}	=	Minimum Power Velocity
$V_{min_{Sink}}$	=	Minimum Sink Velocity
V_{min_T}	=	Minimum Thrust Velocity
V_{stall}	=	Stall velocity
V_t	=	Fuel Volume
V_{tip_h}	=	Helical tip speed
V_{tip_s}	=	Static tip speed
$V_{v_{glide}}$	=	Vertical Glide Velocity
$V_{v_{rate}}$	=	Vertical Velocity Rate

$V_{vertical}$	=	Vertical velocity
Vol_{int}	=	Internal fuselage volume
W	=	Weight
W_{HT}	=	Horizontal Tail Weight
W_{VT}	=	Vertical Tail Weight
W_{av}	=	Avionics Weight
W_{crew}	=	Crew weight
W_{climb}	=	Climb weight
W_{cruise}	=	Cruise weight
W_{dg}	=	Design Weight
W_{elec}	=	Electronics Weight
W_{empty}	=	Empty weight
W_{fc}	=	Flight Control System weight
W_{fs}	=	Fuel System weight
W_{fuse}	=	Fuselage weight
W_h	=	Hydraulics Weight
W_i	=	Segment Weight
$W_{landing}$	=	Landing weight
W_{nw}	=	Weight on nose wheel
W_{mlg}	=	Main Landing Gear Weight
$W_{payload}$	=	Payload weight
W_{sc}	=	Surface Control System weight
W_{tail}	=	Tail weight
W_w	=	Weight on wheel
W_{wing}	=	Wing weight
W_0	=	Gross takeoff weight
w_{qc}	=	Wing Quarter Chord
$(x/c)_m$	=	Chord wise location of maximum thickness

\dot{X}_{ac_h}	=	Horizontal Tail Aerodynamic Center-to-Chord ratio
\dot{X}_{ac_w}	=	Wing Aerodynamic Center-to-Chord ratio
\dot{X}_{cg}	=	Aircraft C.G.-to-Chord ratio
\dot{X}_{np}	=	Neutral Point-to-Chord ratio
Y	=	Chordwise Location
\dot{Y}	=	Spanwise location of mean aerodynamic chord
z_v	=	Vertical Distance between Vertical Stabilizer and Aircraft C.G.
z_w	=	Vertical Distance from Wing Root Chord to Fuselage Centerline

Symbols

β (BETA)	=	Prandtl-Glauert compressibility correction
$\Delta\alpha_{0L}$ (DELTA-alpha)	=	Change in Aft Tail Zero-Lift Angle
δ_e (delta-p)	=	Elevator Deflection Angle
η_p (eta-P)	=	Propeller efficiency
η_s (eta-S)	=	Shock absorber efficiency
η_T (eta-T)	=	Tire efficiency
η_{af} (eta-af)	=	Airfoil efficiency
η_h (eta-h)	=	Tail to Freestream Dynamic Pressure Ratio
Γ (GAMMA)	=	Dihedral
γ_{climb} (gamma-climb)	=	Climb Angle
γ_{angle} (gamma-angle)	=	Best Climb Angle
λ (lambda)	=	Taper ratio
λ_{VT} (lambda-VT)	=	Vertical Tail Taper ratio
μ (mu)	=	Dynamic Viscosity
μ_r (mu-r)	=	Ground Roll Resistance
$\dot{\Psi}$ (psi)	=	Turn Rate

ρ (rho) = air density
 σ (sigma) = Density ratio

1. INTRODUCTION

1.1 MOTIVATION

The motivation behind this project is to fill a niche in the agricultural aircraft market place. Unmanned Aerial Vehicles (UAV) have entered the agricultural aircraft market, and fulfill important roles like flying reconnaissance over crops and spot aerial spraying. UAVs have not moved past spot aerial spraying, however, and are currently incapable of aerial spraying large fields in a timely manner. This is due to the Federal Aviation Administration (FAA) not allowing the use of larger UAVs that would be capable of spraying larger fields. In May 2015, the FAA approved the Yamaha RMAX for aerial spraying, with restrictions. With the increase of UAV popularity, and the growing UAV market place, it is reasonable to expect larger crop dusting UAVs to attempt become certified and enter the agricultural market place.

1.2 OBJECTIVE

The primary objective of this report is to design a fixed-wing UAV that has a hopper capacity of 50 gallons of pesticide that meets both the FAA requirements for crop dusters and as many new FAA requirements for the Yamaha RMAX as possible. Literature research will be conducted to document available crop dusting technologies and determine how variables like release height and airspeed affect crop dusting. Market research will be conducted to determine economic viability of a fixed-wing UAV and to compare current crop dusting options. An initial configuration layout will be designed including wing, empennage, initial sizing, electronics and landing gear. Potential propulsion systems will be discussed with one being selected and integrated into the aircraft. Aerial spray system types and configurations will be compared and integrated into the aircraft. Then the correlation between hopper

capacity and fuel needs will be discussed. The aerodynamics of the UAV will be analyzed and discussed. Weight analysis will be conducted to determine viability of the configuration. Stability and control analysis will be conducted to determine the stability of the UAV. The performance capability of the UAV will then be examined. Finally, the overall design and ability to meet the requirements will be discussed.

2. LITERATURE REVIEW

In this section, a brief history of crop dusting will be discussed, along with aerial application of pesticide and UAV crop dusting studies. Finally, market research will be presented to show the economic viability of this concept.

2.1 HISTORY OF CROP DUSTING

Eldon Downs and George Lemmer researched aerial crop dusting in the United States from the 1870's until the 1960's for the Agricultural Historical Society. According to Downs and Lemmer, the United States Department of Agriculture (USDA) began to focus on helping farmers control the insect population starting in the 1870's. At the beginning of the 20th century, this focus began to include insecticides and fungicides. The addition of aircraft slowly revolutionized the USDA's ability to control the pest population. Aircraft were initially used to search for outlaw cotton fields, seed sowing, and crop dusting fields and forests. The original crop dusting experiment was dusting catalpa trees in Troy, Ohio¹. The success of this experiment encouraged further experiments with dusting cotton fields. The successes of these subsequent experiments caused the USDA, partnering with the U.S. Army Air Service, to experiment on all kinds of pesticides.

Eldon Downs and George Lemmer go on to mention that the aircraft available during the early years of crop dusting were not well suited to crop dusting. The Curtis JN-6 and de Havilland DH-4 were the primary aircraft used for crop dusting, however, neither aircraft was powerful or stable enough to fly safely at the low altitudes necessary for effective crop dusting¹. Downs and Lemmer go on to say that the first hopper was created by the Engineering Division at McCook field in Ohio and could only hold 32 gallons. Throughout the 1920's, experiments were conducted with new equipment and techniques to improve efficiency dusting both fields and forests. In 1926, a commercial company called Huff-Daland dusted several thousand acres of tomato plants, where two pilots, one mechanic, and one aircraft performed work that would have required up to 2,000 men¹. The work done by Huff-Daland helped show how much more efficient aerial crop dusting could be when compared to ground dusting.

Improvements in aerial crop dusters progressed slowly until major improvements were made after World War II. These improvements lead to a large increase in the usage of aircraft for crop dusting. In 1958, 21 million acres were crop dusted by aircraft¹. The potential dangers of crop dusting started to become evident, and in 1964, a reduction in the use of crop dusting started. Some of these potential dangers are shown in a report produced by the American Journal of Public Health. Dr. McConnell, Dr. Anton, and Ralph Magnotti traveled to Nicaragua's largest crop dusting airport to evaluate the exposure levels of crop dusting mechanics. They found the mechanics had an incredibly high risk of pesticide overexposure, and many had been to the hospital with symptoms of pesticide overexposure. In addition, constant low level exposure to certain chemicals can reduce the number of symptoms relative to a larger single exposure, reducing the likelihood of the patient seeking treatment². This

study did not include pilots from Nicaragua, however, the exposure experienced by mechanics shows pilots are at risk as well.

UAVs started to become more prominent around the same time the dangers of pesticide were exposed. The United States Air Force (USAF) pioneered the first mass produced, long range UAVs, whose primary initial mission was reconnaissance³. The Ryan model 147, renamed the AQM-34 Lightning Bug, was in operational use from the 1960's until 2003. During this time period, many technological advancements were made that pushed UAV aircraft from missions of reconnaissance to all of the missions they fulfill today. The United States Navy (USN) developed the QH-50 DASH, which was in operation throughout the 1960's and 1970's³. The use of the QH-50 DASH created several firsts for UAVs. The QH-50 DASH was the first UAV helicopter and the first UAV to take off and land on a ship at sea³. The rapidly developing UAV technology allowed UAVs to expand their capabilities to include agriculture.

Crop dusting UAVs were first introduced in the 1980's. They are typically heavier and have higher payloads than other agricultural UAVs, but they are also able to support longer flight endurance⁴. The crop dusting UAVs typically used are helicopters and rotocopters, with Yamaha being at the forefront of crop dusting UAV development. The first Yamaha aerial sprayer, RCASS, was built in 1980. The R50 was introduced in 1990 with a 20 kg payload and laser height-determination system. The Yamaha RMAX was introduced in 1997, and has flown over 2.0 million flight hours and sprays 2.4 million acres annually in Japan⁵. Starting in 1991, there were fewer than 100 registered Yamaha unmanned helicopters, and by 1999 there were 1,200⁶. On May 1, 2015, the Federal Aviation Administration (FAA)

authorized the Yamaha RMAX for crop dusting within the United States National Airspace (USNAS).

2.2 CROP DUSTING STUDIES

At the 1998 North American Conference on Pesticide Spray Drift Management, Dennis Gardisser listed some application factors that help minimize spray drift. First, the goal should be to create as many droplets at the optimum size as possible. The optimum size will vary based on spray nozzle, type of pesticide, etc. Second, Gardisser mentions the effect of nozzle design on spray drift:

The best nozzle design seem to be those that take advantage of the airflow. Spray should be eliminated parallel to the dominant airflow direction to avoid aerodynamic shear. Flat fan, sheet, and straight stream type nozzles are being incorporated by many operators to maintain good droplet size characteristics. These nozzles may also direct all the spray parallel to the air stream and/or slightly down – in the direction of the crop...As the aircraft speed increases, attention to air shear becomes more important. (86)

Third, the nozzles should be moved away from aerodynamic obstructions created by other parts of the aircraft, and half-boom shut-offs are useful for reducing drift on edges of the field perimeter. Finally, he mentions that aerodynamic ground effects may increase the drift of pesticides⁷.

At the same conference, I.W. Kirk summarizes the main problems associated with drift, and studies done to prevent it. The main problems associated with spray drift are the damage done to areas outside the spray perimeter and the environmental damage. It is also a waste of materials and can create a negative public perception of crop dusting.

The first study Kirk summarized was focused on drift reduction, written by Valco, et al. In 1990, Environmental Protection Agency (EPA), a group of synthetic insecticide

producers called the Pyrethroid Working Group (PWG), and the National Agricultural Research and Education Foundation contacted USDA Agricultural Research Service (ARS) to develop a program to reduce the hazards of aerial spray drift. The test was conducted in 11 states during spring of 1991. The test was conducted by placing spray droplet collection cards 100 ft. downwind at 10 ft. intervals on the spray swath centerline to measure coverage percentage. Monofilament lines were stretched between poles at 5, 10, 15, and 20 ft. heights parallel to the spray swath centerline to measure the density of the spray drift. Nozzle orientation, aircraft speed, boom percentage, and flight height were some of the variables tested. The results show nozzles pointed back produced less drift than nozzles pointed down, nozzles to three quarters wing length produced less drift than nozzles to full wing length, lower speed produced less drift than high speed, and lower flight height produced less drift than higher flight height⁸.

The second study summarized by Kirk aimed to determine effects of nozzle selection on drift reduction, performed by Bouse, et al. in 1994. The aircraft used was an Air Tractor AT-502. The nozzles included a narrow angle flat-fan 4020 Quick Veejet and a whirl-type hollow cone 1/8B10-8 WhirlJet. The tests were conducted at 120, 135 and 150 mph for each nozzle. The spray deposits were collected on Mylar cards placed across the spray swath and downwind to 450 ft. At 450 ft., cotton strings were hung between poles at 6 ft. intervals, with a maximum height of 30 ft. The study showed the narrow angle flat-fan produced larger droplets than the whirl-type hollow cone at every speed, and droplet size decreased for both nozzles as the speed increased. The study determined larger droplets produced less spray drift⁸.

The third study summarized how a hydraulic nozzle might reduce spray drift, performed by Kirk in 1997. A hydraulic nozzle works by using 4 orifices and 3 deflector plates to produce different droplet sizes and spray rates. The test was performed in a wind tunnel with airspeed varying from 100 to 160 mph with a CP nozzle orifice size of 0.125", 30°, and 30 psi. The study showed the smallest number of small droplets were formed at 110 mph, and the number of small droplets increases by 4.3 times when airspeed was increased to 160 mph⁸. This study helps prove higher airspeed increases air shear, resulting in smaller droplets and more drift.

Finally, Kirk describes a study that compares a turbine-engine-powered Thrush and a larger, heavier radial piston-engine-powered M-18 Dromader, performed by Howard in 1994. The Dromader was tested with both 50% and 70% boom length relative to the wing, while the Thrush was only tested with the 70% boom length. The Dromader and Thrush were flown at 110, 120, and 130 mph and at 120, 130, and 140 mph respectively. The aircraft were flown upwind at an angle of 45° for a 2,200 ft. sample line. CP nozzles were used on the boom. The study shows the spray drift increased with increased airspeed, in agreement with other studies. The drift for the Dromader increased when the boom length percentage was increased from 50 to 70, which also agrees with other studies. The Thrush was shown to reduce drift more than the Dromader. In fact, the Thrush flying at 140 mph reduced spray drift more than the Dromader flying at 110 mph with a 50% boom length⁸. In addition to these studies, Kirk mentions the potential of aerial electrostatic systems to help reduce spray drift. These systems will be discussed in other studies later on.

The Spray Drift Task Force (SDTF) is a joint project of 40 agricultural chemical companies formed in 1990. The EPA Office of Pesticide Programs (OPP) required chemical

manufacturers to provide droplet-size spectrum measurements and field-drift evaluations if unintended targets were at risk of adverse effects⁹. The fundamental premise of the SDTF is spray drift is primarily due to application techniques, environmental conditions, and the properties of the tank mix. The SDTF database was created with three assumptions. The first assumption was the active ingredient analyte has a degradation or volatilization time that is too rapid for effectiveness in the field. The second assumption is the physical properties of the chemical should be measured in the tank mix and tracer levels would correlate to full active-ingredient rates⁹. The third assumption is the risk to unintended targets can be evaluated in a two-step process that determine concentration and then determine risk.

The overall objective of the SDTF was the quantification of downwind sedimentation deposition for a wide range of pesticide label conditions and atomization characteristics. Since meteorological variables can have a large impact on spray drift, this study was done to quantify the response of drift to these variables, resolve discrepancies on importance of application parameters, and account for the effects of meteorological variables on application variables. Helicopters were flown at a speed of 11 to 33 m/s, fixed-wing piston aircraft with a speed of 33 to 50 m/s, and turbine engine fixed-wing aircraft greater than 50 m/s. Most of the applications were sprayed at 1.5 m to 3 m above the crops, and the nozzles were typically oriented 45° backward on booms positioned either below or behind the trailing edge.

Based on the results, spray drift was highest within 10 m of the intended target, with the amount of drift trailing off rapidly as the distance from target was increased. The mean airspeeds for the SDTF study were 28, 48, and 68 m/s. Increasing the speed led to an increase in finer sprays due to air shear. The higher speeds also produced higher downwind deposition rates. Increasing the release height and the boom length percentage also led to an increase in

the downwind deposition rates. One significant result from the table shows nozzles pointed back produced the least amount of droplets of the size many consider to be more likely to drift under favorable conditions.

In addition to the SDTF study, an off-site drift and deposition model was created called AgDRIFT. Both the STDF and the EPA OPP support the use of drift modeling tools to improve the efficiency, cost effectiveness, and reliability of product evaluation¹⁰. AgDRIFT was compared to the studies done by the SDTF, and overall, AgDRIFT was able to predict the average field deposition levels reasonably well for a variety of aerial agricultural applications¹⁰. There are some issues with the results produced by AgDRIFT. The SDTF studies only used one helicopter, and the number of tests performed was small, creating an inability to accurately model helicopter drift compared to fixed-wing drift. There is also an issue of AgDRIFT being sensitive to evaporation effects. In general, AgDRIFT is a reasonable model to use to simulate the drift produced by the aerial application of pesticide.

Frank et al., (1993) were interested in trying to determine if buffer zone guidelines could be developed for different pesticide application techniques. This study was conducted over a three year period at 26 different sites in Ontario. The different application techniques used for the study are aerial application via helicopter and fixed-wing aircraft, ground concentrated air blasts (CAB), ground high-pressure booms, and ground low-pressure booms. Data collection was conducted by placing filter paper in petri dishes both parallel and perpendicular to the flight path. Wind speed and direction, air temperature, flight path direction and release height during spraying were all recorded. A Piper Pawnee -D was used for the fixed-wing aircraft, and was flown 3-5 m above the crops, with a speed of 155-160 km/h.

During the 1983 tests performed by Frank et al., mancozeb was recorded as having drifted 24 m parallel to the flight path and 18 m perpendicular to the flight path. 42.6 mg of mancozeb was measured parallel to the flight path and 17.5 mg was measured perpendicular to the flight path. Both of those quantities are greater than what was recorded during the helicopter test¹¹. During the 1984 tests, metalaxyl was used and was found to have a different drift pattern than the 1983 mancozeb test. Both the 1983 and 1984 tests were performed under windless conditions. Despite having different metrological variables at 26 different test sites, the drift pattern and deposits were similar for all the systems tested. Detectable deposits from the three helicopter and fixed wing aircraft drifted from 15 to 76 m parallel to the flight path and 3 to 84 m perpendicular to the flight path¹¹. The amount of drift was dependent on many factors, including the physical properties of the pesticide being applied. The low pressure boom had the lowest drift potential of the 3 ground application methods tested.

Nuyttens et al., (2009) sought to determine the droplet size and velocity characteristics of different nozzles, sizes, and spray pressures. This study was performed because of the complexity of modeling the droplet movement under a spray model. The ideal nozzle-pressure combination should improve efficacy by increasing on target deposition rate, while minimizing drift and user exposure¹². The droplet diameter when released is strongly correlated to the velocity of the droplet. In this study, there were 13 different nozzles of 3 different types (standard flat-fan, low-drift flat-fan, and air-inclusion), sizes (ISO 02, 03, 04, 06), and spray pressures (2.0, 3.0, and 4.0 bar)¹².

Nuyttens et al., found that for nozzles of the same size and pressure, the standard flat-fan nozzles produce the finest droplets, which are more prone to drift, followed by low-drift and air inclusion nozzles. The downside to the larger droplets created by the low-drift and air

inclusion nozzles is an increased chance of runoff. Another result found from this study is the larger the ISO size, the coarser the droplets at the same operating pressure, however, the standard flat-fan nozzles are more effected by this than the other two nozzles. In general, bigger droplets correspond with higher drop velocities, and smaller droplets with lower velocities¹². After a certain droplet size is achieved, the drop velocity will stabilize. One important difference between the flat-fan nozzles is that the standard nozzle will produce faster droplets for the same droplet size and operating pressure when compared to the low-drift flat-fan nozzle. For all nozzle types, a bigger ISO nozzle will correspond with higher drop velocity characteristics¹².

Huang et al., (2009) sought to develop a spray system for an unmanned helicopter for both agricultural spraying and vector control. The UAV selected as the platform was the Rotomotion SR200. The spray system was interfaced with the UAV's electronic control systems to trigger spray based on the GPS coordinates. The spray system consisted of a boom with spray nozzles, a hopper for the spray, a liquid gear pump, and a spray control activation mechanism. The goal of the UAV was to spray 34.59 acres on a single load with 4.2 L of chemical, while flying at 2.2 m/s¹³. Four spray nozzles were tested for droplet size and flow rate, with the Micronair ULV-A+ being chosen due to the better spray atomization pattern. The results of the testing show that a UAV with a 30 m spray at a release height of 6 m and aforementioned airspeed, the system would be able to spray 1 acre/min¹³. This system was designed for low acre spraying or spot spraying large fields, but was not designed to spray a large acreage plot.

Edward Law (2001) researched and reviewed the research and development of agricultural electrostatic spray throughout the 20th century. The Lorentz equation is used to

quantify the force on a particulate given a certain charge and velocity when acted on by an electric and magnetic field. Law describes how this is applied in agricultural spraying:

For fixed or relatively slow moving charged bodies, the electric force component dominates the negligible magnetic component. This provides that basis for numerous electrostatic processes in which dynamic control of particulate trajectories is achieved for purposes of dispersion, propulsion, attraction, deposition... For finely divided liquid and solid matter of diameters under several hundred micrometers, common particulate-charging methods... impart charge-to-mass ratios quite adequate to provide electrostatic forces 10-50 fold dominate over gravity in electric fields well under the 30kV/cm dielectric strength typical of air. Thus, technological implementation of electrostatic forces for a number of agricultural and biological usages is quite feasible—charged powder and droplet applications being prime ones. (26)

Despite being relatively effective, chemical pesticides add over \$25 billion annually to the world's crop-production costs and disperse 2.25 billion kg of active ingredients world-wide¹⁴. One of the ways to improve efficiency is to find a way to evenly apply pesticide to each plant instead of using the conventional gravitational and inertial forces. There are some technical issues associated with charged airborne pesticide. The main issue is airborne pesticide spray can lose as much as 80% of the charge exchanged between a pesticide spray cloud and the intended target, a problem worsened by using a positively-charged spray¹⁴. Law presents some efficiency evaluations that show the finely atomized electrostatically applied sprays can achieve equal protection to conventional spray methods while using only half the pesticide. In addition to the study by Law, there have been other studies showing increased efficiency with electrostatic spray.

Durham Giles and T. Blewett sought to determine the potentially hazardous effects of conventional and reduced-volume charged sprayers on strawberry harvesters. The chemical captan is typically applied every 14 days when fruit is being produced.

Strawberries are then harvested every 3-5 days and the harvesters are continually exposed to captan. The reduced-volume charged spray has the potential to reduce the applicator exposure, but it also has the potential to increase crop picker exposure¹⁵. The reduced-volume spray was tested 3 times at 80 L/ha, 23 times less than the conventional spray. Both sprays used 2.24 kg/ha., consistent with the conventional full-rate treatment, resulting in the reduced volume spray being 23 times more concentrated.

The results from the tests show that the reduced-volume charged spray was more effective at sticking to the strawberry foliage. The decay rate of captan per cm² of leaf area was similar for the conventional full-rate and charged half-rate applications¹⁵. The half-rate charged spray was deposited more than the conventional full-rate. As was expected, the increase in pesticide deposit led to an increase in exposure of the crop pickers. This increase in exposure was not found to be any more dangerous than exposure from the conventional spray, however, a full-rate charged application could increase worker exposure by 70%¹⁵.

Kirk et al. (2001) researched and summarized several studies done with the USDA-developed aerial electrostatic spray system. After 5 years of testing, the final prototype was composed of 88 electrostatic nozzles with TX-VK6 orifices, calibrated for 9.4 L/ha at 483 kPa, and bipolar charging with inboard nozzles on each boom separated by 1.8 m¹⁵. A conventional aerial applicator on the same aircraft was tested for comparison purposes. The conventional application used either 32 CP nozzles calibrated for 46.8 L/ha at 193 kPa, or a ULV application arrangement of 10 to 13 8002SS nozzles calibrated for 0.9 to 1.2 L/ha at 276 kPa¹⁶. The tests were performed on cotton to test effectiveness against the whitefly and boll weevil. The spray rates for the

whitefly were 4.7 L/ ha for the electrostatic and 46.8 L/ha for the conventional, however, there was not a significant difference between the effectiveness of either method, with the conventional method proving to be the more effective of the two¹⁶.

Unlike the whitefly study, the boll weevil studies compared the effectiveness of the electrostatic and ULV application methods. The first of the two boll weevil studies, using Fipronil, showed that both methods had over 95% weevil mortality the day after spraying, the electrostatic method having significantly higher weevil mortality rates on day 3, and the mortality rates of both methods dropped to 2% or less by day 7¹⁶. The second study, using EC Malathion 5, showed the electrostatic method to have a 97% mortality rate on the day of application, then drops drastically to 29.8% on day 3, and appears to stabilize there through day 6, while the ULV method starts at 88.7% on the day of application, drops to 56.1% on day 3, and finishes at 43.1 on day 6¹⁶. Kirk et al. concluded the study saying:

These studies show some situations where field performance of the aerial electrostatic spray system exceeds that of conventional sprayers, and vice versa. That is neither unusual nor unexpected. Most application of technologies have niches in which they are best adapted. However, in general terms, aerial electrostatic application methodology has been shown to have spray deposits and efficacies that are not markedly different from conventional aerial application methodologies. Other factors, such as operational efficiencies associated with low spray rates of electrostatic systems, could be an important factor favoring aerial electrostatic applications. (1092)

2.3 MARKET ANALYSIS & RESEARCH

Before determining if there is a place in the market for a new crop dusting UAV, research must be done to determine the economic feasibility of entering the market. There must be enough money and demand to warrant the startup, production, and maintenance costs

of developing a UAV. In 2010, agricultural aviation contributed \$214 million to Iowa's state economy due to increased crop productivity, and the small airfields used by crop dusters contributed over \$400 million to the state's economy¹⁷. Both of those economic figures show there is money in crop dusting, but they do not address demand. In Iowa alone, over 4 million acres are treated by air annually, at \$15 to \$25 per acre¹⁷. There are also incentives to crop dust fields. Treated corn can yield an additional 10-30 bushels of corn, and aphids can cause a reduction of 20 bushels or more of soy beans per acre¹⁷. As of September 29, 2015, soy beans were \$9.77 per bushel, meaning an aphid infestation could cost \$200 per acre, whereas spraying is only \$15 to \$25 per acre. Introducing UAVs into the market place could reduce the spraying price per acre, meaning more farmers might be inclined to pay for crop dusting.

At the Association for Unmanned Vehicle Systems International (AUVSI) conference in Kansas, the potential economic impact of agricultural UAVs were presented. Michael Toscano states that UAV integration into USNAS will create an economic impact of over \$13.6 billion in the first 3 years, with more than \$82.1 billion in the decade after that¹⁸. He goes on to mention that agricultural UAVs would have a \$66 billion economic impact over first 11 years of integration¹⁸. There is a discrepancy with the numbers at this conference. It could be because of the location, but the price of manned crop dusters is said to be \$8.00 per acre, different from the manned crop duster numbers mentioned in the previous paragraph, with UAVs coming in at \$2.00 per acre¹⁸. At a 2013 American Institute of Aeronautics and Astronautics (AIAA) conference in California, AUVSI projected the economic impact to be \$30 billion over the first 10 years in California alone¹⁹. These economic figures show that there is enough money and demand to design new crop dusting UAVs. Now a niche in the market must be found.

The Air Tractor AT-401B, Thrush 510G, PZL Mielec Dromader, Pacific Aerospace Cresco, and Embraer Ipanema basic specifications will all be compared to determine the part of the market covered by manned aircraft. Both Air Tractor and Thrush produce multiple models of manned crop dusters, both at this size and larger. It is also important to note that there were no Cresco or Ipanema aircraft listed under the FAA Aircraft Registry. It is unclear if this is a certification issue or if there are simply not any registered.

Table 1. Basic Specifications of Manned Crop Dusters

Specs	AT-401B ²⁰	510G ²¹	Dromader ^{22,23}	Cresco ^{24,25}	Ipanema ²⁶
Length (ft.)	27.33	32.33	31.08	36.33	24.38
Height (ft.)	9.50	9.33	12.16	11.9	7.28
Wing Span (ft.)	51	47.5	58.07	42	36.32
Wing Area (ft. ²)	306	365	430.6	294	201.2
Fuel Capacity (gal.)	126	228	191.79	130	70
Engine	P&W R1340	GE H80	Asz-62IRM18	P&W PT6-34	Lycoming 300HP
Empty Weight (lb.)	4244	4,700	5975	2950	NA
Maximum Takeoff Weight (lb.)	NA	NA	9259.4	7,000	3968.3
Hopper Capacity (gal.)	400	510	660.43	500	250
Operating Speeds (mph)	120-140	90-150	NA	NA	NA
Maximum Payload (lb.)	NA	NA	4409.25	NA	NA

The Ipanema is the smallest aircraft with the lowest fuel and hopper capacity. The AT-401B is the smallest of the three aircraft that are definitely FAA certified. The 510G can operate at a lower speed than the AT-401B, leading to less air shear, and potentially less drift. The Cresco has a crew of two and can hold up to seven passengers, leading to the longer length and larger height of the aircraft. In comparison to the UAV helicopters, it is relatively common for these aircraft to spray 1,000 acres or more in a day. Manned aircraft require the use of a runway for take-off and landing, and the ferrying time from airport to field wastes

both time and money. One noticeable aspect of all five of these aircraft are how large the smallest aircraft is. The size of the UAVs will pale in comparison to the size of the manned aircraft.

The UAV crop dusters that will be compared are the Rotomotion SR 200, the AG-RHCD 01, and the Yamaha RMAX.

Table 2. Basic Specifications of UAV Crop Dusters

Specs	SR200 ²⁷	AG-RHCD 01 ²⁸	RMAX ⁵
Length (in.)	110	70.9	108.3
Width (in.)	30	21.7	28.3
Height (in.)	34	27.6	42.5
Main Rotor Diameter (in.)	118	77.2	123.2
Maximum Payload (lb.)	50	20.9	35.3
Engine	150 cc, 16 HP, 2-stroke gasoline engine	NA	246 cc, 2-stroke, 2-cylinder
Endurance (hrs.)	5+	NA	1
Dry Weight (lb.)	55	45.2	141
Operating Speed (mph)	NA	6.7-13.4	12.4
Hopper Capacity (gal.)	NA	2.1	4.2
Spray Rate (gal/min)	NA	0.21-0.32	0.34-0.53

The Yamaha RMAX and SR 200 are both larger than the AG-RHCD 01, but the largest hopper capacity is only 4.2 gallons. Yamaha has spent a large amount of resources creating UAV helicopters specifically for crop dusting, so it makes sense that the RMAX is the most robust of the three UAVs. The SR 200 is more of a general UAV that can be modified to become an aerial sprayer. The AG-RHCD 01 and RMAX can only spray for 7 or 8 minutes if the maximum spray rate is used. These UAVs are capable of taking off from anywhere, so there is no ferrying time. Unfortunately, the UAVs have much smaller fuel tanks and hopper capacities, resulting in regularly refueling and refilling the hopper. It is clear from the hopper capacity, spray rate, and operating speeds that these UAVs are built for spot spraying or very small fields, but they cannot handle the larger fields that manned crop dusters spray.

There is a large gap in capabilities between the manned and UAV crop dusters. The manned aircraft perform better on larger fields, but are not as useful on smaller fields due to the inability to precisely apply pesticides and cost inefficiencies. The UAV helicopters can precisely apply pesticides, but are not practical for larger fields. Unlike the manned aircraft, the UAVs do not have to account for a pilot on board resulting in a smaller chance of injury and an ability to push the design envelope. The UAVs are also capable at operating at speeds that minimize drift, improving application efficiency. Based on the market analysis, there is a niche in the crop dusting market between the manned aircraft and UAV helicopters that is not currently filled, with an economic incentive to fill that niche.

3. MISSION SPECIFICATIONS

3.1 MISSION REQUIREMENTS

The mission requirements for this aircraft will include the FAA requirements for crop dusting aircraft, particularly Title 14 Sections 91.313 and 137.51, and the Yamaha RMAX requirements. Due to mission requirements, some of the Yamaha RMAX exemptions will have to be disregarded as they would make the aircraft impossible to design. All of the FAA requirements will be provided in the Appendices. The payload, takeoff distance, and velocity requirements will be the requirements that influence the design of the aircraft the most.

3.2 GENERAL FLIGHT

The aircraft must be operated within the visual line of sight (VLOS) of the pilot in command (PIC) and visual observer. The pilot having to maintain VLOS presents a problem when it comes time to applying the pesticide. It means a third person will have to watch the video feed, control the spraying, and make sure the UAV is spraying in the right area. A third

person will allow the pilot to focus solely piloting the aircraft. Aerial spraying can be made easier by putting a dye in the pesticide to make it more visible. The UAV can only be operated during daylight hours and in good weather. The maximum altitude will be 400 ft. above ground level (AGL), typically being flown at 15 to 20 ft. over an agricultural area. The UAV will take off at an altitude of 1,000 ft., instead of sea-level, to account for various altitudes across the country.

3.3 PAYLOAD

The UAV must be capable of carrying 50 gallons of pesticide (417 lb.). It will also have to carry various electronic equipment like cameras and avionics.

3.4 FLIGHT SPEED

The preferred maximum speed for this aircraft will be 45 mph, just like the RMAX, however, if the 45 mph maximum speed constricts the design space too much, it will be increased. The UAV will fly at 40 mph when applying pesticides. If the maximum speed is modified, then the chosen application airspeed will be modified accordingly. The flight speed analysis is provided in Appendix C.

3.5 ENDURANCE

The runway where the UAV will be taking off will be located 5 miles away from the intended spray area. The 5 mile distance is used because a suitable road might not be located right next to the intended spraying area. The aircraft must have a large enough fuel tank to account for varying spray rates per acre.

3.6 TAKEOFF AND LANDING

The aircraft must be capable of taking off and landing on dirt roads close to the intended spraying area. The runway will be limited to 500 ft. during takeoff. The preferred landing distance is 1,000 ft., but it can be increased if necessary.

3.7 CREW

The crew will consist of three people. The aircraft will have a pilot and a visual observer who must be able to communicate verbally at all times. The third person will be needed to transport the crew to where the UAV takes-off and to the agricultural area where pesticide will be sprayed. The third crew member will also have to monitor the cameras and avionics, as well as be in control of the pesticide.

3.8 MISSION PROFILE

The profile of the mission is shown in Figure 1. The details for each phase are:

- Phase 1: The UAV will takeoff from a dirt road within a distance of 500 ft. during daylight hours.
- Phase 2: The UAV will proceed to climb to a cruise altitude of 300 ft.
- Phase 3: The UAV will cruise for 5 miles once it reaches a cruise altitude of 300 ft.
- Phase 4: The UAV will then begin descent until it is 15 to 20 ft. above the ground.
- Phase 5: Once at the altitude of 15 to 20 ft., the UAV will proceed to fly at 40 mph while spraying pesticide over the agricultural area. The effective spray swath will be assumed to be the wing span of the aircraft.
- Phase 6: Once the hopper has emptied or work has been completed, the UAV will climb back up to a cruise altitude of 300 ft.
- Phase 7: Once at a cruise altitude of 300 ft., the UAV will proceed to fly 5 miles back to where it took off.
- Phase 8: At this point, the UAV will begin descent until the wheels reach the ground.

- Phase 9: Once the wheels touch the ground, the UAV will reach a complete stop.

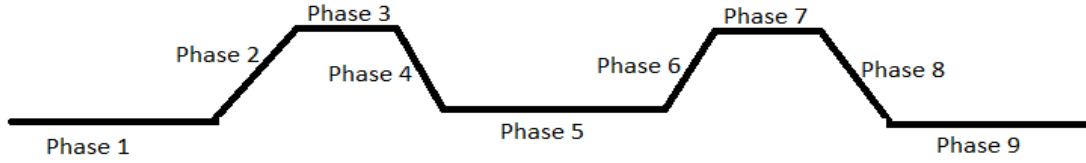


Figure 1. Mission Profile

4. INITIAL CONFIGURATION

4.1 DESIGN TAKEOFF WEIGHT

The first step in attempting to size this agricultural UAV will be to use a quick sizing method to create a rough guess for the takeoff gross weight as proposed by Daniel Raymer.

The design takeoff weight can be written as shown in Eq. (4.1)²⁹:

$$W_0 = W_{crew} + W_{payload} + W_{fuel} + W_{empty} \quad (4.1)$$

To guess an initial takeoff gross weight, (4.1) needs to be modified to make the fuel and empty weights fractions of the total weight. The payload weight is found by multiplying the hopper capacity by the weight of 1 gallon of water in pounds. Also, as there is no crew, the crew weight is 0 lb. These modifications are shown in Eq. (4.2)²⁹:

$$W_0 = \frac{W_{payload}}{1 - \frac{W_{fuel}}{W_0} - \frac{W_{empty}}{W_0}} \quad (4.2)$$

The empty weight fraction can be estimated from historical values for agricultural aircraft provided by Raymer and using Eq. (4.3)²⁹:

$$\frac{W_{empty}}{W_0} = (0.95) 0.74 W_0^{-0.03} K_{vs} \quad (4.3)$$

The UAV will not use swept wings, resulting in a K_{vs} is 1. If composites are used, then the empty weight fraction should be multiplied by 0.95. The fuel weight fraction uses different fuel requirements, based on mission segment, to estimate the weight. At this stage, only takeoff, climb, cruise, and landing are used, producing an underestimate of the weight fraction. Also, the fuel required during aerial application is not known at this time. The historical mission-segment provided by Raymer are 0.97, 0.985, and 0.995 for takeoff, climb, and landing respectively²⁹. The cruise segment weight fraction is found using a modified Breguet range equation shown in Eq. (4.6)²⁹:

$$C = C_{bhp} \frac{V}{550 \eta_p} \quad (4.4)$$

$$R = \frac{V}{C} \frac{L}{D} \ln \frac{W_{i-1}}{W_i} \quad (4.5)$$

$$\left(\frac{W_i}{W_{i-1}} \right)_{cruise} = e^{\frac{-RC_{bhp}}{550 \eta_p \frac{L}{D}}} \quad (4.6)$$

The maximum lift-to-drag ratio of 11.5 was estimated based on a figure provided by Raymer, and the propeller efficiency was assumed to be 0.8 in cruise. Once all of the mission segment fuel weight fractions are found, they are multiplied together and then by 1.06, to account for reserves and trapped fuel, and the product is the fuel weight fraction. After all of these calculations were made, Eq. (4.2) was used to estimate the gross takeoff weight, and the results are presented in Table 3.

Table 3. Estimated Gross Takeoff Weight

W ₀ Guess	W _f	W _e	W ₀ Calculated
600	44.1	348.1	1203.38
700	51.5	404.3	1194.15
800	58.8	460.2	1186.30
900	66.2	515.9	1179.48
1000	73.5	571.4	1173.47
1100	80.9	626.8	1168.11
1110	81.6	632.3	1167.60
1120	82.3	637.8	1167.10
1130	83.1	643.3	1166.60
1140	83.8	648.9	1166.11
1150	84.5	654.4	1165.62
1160	85.3	659.9	1165.14
1161	85.3	660.5	1165.10
1162	85.4	661.0	1165.05
1163	85.5	661.6	1165.00
1164	85.6	662.1	1164.95
1165	85.6	662.7	1164.90

The initial takeoff gross weight is 1,165.0 lb. as shown in Table 3.

4.2 INITIAL WING CONFIGURATION

The initial wing configuration will focus more on historical trends and qualitative observations than quantitative analysis. The NACA 4415 airfoil was chosen due to its popularity in the agricultural aircraft industry. Airfoils with thicker, flatter trailing edges are more advantageous for crop dusting due to the ease of attaching the applicator. High wing position was chosen for multiple reasons. High wings are useful for short runways, prevents the ground effect from increasing lift as the UAV approaches the ground, and will help protect the sprayer and wing from any debris during takeoff and landing. The initial wing dihedral will be 1° to provide more dihedral without creating an excess of dihedral. Raymer provides a typical agricultural aircraft aspect ratio of 7.5²⁹. As the UAV will fly no faster than 45 mph, there is no need to use wing sweep to reduce adverse effects of transonic and supersonic flow.

The wing will have no taper or twist. According to Raymer, general aviation aircraft typically have 2° of incidence with no twist²⁹.

4.3 INITIAL TAIL CONFIGURATION

The initial tail configuration will also focus on historical trends and qualitative observations. The conventional tail was chosen primarily due to the weight difference between the conventional and t-tail. The conventional tail elevator position could pose a problem due to wing wake, nevertheless, with the aircraft never flying above subsonic speeds, the position should be acceptable. The horizontal tail will use the NACA 0009 for its airfoil. The horizontal tail must behave similarly for positive and negative angles of attack, making the symmetric airfoil a suitable choice. Also, the symmetric NACA airfoils are a popular choice for horizontal tails. The vertical tail will also use the NACA 0009 for its airfoil. Unlike the horizontal tail, the vertical tail will need a small degree of incidence, 1 or 2° , to account for the moment produced by the single engine propeller. Both the horizontal and vertical tails will have aspect ratios of 4 and 1.5 and taper ratios of 0 and 0.4 respectively.

5. INITIAL SIZING

The first step in sizing the UAV will be to calculate the thrust-to-weight ratio and the wing loading. The thrust-to-weight ratio will determine how large the engine will need to be. The wing loading will be used to find the area of the wing. Once the area is known, the information from the previous section can be used to complete the initial design of the wing, fuselage, and tail.

5.1 THRUST-TO-WEIGHT RATIO

When discussing thrust-to-weight ratio for propeller aircraft, it is important to note that power loading is typically used instead of thrust. A small engine will have a high power loading and vice-versa. Agricultural aircraft typically have a power loading of 11 lb./hp²⁹. The propeller produces the thrust for propeller aircraft, which leads to modifications to the thrust-to-weight ratio equation, shown in Eq. (5.1)²⁹:

$$\frac{T}{W} = \frac{\eta_p}{V} \frac{P}{W} = \frac{550 \eta_p}{V} \frac{hp}{W} \quad (5.1)$$

The thrust-to-weight ratio will be solved using two different methods, and the higher value will be used as the initial T/W . Statistical estimation can be used to determine a first estimate for P/W and T/W . This statistical estimation involves using historical factors for agricultural aircraft, as shown in Eq. (5.2)²⁹:

$$\frac{P}{W_0} = 0.009 V_{max}^{0.5} \quad (5.2)$$

Once Eq. (5.2) is solved, the value can be used in Eq. (5.3) to solve for the thrust-to-weight ratio. Hp/W and T/W are equal to 0.0563 and 0.663 respectively.

The second method used is thrust matching. This method assumes that the aircraft is cruising at the optimum altitude for an unknown wing loading²⁹. The thrust-to-weight ratio is equal to the inverse of the lift-to-drag ratio as shown in Eq. (5.3)²⁹:

$$\left(\frac{T}{W} \right)_{cruise} = \frac{1}{\left(\frac{L}{D} \right)_{cruise}} \quad (5.3)$$

The cruise T/W value is equal to 0.087, however, the thrust-to-weight ratio during cruise is typically only a fraction of the climb thrust-to-weight ratio. The climb T/W adds a velocity component, as shown in Eq. (5.4)²⁹:

$$\left(\frac{T}{W}\right)_{climb} = \frac{1}{\left(\frac{L}{D}\right)_{cruise}} + \frac{V_{vertical}}{V} \quad (5.4)$$

The rate of climb was selected to be 15 fps. The climb velocity is approximately 1.2 times the stall value. The climb T/W value is equal to 0.333, about 4 times larger than the cruise value. The thrust matching values obtained with Eqs. (5.3) and (5.4) must be converted back to the takeoff conditions so it can be compared properly with the statistical estimation values, as shown in Eqs. (5.5) and (5.6)²⁹:

$$\left(\frac{T}{W}\right)_{takeoff} = \left(\frac{T}{W}\right)_{cruise} \frac{W_{cruise}}{W_{takeoff}} \frac{T_{takeoff}}{T_{cruise}} \quad (5.5)^2$$

$$\left(\frac{T}{W}\right)_{takeoff} = \left(\frac{T}{W}\right)_{climb} \frac{W_{climb}}{W_{takeoff}} \frac{T_{takeoff}}{T_{climb}} \quad (5.6)$$

The weight of the aircraft as a percentage of the total weight for the different segments are the same as those used in determining the initial takeoff weight. The thrust ratios are the density percentage difference between the two mission segments. The cruise T/W was found to be 0.0838 and the climb T/W was found to be 0.326. Only the initial climb and cruise T/W were analyzed due to the second climb and cruise phases having much lower weight ratios, reducing the thrust-to-weight ratios. The statistical estimation is the largest value between the two methods, and will be used for engine sizing. An hp/W value of 0.0563 hp/lb. means an initial weight of 1165 lb. requires 66 horsepower.

5.2 WING LOADING

With the initial thrust-to-weight ratio found, the wing loading for various phases of flight can be calculated. The wing loading for climb, cruise, stall conditions, takeoff, and landing will be calculated, with the smallest value being selected as the design wing loading. It is important to note that the climb and cruise wing loadings will need to be multiplied by a ratio to make them comparable with the takeoff wing loading. The takeoff wing loading is based on a takeoff factor taken from Raymer, 85.8 for this UAV, along with the chosen power loading, and lift coefficient as shown in Eq. (5.9)²⁹:

$$C_{L_{max}} = 0.9C_{l_{max}} \quad (5.7)$$

$$C_{L_c} = \frac{C_{L_{max}}}{1.21} \quad (5.8)$$

$$\left(\frac{W}{S}\right)_{takeoff} = 85.8 \sigma C_{L_c} \frac{hp}{W} \quad (5.9)$$

The takeoff wing loading was found to be 5.18. The airfoil maximum lift coefficient used was 1.5, at a Reynolds number of 1,000,000. The stall wing loading calculation is shown in Eq. (5.10):

$$\left(\frac{W}{S}\right)_{stall} = \frac{1}{2} \rho V_{stall}^2 C_{L_{max}} \quad (5.10)$$

The stall wing loading value is 3.98, with a stall speed of 34.6 mph. The climb and cruise wing loading are shown in Eqs. (5.13) and (5.14) respectively²⁹:

$$G = \frac{V_{vertical}}{V} \quad (5.11)$$

$$q = \frac{1}{2} \rho V^2 \quad (5.12)$$

$$\left(\frac{W}{S}\right)_{climb} = \frac{\frac{T}{W} - G \pm \sqrt{\left(\frac{T}{W} - G\right)^2 - \frac{4C_{D_0}}{\pi A Re}}}{2} \quad (5.13)$$

$$\left(\frac{W}{S}\right)_{cruise} = q_{cruise} \sqrt{\pi A Re C_{D_0}} \quad (5.14)$$

The Oswald efficiency and the zero-lift drag coefficient are assumed to be 0.8 and 0.02 respectively. The cruise wing loading for segments 3 and 5 are 3.06 and 2.42. The wing loadings for climb and cruise must be ratioed up to allow for analysis when compared to the takeoff wing loading. This is done by taking the loading values and dividing by the percentage weight difference at the beginning of the segment and the takeoff weight. The wing loadings for segments 3 and 5 are 3.20 and 2.55 respectively. The wing loading for flight segment 7 was ignored as it is ratioed up to a larger number than segment 3. It is important to note that the cruise wing loading is an aerodynamic optimization, meaning it can be ignored if the wing loading produced differs from the other values. This allows for ignoring wing loading for flight segments 3 and 5 if they are much smaller than the other values.

The wing loading during climb is largely dependent on the stall speed, design T/W , and the climb gradient. The approach speed was selected to be the maximum aircraft flight speed, 45 mph, as approach speed is must be at least 1.3 times the stall speed, and the stall speed was chosen to be 34.6 mph. The climb airspeed must be at least 1.2 times the stall speed according to the FAA. The vertical velocity during climb was set to 10.2 mph (15 fps).

The wing loading during climb was found to be 32.0 after being ratioed up. It is important to note that for Eq. (5.13), the solution where the square root is subtracted is ignored. This is due to creating infeasible designs.

Landing distance, also known as the landing ground roll, starts as soon as the wheels first touchdown, and it is dependent on wing loading. Raymer says a reasonable initial guess for the landing distance is 0.3 times the square of the approach speed in knots, as shown in Eq. (5.15)²⁹:

$$d_{landing} = 0.3 V_{app}^2 \quad (5.15)$$

The approach velocity used was 39.1 kt., which is equal to 45 mph, and resulted in a landing distance of 459 ft. The landing distance for a 7° glideslope can be calculated as shown in Eq. (5.16)²⁹:

$$d_{landing} = 80 \left(\frac{W}{S} \right) \left(\frac{1}{\sigma C_{L_{max}}} \right) + 450 \quad (5.16)$$

The landing distance for the UAV should be less than 1,000 ft., but the main goal is to make sure the landing wing loading is larger than the stall wing loading. The landing wing loading was found to be 0.19, resulting in a wing loading that is not viable for design. It was found that an approach speed of 49 kt., 82.7 fps, resulted in a wing loading of 6.03, larger than the stall wing loading. This leads to a landing distance of 720.3 ft. Since the approach speed is now larger than 45 mph, the maximum velocity, a new T/W value has to be found. The new value was found to be 0.5657, which is still larger than larger than the thrust-matching value, meaning 0.5657 is the design T/W value. This means the new hp/W is 0.063. The cruise velocities will not be altered at this point, even though the maximum velocity is now larger

than 45 mph. The maximum velocity increase changed the takeoff and climb wing loadings, which are given in Table 4, with Table 3 showing the flight conditions.

Table 4. Flight Speeds

Flight Speeds	(feet per second)
Stall	50.769
Takeoff	56.1
Climb	61.2
Vertical	15
Approach	82.7

Table 5. Wing Loadings

Wing Loading	(lb./ft ²)
Stall	3.98
Takeoff	5.81
40 mph Cruise	2.55
45 mph Cruise	3.20
Climb	26.3
Landing	6.03

Table 5 shows the stall wing loading is the smallest, with the cruise wing loadings being ignored because they are optimizations. The stall wing loading can be increased by using a more accurate Reynolds number and comparing some different airfoils. This is due to the dependence of the stall wing loading on the maximum lift coefficient. Three airfoils will be compared and they are the NACA 4415, the Eppler 1210, and the USA 40B. Using the wing chord length and an airspeed of 40 mph, the Reynolds number was found to be approximately 2,500,000. This Reynolds number was then used in Xfoil to find the maximum lift coefficients for each airfoil. The Xfoil results are presented in Appendix D. These lift coefficients were then used to resize the UAV. The results are presented below.

Table 6. Airfoil Comparison

	NACA 4415	Eppler 1210	USA 40B
--	-----------	-------------	---------

Maximum C_l	1.772	2.041	1.935
W/S_{stall}	4.701	5.415	5.126
W/S_{takeoff}	6.858	7.898	7.489

Both the Eppler and USA airfoils produce stall wing loadings larger than the climb wing loading, reducing the size of the wing. The climb and cruise wing loadings are not dependent on the wing lift coefficient, so they have not changed. Moving forward, the Eppler 1210 will be the design airfoil.

5.3 REFINED INITIAL WEIGHT SIZING

Before the configuration of the aircraft can begin, it is important to use a more accurate weight sizing to properly size the wing. This is done using more accurate empty weight and fuel weight calculations. The fuel weight calculations will be done using a fixed-engine sizing method with the range of the aircraft used as the primary design factor. Range is selected so it can be varied during the aerial application process. This must be done to account for an initial weight guess changing the wing span, resulting in either a larger or smaller spray swath. If the spray swath is larger, the aircraft will have a smaller range due to covering more ground during a single pass and vice versa, as shown in Eqs. (5.17) and (5.18):

$$S = \frac{W_0}{\left(\frac{W}{S}\right)_{\min}} \quad (5.17)$$

$$b = \sqrt{ARS} \quad (5.18)$$

$$c = \frac{S}{b} \quad (5.19)$$

The taxi and takeoff, climb, descent, and landing and taxi values are based on historical values presented by Raymer and are 0.99, 0.985, 0.9925, and 0.9945 respectively. Before the

cruise segment weights are found, a new method to calculate L/D is used as shown in Eq.

(5.20)²⁹:

$$\frac{L}{D} = \frac{1}{\frac{q_{cruise} C_{D_0}}{\frac{W}{S_{cruise}}} + \frac{1}{q_{cruise} \pi A R e} \frac{W}{S_{cruise}}} \quad (5.20)$$

Once the new L/D is found, it can be plugged into Eq. (4.6) to solve the cruise segment weights. The fuel weight of segment 5 will vary based on how the gross takeoff initial weight affects the range of the aircraft. Once all of the segment fuel weights are found, they are summed and multiplied by 1.06 to find the fuel weight estimate.

Table 7. Refined Segment Fuel Weights

	Fuel Ratio	Fuel Spent	New Weight
Segment 1	1.0	14.5	1435.5
Segment 2	1.0	21.5	1414.0
Segment 3	1.0	0.6	1413.4
Segment 4	1.0	10.6	1402.8
Segment 5	1.0	1.3	1401.4
Segment 6	1.0	21.0	1380.4
Segment 7	1.0	0.6	1379.8
Segment 8	1.0	10.3	1369.4
Segment 9	1.0	7.5	1361.9
Segment Sum	0.9	88.1	
Total Fuel Weight		93.4	

The empty weight of the aircraft must be found before the weight estimate can be refined, as shown in Eq. (5.21), using parameters provided by Raymer²⁹:

$$\frac{W_e}{W_0} = 0.98 \left(1.67 W_0^{-0.14} AR^{0.07} \left(\frac{hp}{W_0} \right)^{0.1} \left(\frac{W_0}{S} \right)^{-0.1} V_{max}^{0.11} \right) \quad (5.21)$$

As Eq. (5.21) shows, the empty weight fraction estimation will vary based on the initial gross takeoff weight guess. Composites are taken into account by multiplying Eq. (5.21) by 0.95. Now that all of the weight estimation equations are known, it is possible to determine a more refined weight estimation. It is important to note that an increase in the maximum airspeed may increase the weight of the aircraft, resulting in a larger wing, despite a larger wing loading.

Table 8. Refined Weight Estimate (lb.)

W ₀ Guess (lb.)	W _f (lb.)	W _e (lb.)	W ₀ Calculated (lb.)
1000	64.5	673.0	1154.5
1250	80.5	815.4	1312.9
1400	90.2	907.9	1415.1
1450	93.4	939.6	1450.0

The refined weight estimate is 1450.0 lb. With an hp/W of 0.063, a minimum of 92 horsepower is needed. The excel sheet used to create the refined weight estimate is provided in Appendix E.

5.4 FUSELAGE AND WING SIZING

With the refined gross takeoff weight estimate, the fuselage length can be estimated as shown in Eq. (5.22), using the historical statistic data for agricultural aircraft²⁹:

$$l_{fuselage} = 4.04 W_0^{0.23} \quad (5.22)$$

The length of the fuselage was found to be 21.6 ft. With the new takeoff weight, Eqs. (5.17), (5.18), and (5.19) can be used to find the wing area, wingspan, and chord length, which are 267.8 ft.², 44.8 ft., and 6.0 ft. respectively. Since the wing is a straight wing, the mean aerodynamic chord is just the chord, with the location of the mean aerodynamic chord being half of the semispan of the wing.

5.5 TAIL SIZING

The tail will be initially sized using the tail volume coefficients, wing sizing, and fuselage sizing. According to Raymer, typical tail volume coefficients for agricultural aircraft are 0.5 and 0.04 for the horizontal and vertical tails respectively. These values are used to find the tail areas as shown in Eqs. (5.23) and (5.24):

$$S_{HT} = \frac{c_{HT} \dot{C}_w S_w}{L_{HT}} \quad (5.23)$$

$$S_{VT} = \frac{c_{VT} b_w S_w}{L_{VT}} \quad (5.24)$$

$$c_{root} = \frac{2S}{b(1+\lambda)} \quad (5.25)$$

$$c_{tip} = \lambda c_{root} \quad (5.26)$$

$$\dot{C} = \frac{2}{3} c_{root} \frac{1+\lambda+\lambda^2}{1+\lambda} \quad (5.27)$$

$$\dot{Y} = \frac{b}{6} \frac{1+2\lambda}{1+\lambda} \quad (5.28)$$

The tail arm for a front-mounted fuselage is typically around 60 percent of the fuselage length for agricultural aircraft²⁹. The values for the tail areas are presented in Table 9. With the tail areas known, Eqs. (5.18), (5.19), and (5.23)-(5.28) can be used to finish sizing the tail, with Eqs. (5.25)-(5.28) only being used on the vertical tail because it has a taper ratio. It is important to note when finding the spanwise location of the mean aerodynamic center of the vertical tail, the value obtained must be multiplied by 2 to account for the total area of the

vertical tail being half the volume if it were to be laid out flat like the wing and horizontal tail. These values are also presented in Table 9.

Table 9. Initial Tail Sizing

	Horizontal Tail	Vertical Tail
S (ft ²)	61.9	37.1
b (ft.)	15.7	7.5
c_{root} (ft.)	-	7.1
c_{tip} (ft.)	-	2.8
\hat{C} (ft.)	3.9	5.3
\hat{Y} (ft.)	3.9	3.2

The initial sizing is in between the Pacific Aerospace Cresco and the Embraer Ipanema, despite having a much lower maximum takeoff weight. This is most likely due to the minimum wing loading for this UAV being much lower than is typical for single engine general aviation. Raymer provides historical trends for the wing loading, with single engine aircraft having a wing loading of 17 lb./ft², and sailplanes having wing loadings of 6 lb./ft², both larger than the wing loading for this UAV. Nothing can be done about the stall wing loading without increasing the stall speed or using an airfoil with a much higher lift coefficient.

5.6 CONTROL SURFACE SIZING

The initial aileron, elevator, and rudder sizing will be based on historical guidelines provided by Raymer. The aerial applicator wing percentage will determine how large the aileron span can be. Based on literature, an increase in aerial applicator wing percentage

increases drift. Also, the aerial application airspeed was determined with a 65 percent aerial applicator wing percentage, which will be the percentage moving forward. This means the aileron will be approximately 30 percent of the wing span. Based on historical guidelines, the aileron chord ratio will have to be about 35 percent. The elevator and rudder will both span the entire length of the horizontal and vertical tails. The elevator will be 45 percent of the horizontal chord, and the rudder will be 40 percent of the vertical chord.

6. INITIAL LAYOUT

6.1 PROPULSION AND FUEL SYSTEM

A comparison of two engines will be used to select an appropriate engine. The selection of an engine will be heavily influenced by the weight of the engine and size of the required propeller.

Table 10. Engine Comparison

	Rotax 912 100 HP ³⁰	Lycoming O-235-C ³¹
Maximum Horsepower (hp.)	100	115
Maximum Sustained Horsepower (hp.)	95	115
RPM	5800	2800
Time Between Overhauls (hr.)	1500	2400
Compression Ratio	10.5:1	6.75:1
Weight (lb.)	124.7	245
Length (in.)	22.1	30
Width (in.)	22.7	32
Height (in.)	14.6	22.4

Before determining which engine will be selected, analysis will be done with both engines to size the propeller. This is due to the rotations per minute (rpm) of each engine potentially affecting the diameter of the propeller. The propeller diameter must be calculated to properly design a layout. When designing the propeller, there must be at least 9 in. of clearance at all altitudes. The tip of the propeller must be less than the critical Mach number

of the propeller airfoil, meaning the helical tip velocity should be less than 950 fps at sea level for a metal propeller. For this UAV, the helical tip velocity will be kept to approximately 700 fps to help eliminate noise. This will allow for easier communication between crew members. The diameter of the propeller can be calculated two different ways, and the smaller value should be used. These two methods are the statistical method, shown in Eq. (6.1), and the tip speed method, shown in Eqs. (6.2) and (6.3), as shown below²⁹:

$$D = K_p \sqrt[4]{hp} \quad (6.1)$$

$$V_{tip_s} = \frac{\pi n D}{60} \quad (6.2)$$

$$V_{tip_h} = \sqrt{V_{tip_s}^2 + V^2} \quad (6.3)$$

The statistical method diameter will vary based on the number of blades varying K_p , which has a value of 1.7, 1.6, and 1.5 for 2, 3, and 4 blades respectively. The maximum speed was chosen for analysis because that is when the tip speed will have to be the lowest, resulting in the smallest diameter propeller. Analysis with both engines and differing numbers of blades is presented in Table 11.

Table 11. Engine and Propeller Analysis

	Statistical Method						Tip Speed	
	2 blades		3 blades		4 blades			
Engine	912	O-235	912	O-235	912	O-235	912	O-235
Diameter (ft.)	5.3	5.3	4.9	4.9	4.6	4.6	2.3	4.7
V_{tip_s} (fps)	1596	771	1502	725	1408	680	695	695
V_{tip_h} (fps)	1598	775	1504	730	1411	685	700	700

The smallest diameter was found to be 2.3 feet with the Rotax engine. With a smaller propeller and less weight, the Rotax engine was selected and has a clear advantage when compared to the Lycoming engine. The main disadvantages with the Rotax engine are the

short time between overhauls and less horse power. The time between overhauls can be avoided if the UAV flies less than 1500 hours during spring, summer, and fall. If it flies less than 1500 hours during that time frame, which is a reasonable assumption, the engine can be overhauled in the winter, which would be a prudent decision anyways. The second disadvantage is somewhat mitigated because Rotax has a slightly more powerful engine that can be replace the Rotax 912. This is still a concern, because if there is a drastic weight increase further in the design process, it may be necessary to switch to a Lycoming engine. This would mean a new initial layout may have to be created. Despite the drawbacks of the Rotax engine, it will be selected due to the weight and propeller size advantages.

The selected propeller is the Sensenich 2 blade FP made from composites. This propeller was chosen due to the ability to customize the material and size. This UAV will use the tractor installation, also known as a puller, primarily due to the simplicity of the design and the effect on the weight balance. With the aircraft losing approximately 500 lb., over one-third of its weight, during the course of its mission, it makes sense to place the engine as far fore as possible to keep the aircraft stable. The engine needs to be cooled by incoming air to function properly. The area needed can be calculated as shown in Eq. (6.4)²⁹:

$$A_{cooling} = \frac{hp}{2.2 V_{climb}} \quad (6.4)$$

The engine cooling area was found to be 0.69 ft². The UAV will be using updraft cooling. This means the air entering the engine will be warmer, but updraft cooling tends to be more efficient due to a suction effect. Since this is a UAV and not a manned aircraft, there is no need to worry about hot air or an oil leak coating the windscreen. Typically, the engine needs

about 1 lb. per second for every 100 horsepower. The preliminary layout will use a ratio of A_{exit}/A_{inlet} of 0.8. The use of adjustable cowl flaps can increase this ratio to 2 or more.

The fuel tank will be a discrete fuel tank, located behind the engine. A total fuel weight of approximately 93.4 lb. corresponds to approximately 15.6 gallons of aviation gasoline. This requires approximately 2.1 ft³.

6.2 PESTICIDE DISPERSAL METHOD

The pesticide dispersal method effects drift, flight time, and the amount of pesticide needed. A comparison of the advantages and disadvantages of the conventional system, the ultra-low volume system, and an electrostatic spray system will be used to select a dispersal system.

Table 12. Conventional Spray Method³²

Advantages	Disadvantages
<ul style="list-style-type: none"> All pesticides available 	<ul style="list-style-type: none"> Waste of pesticide
	<ul style="list-style-type: none"> Drift
	<ul style="list-style-type: none"> Water needed

Table 13. Ultra-Low Volume Spray Method³²

Advantages	Disadvantages
<ul style="list-style-type: none"> No water is needed 	<ul style="list-style-type: none"> Waste of pesticide
	<ul style="list-style-type: none"> Drift
	<ul style="list-style-type: none"> Few available pesticides
	<ul style="list-style-type: none"> Uneven coverage

Table 14. Electrostatic Spray Method³²

Advantages	Disadvantages
<ul style="list-style-type: none"> Minimized drift 	<ul style="list-style-type: none"> Only applicable to foliage
<ul style="list-style-type: none"> Adheres to foliage 	<ul style="list-style-type: none"> Water needed
<ul style="list-style-type: none"> More even coverage 	<ul style="list-style-type: none"> Needs power source

Based on the advantages and disadvantages of each application method, the electrostatic sprayer was selected due to the minimized drift and the need for less pesticide

compared to the conventional sprayer. The Spectrum electrostatic spray system was chosen for the applicator. It can vary application rates from less than one gallon per acre to four gallons per acre. The size of the hopper will have to be 6.7 ft.³ to hold 50 gallons. The initial placement for the hopper will be in the wing and the wing box, with the option to be moved closer to the engine to help with stability.

6.3 AVIONICS

When sizing the avionics, it is necessary to obtain the component weights, geometries, power, and cooling requirements from the manufacturers. Until all of the avionics components are defined, the total volume of the avionics can be approximated. For single engine general aviation, avionics are typically 1 to 3% of the total empty weight, with the density of the avionics ranging from 30-45 lb./ft³. 3% and 37.5 lb./ft³ were chosen, resulting in an approximated avionics weight and volume of 28.2 lb. and 0.75 ft².

6.4 FLIGHT CONTROL SYSTEM

As with any aircraft, this UAV needs a mechanism or mechanisms to allow for controlled flight. Unlike manned aircraft, control rods and cable/pulleys systems are less feasible due to the control stick not being on the aircraft. This means that an actuator will be used to control the aircraft. Electro-Hydrostatic Actuators (EHA) are state-of-the-art and they provide more efficient flight control actuation³³. This increase in efficiency is due to the EHA returning to a dormant state, where only the control electronics are using power, after the demand is completed. As there is less power being used, a smaller power source can be used, resulting in space and weight savings, both of which are crucial to designing an efficient aircraft.

To increase the safety of the aircraft, fly-by-wire (FBW) control laws will be used to create a smaller chance of loss of life, and to provide assistance transporting over 500 lb. of flammable liquid. A crash landing of this aircraft has a much lower chance of resulting in civilian casualties, as there will be no one on the aircraft and the aircraft will be flying short distances over mostly unpopulated fields. This means the level of redundancy can be reduced. The initial state will be normal control laws, which include the basic control laws with additional features. If there are failures, the FBW system will switch to the alternate laws, which are primarily just the basic control laws. Direct control laws will only be used as a last resort. There will be no mechanical backup laws as there is no pilot on board to operate the mechanical systems. Also, the mechanical backups would take up valuable weight and space that could be utilized more effectively.

6.5 ELECTRONICS

This UAV is entirely dependent on electronics to fulfill its mission. It will need two or three cameras to fly safely and to make sure pesticides are being sprayed in the correct location. It will need a C-band radio in the 4 to 8 GHz range to communicate with the ground control station. Of the three cameras needed for this mission, two of them will need to be able to identify where pesticides have been sprayed. This will require the use of multispectral cameras. The third camera will just be a regular video camera that will be used to view above the UAV. This is to make sure that there will be no collisions when the UAV starts its climb. The camera that will monitor the spray path from the bottom of the aircraft will be the CM100 from UAV Vision. The cameras used to pilot the UAV will be the Tau 2 336, also from UAV Vision. Two cameras may be needed, one on each wing, to effectively pilot the aircraft. If that is too heavy, some thermal cameras from Microdrones would be used instead. The final

aircraft camera, that will monitor the space above the aircraft, will be a daylight camera from Microdrones. These are just some of the electronic instruments needed for the aircraft to safely conduct its mission.

6.6 WETTED AREAS

The wetted areas of the wing and tail need to be calculated to create an initial layout of the aircraft. This can be done as shown in Eq. (6.5)²⁹:

$$S_{wet} = S_{exp} \left[1.977 + 0.52 \left(\frac{t}{c} \right) \right] \quad (6.5)$$

The exposed area is the area that is not part of the fuselage. The wetted area of a long, thin body with a circular cross section can be found as shown in Eq. (6.6)²⁹:

$$S_{wet_{fuse}} = 3.4 \left(\frac{A_{top} + A_{side}}{2} \right) \quad (6.6)$$

The internal volume of the UAV can be found in a similar way, as shown in Eq. (6.7)²⁹:

$$\int \dot{v} = 3.4 \frac{A_{top} A_{side}}{4 L} \quad (6.7)$$

Vol_i

The values from Eqs. (6.5)-(6.7) are presented in Table 15.

Table 15. Wetted Area and Internal Volume

Wetted Fuselage Area (ft ² .)	293.4
Wetted Horizontal Tail Area (ft ² .)	118.2
Wetted Vertical Tail Area (ft ² .)	86.6
Wetted Wing Area (ft ² .)	551.4
Internal Fuselage Volume (ft ³ .)	293.0

6.7 CONFIGURATION

An initial aircraft layout is needed to properly analyze the aerodynamics and size the landing gear. The initial configuration will be presented, and will be used to analyze the initial center of gravity. The first step in analyzing the configuration is taking the reference and wetted areas to find the exposed areas of each component are the area exposed to the airflow, and are based on the reference areas calculated previously and in Figures 2, 3, and 4.

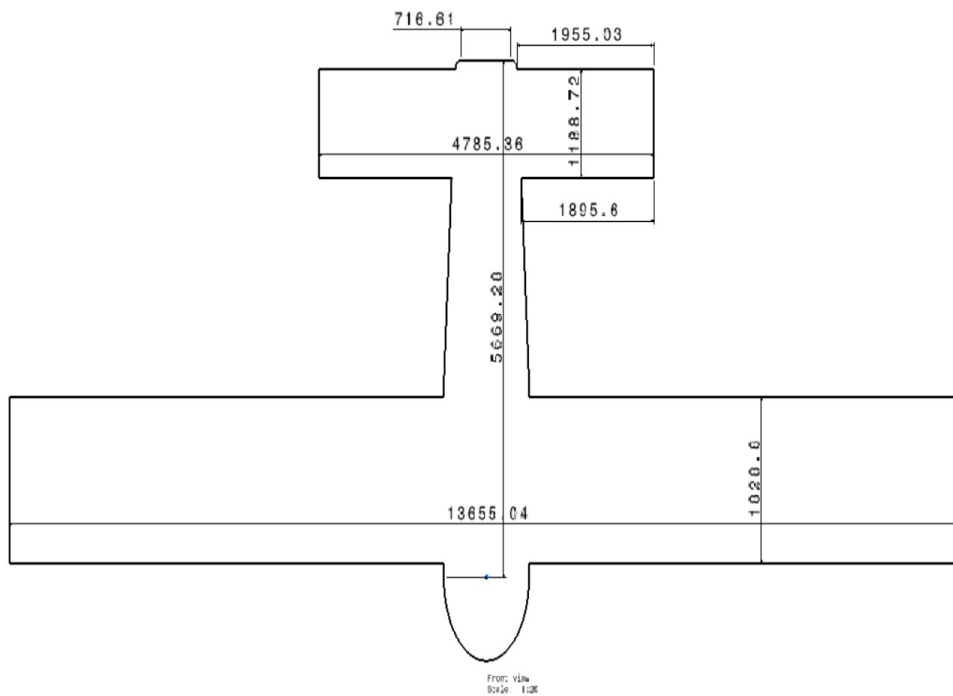


Figure 2. Top View (mm)

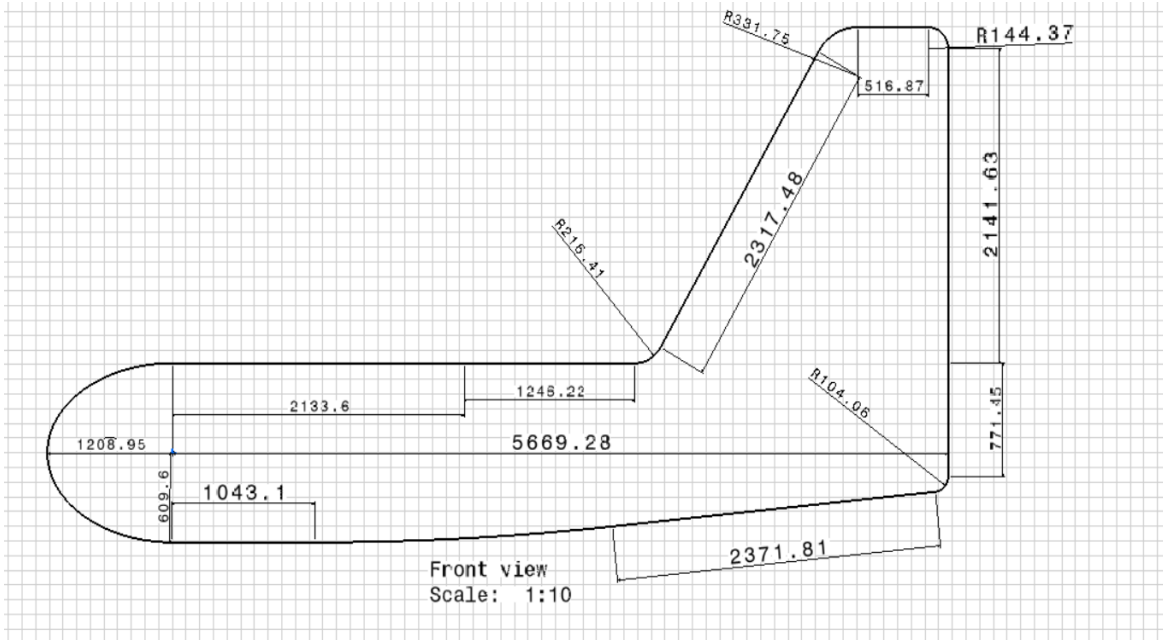


Figure 3. Side View (mm)

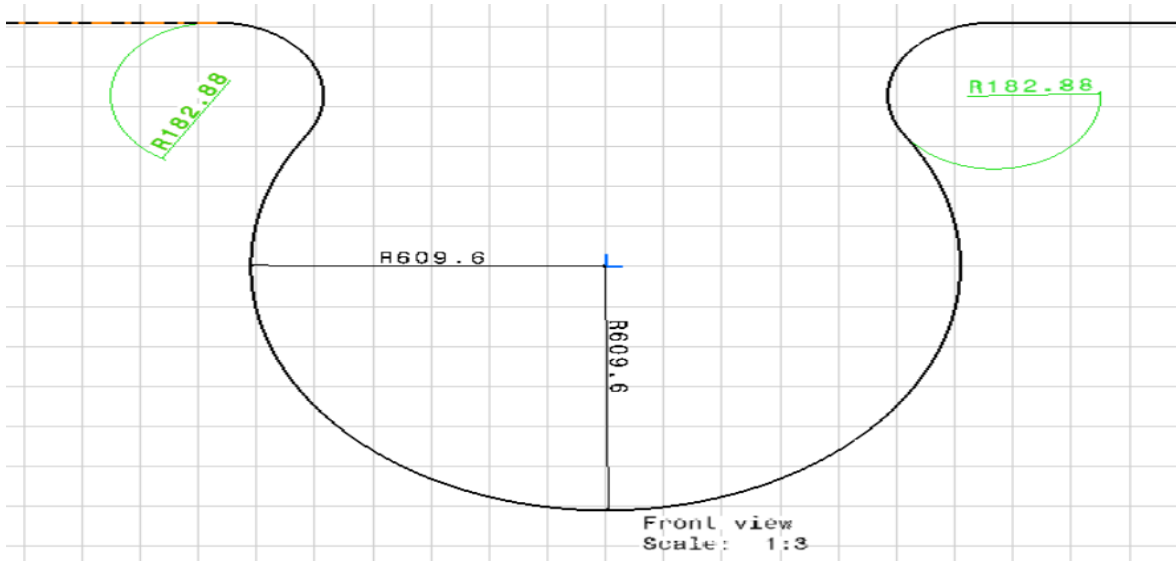


Figure 4. Wing-Fuselage Cross Section (mm)

The reference areas for the fuselage, horizontal tail, vertical tail, and wing are 62.3, 61.9, 37.1, and 267.8 ft.² respectively. The exposed areas of the vertical tail and wing are the same as the reference areas. The exposed areas of the fuselage and horizontal tail are 222.7 and 49.9 ft.² respectively. With the exposed areas calculated, the center of gravity (c.g.)

locations of every component can be calculated, and are provided in Table 16, along with the dimensions of each component.

Table 16. Component Sizes

Component	Dimensions (ft. ² or L-W-H in ft.)	C.G. location (ft.)
Fuselage	222.7	10.9
Horizontal Tail	49.9	19.3
Vertical Tail	37.1	19.3
Wing	267.8	6.83
Landing Gear	2.15	6.83
Propeller	2.3	0
Engine	1.84-1.89-1.22	1.75
Avionics	0.5-1-1	5.83
Fuel	1.5-1.5-1	5.83
Sprayer	29.2-NA-NA	9.33
Aircraft Battery	1.48-0.33-1.25	7.17
Hopper	2.83-1.45-1.63	4.15

6.8 CENTER OF GRAVITY ANALYSIS

The c.g. of the aircraft can be calculated once the fuselage, landing gear, tails, and wing weights are known. These weights can be found using Eqs. (6.8)-(6.11)²⁹:

$$W_{fuse} = 0.95 \left(1.26 S_{exp_{fuse}} \right) \quad (6.8)$$

$$W_{tail} = 0.88 \left(1.76 S_{exp_{tail}} \right) \quad (6.9)$$

$$W_{wing} = 0.9 \left(2.25 S_{exp_{wing}} \right) \quad (6.10)$$

$$W_{lg} = 0.057 W_0 \quad (6.11)$$

Table 17. Aircraft C.G. Calculation

Component	C.G. Location (ft.)	Weight (lb.)	Moment (ft.-lb.)
Fuselage	10.9	296.2	3238.4
Horizontal Tail	19.3	87.8	1697.9
Vertical Tail	19.3	65.3	1262.4
Wing	6.83	602.6	4720.0
Landing Gear	6.83	82.7	564.8
Propeller	0	4.6	0

Engine	1.75	140.6	257.8
Avionics	5.83	28.2	164.5
Fuel	5.83	93.4	544.8
Weight of Sprayer	9.33	29.2	272.5
Aircraft Battery	7.17	59.5	426.8
Hopper	4.15	417	1729.8
Aircraft	7.53	1907.0	

As Table 17 shows, the aircraft center of gravity is behind the center of lift, located at 5 ft., resulting in static instability. The location of the aircraft c.g. is not unexpected due to the large size of the wing and tails, and the lack of component weight to offset the large structural weights. The static instability can be rectified by the use of a FBW control system. Table 17 also shows that the weight of the aircraft is 457 lb. heavier than the refined weight estimate predicted. This means that the Rotax engine selected will not have enough power to takeoff, however, since a more accurate c.g. will be conducted later on in the design process, the engine will not be changed yet. If the engine needs to be changed, either the Lycoming O-235-C or O-320-A will be selected. In an effort to move the c.g. forward, an analysis was done where the length of the fuselage was altered, resulting in changes in tail size. The results are presented below in Figures 5 and 6.

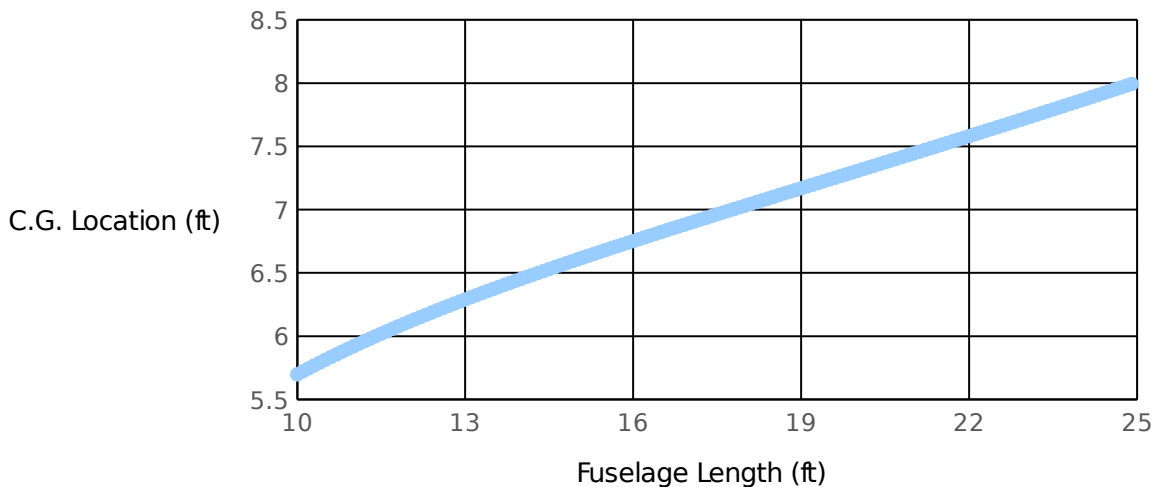


Figure 5. C.G. Location Resulting From Fuselage Length Changes

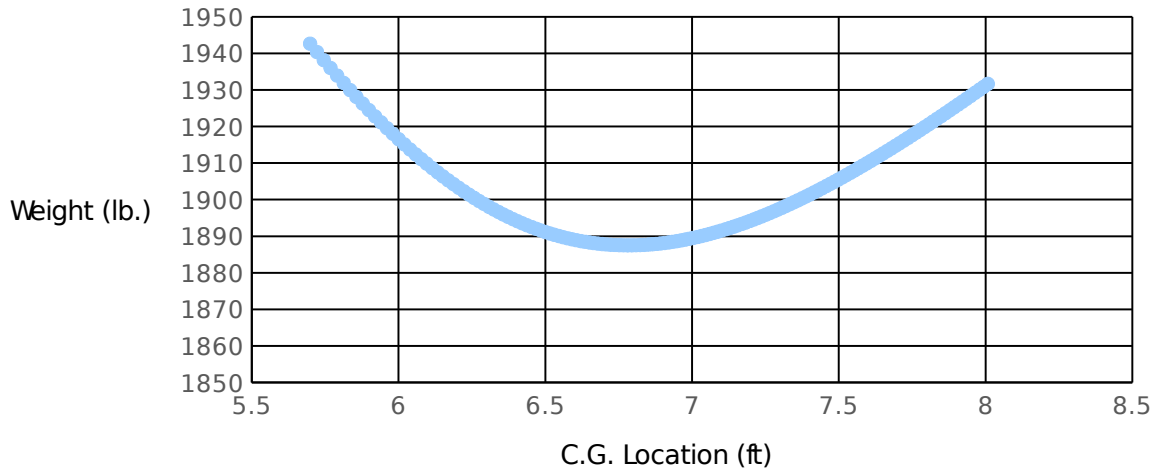


Figure 6. Weight Variance Due to C.G. Location

Figure 6 shows that although the aircraft c.g. moves quite a bit, the weight of the aircraft does not change very much. Also, the c.g. location never moves in front of the center of lift. With that in mind, the initial aircraft configuration will be used going forward. With a configuration chosen analysis was done to find the fore and aft c.g. with results presented in Table 17.

Table 18. Fore and Aft C.G.

Segment Number	Beginning C.G. (ft.)	End C.G. (ft.)
1	7.53	7.54
2	7.54	7.56
3	7.56	7.56
4	7.56	7.57
5	7.57	7.69
5	7.69	7.80
5	7.80	7.92
5	7.92	8.04
5	8.04	8.16
5	8.16	8.28
5	8.28	8.40
5	8.40	8.53
5	8.53	8.57
6	8.57	8.61
7	8.61	8.61
8	8.61	8.63

9	8.63	8.64
---	------	------

Before analyzing Table 18, it is important to note that segment 5, the crop dusting segment, was divided into 9 difference segments to show how the steady release of pesticide was affecting the c.g. Table 18 shows the fore c.g. at 7.53 ft. and the aft c.g. at 8.64 ft. It makes sense for the c.g. to move back throughout the mission as the fuel tank and hopper are both emptied.

7. LANDING GEAR

7.1 LANDING GEAR ARRANGEMENT

The landing gear will use a quadricycle gear arrangement, due to the rough runways that will be used. Unlike the taildragger and tricycle gear arrangements, the quadricycle wheels are all the same size, which will help improve stability while taking off and landing on rough runways. As there are more wheels, each wheel can be smaller, which is important because the landing gear cannot be stored in the wings, due to the use of the high wing. Another benefit of using the quadricycle, is it allows for the possibility of landing in empty fields in case of emergencies. This would not be possible with some of the other landing gear arrangements. Also, due to the rough runways, there will have to be 4 main landing gear, each with two wheels instead of each landing gear only having one wheel. The redundant wheel is to safeguard against one of the tires being rendered unusable during either takeoff or landing.

7.2 TIRE SIZING

Statistical tire sizing is used to initially size the tires, as shown in Eqs. (7.1) and (7.2)²⁹:

$$T_d = 1.51 W_w^{0.349} \quad (7.1)$$

$$T_w = 0.715 W_w^{0.312} \quad (7.2)$$

The initial tire diameter and width were found to be 9.3 and 3.6 in. respectively. As the UAV will be using potentially rough runways, the tire sizes need to be increased by 30%, resulting in a tire diameter and width of 12.1 and 4.7 in. respectively. Once the design layout is finished, Figure 7 and Eqs. (7.3)-(7.8)²⁹ are used to find the smallest tire that can handle the predicted loads. The tires are then selected from a manufacturer's catalog.

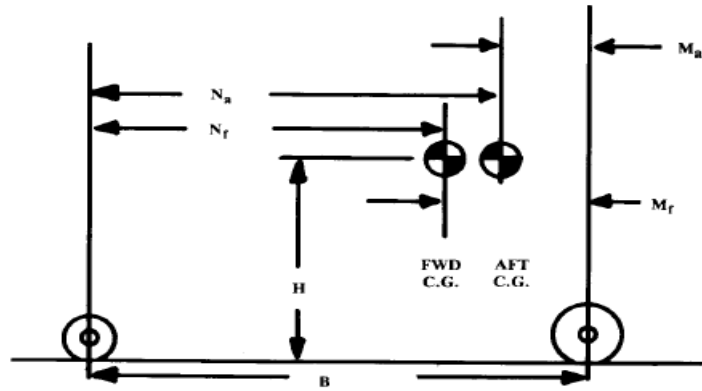


Figure 7. Landing Gear Dimensions [29]

$$S_L = W_w \frac{N_a}{B} \quad (7.3)^2$$

$$S_{L_n} = W_{nw} \frac{M_f}{B} \quad (7.4)^2$$

$$S_{l_n} = W_{nw} \frac{M_a}{B} \quad (7.5)$$

$$D_{l_n} = \frac{10 H W_{nw}}{g B} \quad (7.6)$$

The maximum static load, maximum nose static load, minimum nose static load, and dynamic nose braking load were found to be 141.3, 252.0, 194.1, 66.6 lb. With these values, the tires were chosen to be the Goodyear type III 5.00-4. These tires have a max speed of 120 mph, max load of 2200 lb., psi of 95, max width of 5.05 in., max diameter of 13.25 in., wheel diameter of 4.0 in², and rolling radius of 5.2 in³⁴. Once the tires have been selected, the internal pressure of the tire must be calculated. With the UAV using dirt runways, it is important to lower the internal pressure. Raymer provides a maximum tire pressure for a poor foundation tarmac runway of 50-70 psi, dry grass on hard soil of 45-60 psi, and hard packed sand of 40-60 psi. The maximum tire pressure will have an acceptable range of 50-60 psi as a compromise between the three previously reported tire pressure ranges. It is important to note that if the load is lower than the maximum load, the tire pressure must be proportionally reduced to keep the same tire rolling radius. The pavement contact area and tire pressure can be calculated as shown in Eqs. (7.7) and (7.8)²⁹:

$$A_p = 2.3\sqrt{wd} \left(\frac{d}{2} - R_r \right) \quad (7.7)$$

$$P_t = \frac{W_w}{A_p} \quad (7.8)$$

The pavement contact area was found to be 27.1 in.², and the tire pressure was found to be 8.8 psi, which seems low, but the value makes sense. As the pavement contact area goes up, pressure goes down as shown in Eq. (7.8). Equation (7.7) shows that as the rolling radius approaches half the diameter of the tire, the pavement contact area will decrease, and the pressure will increase. The current rolling radius isn't large relative to the half diameter of the tire, resulting in lower tire pressure. The kinetic energy absorbed by the brakes is used to size the required wheel rim diameter. This is done by finding the kinetic energy during landing, as

shown in Eq. (7.9), dividing by the number of wheels with brakes, and then using a chart provided by Raymer to find a corresponding wheel rim diameter²⁹:

$$KE_{braking} = \frac{1}{2} \frac{W_{landing}}{g} V_{stall}^2 \quad (7.9)$$

The landing weight should be the same as the initial gross takeoff weight, in case the UAV needs to land shortly after taking off. The kinetic energy absorbed by the brakes was found to be 4770.3 ft.lb/s. per brake. Each rear wheel will have a brake, standard for Western designs. This corresponds to a wheel rim diameter range of approximately 7.5 to 9 in²⁹. This is larger than the selected tire wheel rim diameter, meaning a larger tire must be chosen. It may require a specially designed wheel due to the wheel dimensions not fitting any of the Goodyear aviation tire dimensions.

7.3 GEAR SIZING AND RETRACTION

For ground steering, the nose wheels will be capable of being turned, but they will not be free to swivel. The aft wheels will not be able to turn and they will also not be free to swivel. According to Raymer, with steerable nose wheels, the rake angles should be no greater than 15° and the trail should be approximately 20% for small aircraft²⁹.

The final step in designing the landing is designing the gear retraction. Despite flying at relatively slow airspeeds, there is still a need for landing gear retraction due to the drag produced by landing gear that has not been retracted. Allowing for gear retraction will potentially increase the fuselage and fuselage drag, but with the landing gear in the fuselage, the shape of the aircraft will be much more streamlined. The landing gear will have to be either stored in the fuselage, or in pods connected to the fuselage. The pods connected to the fuselage will increase the drag much like landing gear that is not retracted would. This makes

storing the landing gear in the fuselage the only viable option. This is made easier by the fact that there are no passengers, leaving space for the landing gear in the fuselage.

The mechanism for retraction will use a sliding pivot instead of a four bar linkage. This sliding pivot has the potential to be heavier, but that is made up for with simplicity and compactness. As the landing gear will be stored in the fuselage, there will be four different landing gear bays, one for each gear. This is to minimize the volume needed to store the landing gear. There will be 1.5 feet laterally between the landing gear bays that will be used to store the aircraft battery, hopper, etc. The landing gear will connect to the fuselage at the widest possible diameter, to allow for the largest lateral distance between the landing gears.

8. AERODYNAMIC ANALYSIS

Aerodynamic analysis must be performed to properly assess the performance of this UAV. In this section, the following will be found using classical methods:

- Lift-Curve Slope
- Parasitic Drag
- Induced Drag
- Drag Polar

This analysis will be done for both cruise velocities.

8.1 LIFT-CURVE SLOPE

The lift-curve slope is needed to find an appropriate wing incidence angle, and for longitudinal stability analysis, and can be calculated as shown in Eqs. (8.1)-(8.3)²⁹:

$$\beta = \sqrt{1 - M^2} \quad (8.1)$$

$$F = 1.07 \left(1 + \frac{d}{b_w} \right)^2 \quad (8.2)$$

$$C_{L_\alpha} = \frac{2\pi AR}{2 + \sqrt{4 + \frac{AR^2 \beta^2}{\eta_{af}^2}}} \left(\frac{S_{exp}}{S_{ref}} \right) F \quad (8.3)$$

Before calculating the lift-curve slope, it is important to check that wing area ratio multiplied by the fuselage factor is less than 1, as it is unlikely that the fuselage is creating more lift than the part of the wing that is covered. As this value was found to be 1.27, it is changed to 0.98, due to account for the fuselage generating less lift than the wing. The airfoil efficiency for the Eppler 1210 is not known, so the value is approximated to be 0.95, as suggested by Raymer. The lift-curve slope was found for the cruise velocities of 40 and 45 mph. These values were found to be 4.5572 and 4.5584 per radian respectively.

8.2 PARASITIC DRAG

An important aspect of aerodynamic analysis is the calculation of the parasitic drag. As the UAV will be flying in the subsonic region, the parasitic drag will mostly be comprised of skin-friction with a small amount of separation pressure drag. The parasitic drag will be calculated two different ways. The first way is a quick equivalent skin-friction method, which will be used to check the results of the second method. The skin-friction method is presented in Eq. (8.4)²⁹:

$$C_{D_0} = C_{f_e} \frac{S_{wet}}{S_{ref}} \quad (8.4)$$

In Eq. (8.4), the equivalent skin-friction has a value of 0.0055, a value Raymer provided for a single engine aircraft. The parasitic drag found using Eq. (8.4) was 0.0113. The second method is the component buildup method. This method involves calculating the parasitic drag of each component and then summing them together to find the total parasitic drag.

The first step in finding the component parasitic drag is finding the Reynold's number for each component. When calculating the Reynold's number for each component, the characteristic length for the fuselage is the total length, while the characteristic length of the wing or tail is the mean aerodynamic chord length. Once that is done, the cutoff Reynold's number is calculated, with a skin roughness value of $0.7E^{-5}$ for smooth composites. The smaller of these Reynold's numbers is then used to calculate the turbulent skin friction. The turbulent skin friction was used, instead of the laminar skin friction, due to the likelihood of dust, pesticide, and bug buildup on every component of the aircraft. This process is shown in Eqs. (8.5)-(8.7)²⁹:

$$\Re = \frac{\rho V l}{\mu} \quad (8.5)$$

$$\Re_{cutoff} = 38.21 \left(\frac{l}{k} \right)^{1.053} \quad (8.6)$$

$$C_f = \frac{0.455}{(\log_{10} \Re)^{2.58} (1 + 0.144 M^2)^{0.65}} \quad (8.7)$$

The skin frictions are provided in Table 19.

Table 19. Skin Friction

	40 mph	45 mph
Fuselage	0.0031	0.0031
Horizontal Tail	0.0042	0.0041
Vertical Tail	0.004	0.0039
Wing	0.0039	0.0038

Once the skin-friction has been found, a form adjustment factor must be calculated. The form adjustment factor is used to take flow separation into account. Equation (8.8) is used for the wing and tails, while Eqs. (8.9) and (8.10) are used for the fuselage. With the form factor found, the component parasitic drag can be found, as shown in Eq. (8.11)²⁹:

$$FF = \left[1 + \frac{0.6}{(x/c)_m} \frac{t}{c} + 100 \left(\frac{t}{c} \right)^4 \right] [1.34 M^{0.18}] \quad (8.8)$$

$$f = \frac{l}{d} \quad (8.9)$$

$$FF_{fuse} = \left(1 + \frac{60}{f^3} + \frac{f}{400} \right) \quad (8.10)$$

$$C_{D_0} = C_f FF \frac{S_{wet}}{S_{ref_w}} \quad (8.11)$$

When calculating the parasitic drag, the wetted area is the wetted area of that component. It is important to note that the tail parasitic drags had an additional 10% added to account for gaps, and 5% was added to the total drag to account for leakage. The results are presented in Table 20.

Table 20. Parasitic Drag

	40 mph	45 mph
Fuselage	0.0048	0.0047
Horizontal Tail	0.0017	0.0017
Vertical Tail	0.001	0.0011
Wing	0.0095	0.0095
Total	0.0179	0.0179

The total parasitic drags were found to be 0.0179 for both cruise velocities, which is not unexpected due to the relatively small difference between the two velocities and the small difference between the skin frictions at both velocities. These values are also larger by a third when compared to the value predicted by Eq. (8.4).

8.3 INDUCED DRAG

Induced drag is the drag caused due to lift. Classical wing theory states that the most efficient wing has an elliptical lift distribution, and any wing without an elliptical lift

distribution will have an increase in drag. This extra drag is accounted for by calculating the Oswald efficiency factor. The Oswald efficiency factor effectively reduces the aspect ratio of the wing, and is used to calculate the drag due to lift factor as shown in Eq. (8.13)²⁹:

$$e = 1.78(1 - 0.045 AR^{0.68}) - 0.64 \quad (8.12)$$

$$K = \frac{1}{\pi A R e} \quad (8.13)$$

The Oswald efficiency was found to be 0.825, which is within the typical range of 0.7 to 0.85²⁹. The drag due to lift factor was found to be 0.0515. As the UAV will be flying close to the ground for the vital portion of the mission, it is important to investigate how ground effects alter the drag due to lift factor, as shown in Eq. (8.14)²⁹:

$$K_{effective} = \frac{33(h/b)^{1.5}}{1 + 33(h/b)^{1.5}} K \quad (8.14)$$

The ground effect will decrease the drag due to lift factor, but the amount that this value will decrease varies based on the distance between the aircraft and the ground. This is shown in Figure 8.

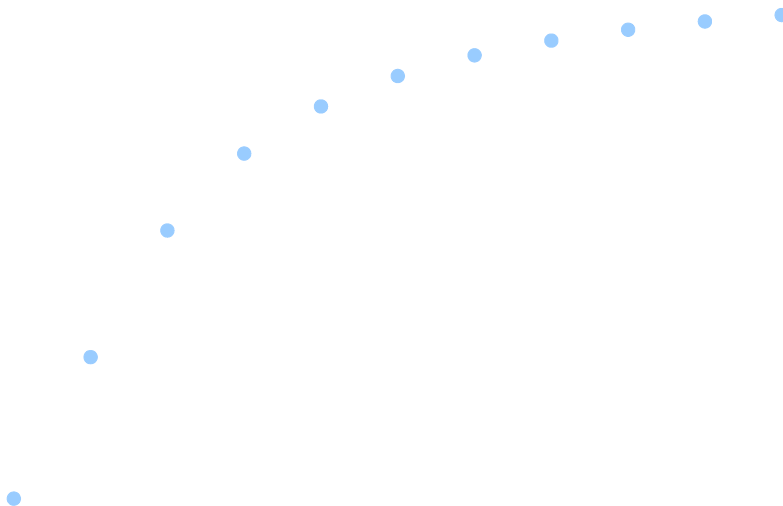


Figure 8. Ground Effects on Drag-due-to-Lift Factor

8.4 DRAG POLAR

With the aerodynamic calculations completed, the drag polar can be calculated. First, the Xfoil results, located in Appendix D, are plotted as the lift coefficient vs the angle of attack.

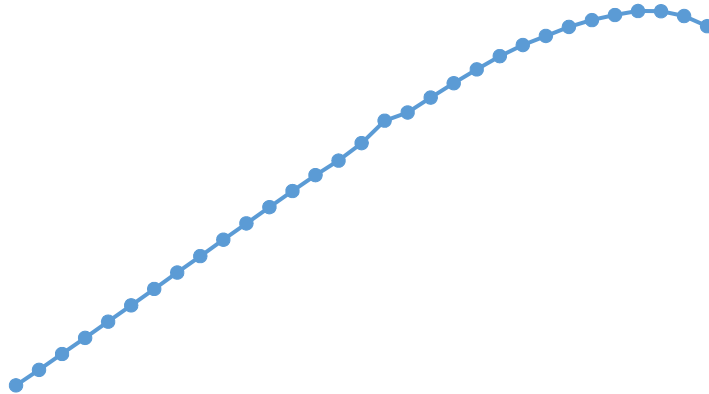


Figure 9. Lift Coefficient Curve

With this information, Eq. (8.15) can be used to plot the drag polar using the parasitic drag and the drag due lift factor:

$$C_D = C_{D_0} + K C_L^2 \quad (8.15)$$

Raymer says moderately cambered airfoils can use the uncambered drag coefficient equation.

The drag polar is presented in Figure 10.

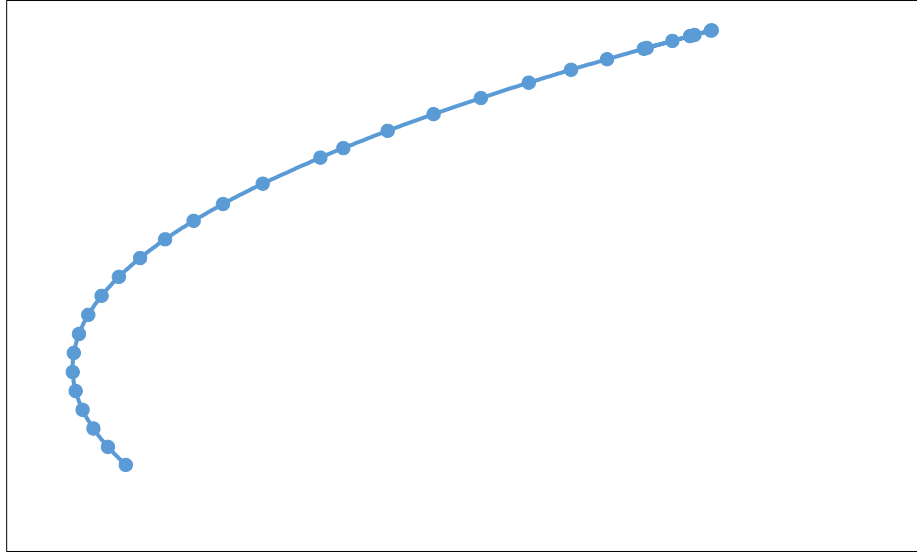


Figure 10. Drag Polar

9. PROPULSION ANALYSIS

With the aerodynamic analysis concluded, the propulsion analysis can begin. Unfortunately, the chosen propeller does not have sufficient information to analyze the propeller, leading to an incomplete analysis of the propeller, and therefore, propulsion. With that in mind, there is some propulsion analysis that can be conducted. When attempting to analyze propulsion, it is important to note that thrust and efficiency are mutually exclusive. This means increasing the thrust will unavoidably decrease the efficiency. There is a similar relationship between thrust and velocity. As the velocity increases, thrust decreases. It is also important to note that the power produced by piston engines is directly proportional to the mass flow into the intake manifold, and that propellers waste approximately 20% of the power when creating thrust, which can be exasperated by an increase in velocity²⁹. When conducting propulsion analysis, some of the important factors include the advance ratio and various coefficients, as shown in Eqs. (9.1)-(9.6)²⁹:

$$J = \frac{V}{n_{rs} D} \quad (9.1)$$

$$C_P = \frac{550 \text{ bhp}}{\rho n_{rs}^3 D^5} \quad (9.2)^2$$

$$C_T = \frac{T}{\rho n_{rs}^2 D^4} \quad (9.3)$$

$$C_S = V^5 \sqrt{\frac{\rho}{P n_{rs}^2}} \quad (9.4)$$

$$T_{ff} = \frac{550 \text{ bhp} \eta_P}{V} \quad (9.5)$$

$$T_s = \frac{C_T}{C_P} \frac{550 \text{ bhp}}{n_{rs} D} \quad (9.6)$$

These values are presented in Table 21.

Table 21. Propulsion Analysis at 40 mph

Advance Ratio (fps/lb.)	0.446
Power Coefficient	0.377
Thrust Coefficient	0.719
Speed-Power Coefficient	21105
Forward Thrust (lb.)	434
Static Thrust (lb.)	412

Unfortunately, due to the lack of test information, the propeller efficiency could not be calculated and had to be assumed at a value of 0.85. This is necessary because the propeller efficiency is required when calculating thrust, and the propeller efficiency is dependent on the thrust, resulting in a propeller efficiency of the assumed value.

The final step in propulsion analysis is calculating the miscellaneous engine drag. This miscellaneous engine drag includes the oil cooler drag, air intake drag, and various other drags, as shown in Eq. (9.7)²⁹:

$$\left(\frac{D}{q}\right)_{misc} = (2 \cdot 10^{-4}) \frac{bhp}{S_{ref}} \quad (9.7)^{29}$$

The miscellaneous engine drag was found to be $6.9E^{-5}$. This value is then added to the parasitic drag, for a total value of 0.0179 for both 40 and 45 mph.

10. STRUCTURAL ANALYSIS

When trying to select aircraft materials, it is important to look at more than just weight or cost. The initial material selection for the entire aircraft will be composites, mostly made up of carbon fiber. Composites will typically offer a large reduction in weight and excellent fatigue performance, at the expense of fabrication, repair, and cost²⁹. There are also hidden costs when manufacturing composites, such as purchasing a crane, finding enough space to operate the crane and storing composite molds. Carbon fiber helps reduce the fabrication cost, as it is easier to mold than other composites. There are also other advantages to using carbon fiber including an excellent strength-to-weight ratio, is very commonly used, and composites can have less material waste compared to other materials like metal. There are other materials that would be used in the construction of this aircraft. Boeing used a graphite-kevlar-epoxy composite on the Boeing 757 fairings and landing gear doors due to the increase in ductility²⁹.

There are some issues with composite materials. Composites tend to have problems handling concentrated loads, especially point loads. Any joints and fittings must be able to smooth these concentrated loads, or the composite will fail. Any cutout and doors can lead to

stress concentrations, meaning these cutouts and doors will need additional structure, resulting in the potential elimination of any weight savings from using composites. This will be an issue when there are 4 separate landing gear bays, a fuel tank opening, a pesticide opening, an opening for avionics and the battery, etc. The wing attachment will also require additional structure. It is also important to note that the strength of composites can be adversely affected by moisture. Some testing will need to be conducted to determine if pesticides lead to a decrease in composite strength, or worse, composite failure. If the pesticides do lead to composite degradation, then materials testing will need to be done to compare aluminum and various other composites to find the most resistant material. The composites would be too costly to continuously manufacture and repair. In any event, a coating will need to be used to prevent pesticide, moisture, and dirt from interacting with the composite, which will increase the weight²⁹.

11. WEIGHT ANALYSIS

11.1 WEIGHT CALCULATIONS

Although two previous weight estimates were performed, the design has progressed far enough to warrant a more accurate weight and c.g. analysis be conducted. Raymer provides equations that to calculate weights for most components, as shown in Eqs. (11.1)-(11.9)²⁹:

$$W_{wing} = 0.9 \left(0.036 S_w^{0.758} AR^{0.6} q^{0.006} \lambda^{0.04} \left(\frac{100t}{c} \right)^{-0.3} (N_z W_{dg})^{0.49} \right) \quad (11.1)$$

$$W_{HT} = 0.88 \left(0.016 (N_z W_{dg})^{0.419} q^{0.168} S_{HT}^{0.896} \left(\frac{100t}{c} \right)^{-0.12} AR_{HT}^{0.043} \right) \quad (11.2)$$

$$W_{VT} = 0.88 \left(0.073 (N_z W_{dg})^{0.376} q^{0.122} S_{VT}^{0.873} \left(\frac{100t}{c} \right)^{-0.49} AR_{VT}^{0.357} \lambda_{VT}^{0.039} \right) \quad (11.3)$$

$$W_{fuse} = 0.95 \left(0.052 S_f^{1.086} (N_z W_{dg})^{0.177} l_t^{-0.051} \left(\frac{l}{d} \right)^{-0.072} q^{0.241} \right) \quad (11.4)$$

$$W_{mlg} = 0.095 (N_l W_{landing})^{0.768} \left(\frac{L_m}{12} \right)^{0.409} \quad (11.5)$$

$$W_{fs} = 2.49 V_t^{0.726} N_t^{0.242} N_{en}^{0.157} \quad (11.6)$$

$$W_{fc} = 0.053 l_f^{1.536} b_w^{0.371} (N_z W_{dg} 10^{-4})^{0.8} \quad (11.7)$$

$$W_h = 0.12 W_0^{0.8} M^{0.5} \quad (11.8)$$

$$W_{elec} = 12.57 (W_{fs} + W_{av})^{0.51} \quad (11.9)$$

Table 22. Component Weight

Component	Weight (lb.)
Wing	244.9
Horizontal Tail	23.1
Vertical Tail	19.8
Fuselage	100.7
Main Landing Gear	39.4
Nose Landing Gear	39.4
Fuel System	4.3
Flight Controls	17.3
Hydraulics	1.1
Electrical	74.2

Before going further with the analysis, the Raymer weight equations for the fuselage, tails, and wing produce estimated weights that seem lower than they should be, especially when compared to the initial weight analysis conducted previously. This does not mean the more detailed calculations are incorrect, but more analysis must be done to determine if the detailed

calculations are accurate. These new calculations, Eqs. (11.10)-(11.18) will be provided by Leland Nicolai³⁵:

$$V_e = \frac{\rho}{\rho_0} V \quad (11.10)$$

$$W_{wing} = 0.8 \left(96.948 \left[\left(\frac{W_0 N_z}{10^5} \right)^{0.65} AR^{0.57} \left(\frac{S_w}{100} \right)^{0.61} \left(\frac{1+\lambda}{2 \frac{t}{c}} \right)^{0.36} \left(1 + \frac{V_e}{500} \right)^{0.5} \right]^{0.993} \right) \quad (11.11)$$

$$W_{HT} = 0.75 \left(127 \left[\left(\frac{W_0 N_z}{10^5} \right)^{0.87} \left(\frac{S_{HT}}{100} \right)^{1.2} \left(\frac{l_t}{10} \right)^{0.483} \left(\frac{b_{HT}}{t_{HR}} \right)^{0.5} \right]^{0.458} \right) \quad (11.12)$$

$$W_{VT} = 0.75 \left(98.5 \left[\left(\frac{W_0 N_z}{10^5} \right)^{0.87} \left(\frac{S_{VT}}{100} \right)^{1.2} \left(\frac{b_{VT}}{t_{VR}} \right)^{0.5} \right] \right) \quad (11.13)$$

$$W_{fuse} = 0.825 \left(200 \left[\left(\frac{W_0 N_z}{10^5} \right)^{0.286} \left(\frac{l_f}{10} \right)^{0.857} \left(\frac{2d}{10} \right) \left(\frac{V_e}{100} \right)^{0.358} \right]^{1.1} \right) \quad (11.14)$$

$$W_{lg} = 0.92 \left(0.054 (L_m)^{0.501} (W_{landing} N_l)^{0.684} \right) \quad (11.15)$$

$$W_{fs} = 2.49 F_g^{0.6} N_t^{0.2} N_{en}^{0.13} \quad (11.16)$$

$$W_{sc} = 1.08 (W_0)^{0.7} \quad (11.17)$$

$$W_{elec} = 12.57 \left(\frac{W_{fs} + W_{av}}{1000} \right)^{0.51} \quad (11.18)$$

Table 23. Comparison Component Weight

Component	Weight (lb.)	Difference (lb.)
Wing	151.2	-93.7
Horizontal Tail	35.3	12.2
Vertical Tail	2.1	-17.7
Fuselage	73.7	-27.0
Landing Gear	123	43.6

Fuel System	12.9	8.6
Hydraulics	NA	NA
Surface Controls	176.4	159.1
Electrical	2.5	-71.7

Unfortunately, the new component weight calculations produce values that are mostly lower than the Raymer values, and in some cases, improbable. With that in mind, the Raymer calculations will be used for the most part. The average of the two methods will be used for the fuel system and flight controls instead of the calculated Raymer values.

11.2 IMPROVED CENTER OF GRAVITY ANALYSIS

An improved center of gravity analysis can be conducted using the new component weights. The weights and c.g. location of each component is provided in Table 24.

Table 24. Component Weight and c.g. locations

Component	Weight (lb.)	Location (ft.)
Wing	244.9	6.5
Horizontal Tail	23.1	19
Vertical Tail	19.8	19
Fuselage	100.7	10.3
Main Landing Gear	39.4	11.5
Nose Landing Gear	39.4	4.6
Fuel System	8.6	3.8
Flight Controls	96.9	11.0
Hydraulics	1.1	11.8
Electrical	74.2	7.2

Engine	140.6	1.4
Avionics	28.2	5.8
Pesticide	417	3.8
Fuel	93.4	5.5
Weight of Sprayer	43.8	9
Propeller	4.6	-0.3
Cameras	3	3.75
Sum	1378.8	
Initial C.G.		6.6
Center of Lift		5

As Table 24 shows, the fore c.g. is 1.6 ft. behind the center of lift, creating a statically unstable aircraft. The position of the c.g. throughout the mission is provided in Appendix F. A comparison was done to see how changing the engine and moving the wing back affected the location of both the c.g. and center of lift. These changes were done in conjunction with Section 12.2 to better analyze the static pitch stability of the aircraft. Changing the engine would require a slight modification of the hopper dimensions. The results are provided in Appendix F.

Table 25. New Design Weight and c.g. location

	Weight (lb.)	Location (ft.)
Sum	1612.5	
Aft C.G.		7.12
Center of Lift		6.728

Although the new design still leaves the center of lift ahead of the c.g., the margin is reduced from 33.6 inches to less than 6 inches, and at least half of the mission now has static stability. As the design of the aircraft has been changed slightly, some component sizes have been altered and some design characteristics have changed. These changes in design are provided in Table 26, where the old and new sizes are provided.

Table 26. Changes in Design

Component	Old	New
Horizontal Tail Area (ft.)	61.9	71.4
Vertical Tail Area (ft.)	37.1	42.8
Tail Moment Arm	0.6	0.52

Engine	Rotax 912 ULS	Lycoming 0-235-F
Installed Engine Weight (lb.)	140.6	350
Propeller Diameter (ft.)	2.3	4.7
Landing Gear Length (ft.)	3.1	3.2
40 mph Parasitic Drag	0.0179	0.0183
45 mph Parasitic Drag	0.0179	0.0184

12. STABILITY AND CONTROL ANALYSIS

12.1 STABILITY CONSTANTS

Before any stability and control analysis is conducted, some constants that are used throughout this section will be found. The aft location of the c.g., the aerodynamic center of the wing, and the aerodynamic center of the horizontal tail are all divided by the wing mean chord, to simplify later equations, as shown in Eqs. (12.1)-(12.3)²⁹:

$$\dot{X}_{cg} = \frac{a_{cg}}{C} \quad (12.1)$$

$$\dot{X}_{ac_w} = \frac{w_{qc}}{C} \quad (12.2)$$

$$\dot{X}_{ac_h} = \frac{h_{qc}}{C} \quad (12.3)$$

The values of these equations were found to be 1.19, 1.12, and 2.99. The fuselage static pitch moment can be found as shown in Eq. (12.4)²⁹:

$$C_{m_{afuse}} = \frac{K_{fuse} d^2 l_f}{c S_w} \quad (12.4)$$

The fuselage static pitch moment was found to be 0.0003 radians. The downwash and downwash derivative angle are dependent on the values of Eqs. (12.5) and (12.6)²⁹:

$$r = \frac{2l_t}{b_w} \quad (12.5)$$

$$m = \frac{2z_t}{b_w} \quad (12.6)$$

These values were found to be 0.5 and 0.09. Using figures presented by Raymer, the downwash derivative was found to be approximately 0.4. The downwash can be calculated as shown in Eq. (12.7)²⁹:

$$\frac{d\alpha_h}{d\alpha} = 1 - \frac{d\epsilon}{d\alpha} \quad (12.7)$$

The value of downwash was found to be 0.6.

12.2 POWER-OFF NEUTRAL POINT

An important aspect of stability control and analysis is determining the static margin. If the c.g. is ahead of the neutral point, then the aircraft will have longitudinal stability. Typical static margin values for general aviation aircraft are larger than 10%²⁹. The neutral point must be calculated to find the static margin, as shown in Eq. (12.8)²⁹:

$$\dot{X}_{np} = \frac{C_{L_\alpha} \dot{X}_{ac_w} - C_{m_{ofuse}} + \eta_h \frac{S_{HT}}{S_w} C_{L_{ah}} \frac{d\alpha_h}{d\alpha} \dot{X}_{ac_h}}{C_{L_\alpha} + \eta_h \frac{S_{HT}}{S_w} C_{L_{ah}} \frac{d\alpha_h}{d\alpha}} \quad (12.8)$$

$$SM = -C_{L_\alpha} \left(\frac{\dot{X}_{np} \dot{C} - a_{cg}}{\dot{C}} \right) \quad (12.9)$$

$$C_{m_\alpha} = -C_{L_\alpha} SM \quad (12.10)$$

The neutral point was calculated to be at 1.3, the static margin is 0.11, and the static pitch stability is -0.52. The static pitch stability is very close to the FAR 23 recommended value provided by Nicolai³⁵. In an effort to provide a worst case scenario for static longitudinal stability, stick-free power-off neutral point analysis was conducted. Stick-free stability states that the elevator contributes nothing to the lift produced by the tail. The stick-free neutral point is typically 2 to 5% ahead of the stick-fixed neutral point²⁹. The stick-free neutral point can be calculated as shown in Eq. (12.11)²⁹:

$$\dot{X}_{np} = \frac{C_{L_{\alpha}} \dot{X}_{ac_w} - C_{m_{fuse}} + .75 \left(\eta_h \frac{S_{HT}}{S_w} C_{L_{\alpha h}} \frac{d\alpha_h}{d\alpha} \dot{X}_{ac_h} \right)}{C_{L_{\alpha}} + .75 \left(\eta_h \frac{S_{HT}}{S_w} C_{L_{\alpha h}} \frac{d\alpha_h}{d\alpha} \right)} \quad (12.11)$$

The stick-free neutral point was calculated to be at 1.26. The static margin and static pitch stability can be found using Eqs. (12.9) and (12.10) and were found to be 0.073 and -0.33. With the neutral point being moved forward, the aircraft is still statically stable. Aircraft that have static margins less than 5%, or are negative, will typically have relaxed static stability that are then dependent on a computerized flight control system to provide static longitudinal stability. The stick-free static margin is about half way to needing relaxed static stability, however, aircraft was already being designed with a computerized flight control system, allowing for the use of relaxed static stability.

12.3 TRIM ANALYSIS

With all of the previous information, it is now possible to calculate the trim needed to fly at various flight conditions. The flight condition that will be analyzed is when the aircraft

is flying at trim, with a moment of 0. The wing moment coefficient, with a value of 0.01, was found using Xfoil. The calculation of the moment is shown in Eqs. (12.12)-(12.14)²⁹:

$$\Delta\alpha_{0_L} = \frac{-.9}{1.9\pi} \frac{dC_l}{d\delta_f} K_f \delta_e \quad (12.12)$$

$$C_{L_h} = C_{L_{ah}} \left[\frac{d\alpha_h}{d\alpha} \alpha - \Delta\alpha_{0_L} \right] \quad (12.13)$$

$$C_{m_g} = C_{L_\alpha} (\dot{X}_{cg} - \dot{X}_{ac_w}) + C_{m_w} + C_{m_{fuse}} + \eta_h \frac{S_{HT}}{S_w} C_{L_h} (\dot{X}_{ac_h} - \dot{X}_{cg}) \quad (12.14)$$

The value for Eqs. (12.12), (12.13), and (12.14) were found to be $0.814 \delta_e$, $2.01\alpha + 2.73\delta_e$, and $-0.57\alpha - 1.18\delta_e$, respectively. Before a trim plot can be created to find the needed elevator deflection required to create a moment of 0, the total lift of the aircraft must be found, as shown in Eq. (12.15)²⁹:

$$C_{L_{total}} = C_{L_\alpha} \alpha + \eta_h \frac{S_{HT}}{S_w} C_{L_h} \quad (12.15)$$

The value of Eq. (12.15) was found to be $5.07\alpha + 0.66\delta_e$. The angle of attack and elevator deflection were varied to create a trim plot. The angle of attack ranged from 0 to 10°, while the elevator deflection ranged from 0 to -6°. The trim plot is presented in Figure 11.

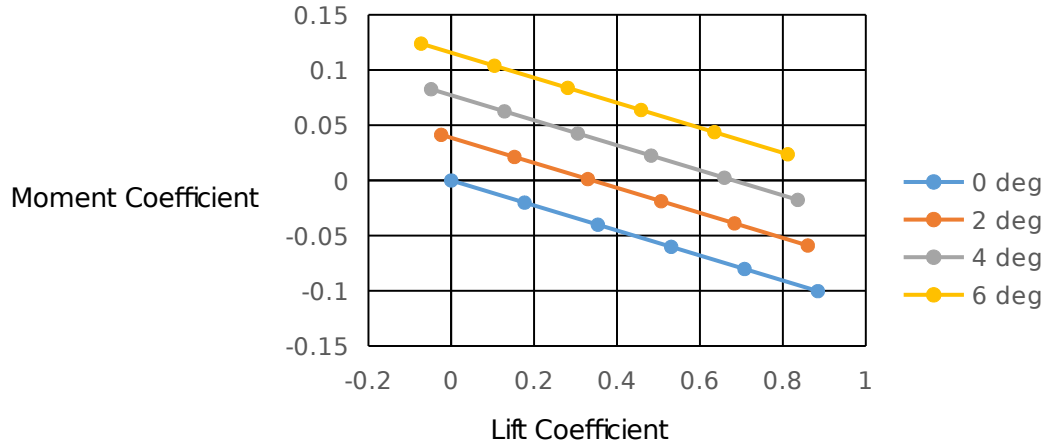


Figure 11. Trim Plot

The lift coefficient must be calculated before Figure 11 is used to find the elevator deflection, as shown in Eq. (12.16):

$$C_L = \frac{W}{qS} \quad (12.16)$$

The lift coefficient was found to be 0.614, which corresponds to an elevator deflection of approximately 3.7°. Using the elevator deflection, the trim via tail incidence was found to be 3.02°.

12.4 SURFACE SIZING

An important aspect of stability and control is designing appropriately sized horizontal and vertical tails. Although these surfaces were sized earlier, stability and control analysis will show if they need to be increased or decreased in size. The horizontal tail surface sizing is based off of the static pitch stability results presented in Section 12.2. These results show that the horizontal tail surface is appropriately sized.

The vertical surface sizing is based off of the results from the static directional stability results presented below. Both Raymer and Nicolai have recommended values for static directional stability of 0.1, but Raymer has a suggested goal of 0.05^{29,35}. The static directional stability of the fuselage can be calculated as shown in Eq. (12.17)³⁵:

$$C_{n_{\beta fus}} = -1.3 \frac{Vol}{S_{ref} b_w} \frac{h}{w} \quad (12.17)$$

The static directional stability of the fuselage was found to be -0.032. The static directional stability of the wing can be simplified, due to a lack of wing sweep, as shown in Eq. (12.18)³⁵:

$$C_{n_{\beta wing}} = C_L^2 \left(\frac{1}{4 \pi AR} \right) \quad (12.18)$$

The static directional stability of the wing was found to be 0.0038. The vertical tail static directional stability and total static directional stability can be calculated as shown in Eqs. (12.19)-(12.21)³⁵:

$$\left(1 + \frac{d\sigma}{d\beta} \right) \frac{q_{VT}}{q} = 0.724 + \frac{3.06 S'_{VS}}{S_w} + 0.4 \frac{z_w}{d} + 0.009 AR \quad (12.19)$$

$$C_{n_{\beta VT}} = c_{VT} C_{L_{\alpha VT}} \left(1 + \frac{d\sigma}{d\beta} \right) \frac{q_{VT}}{q} \quad (12.20)$$

$$C_{n_{\beta}} = C_{n_{\beta wing}} + C_{n_{\beta fus}} + C_{n_{\beta VT}} \quad (12.21)$$

The vertical tail and total static directional stability were found to be 0.17 and 0.14. The vertical tail is about a half larger than the recommended values, however, without wind tunnel data or flight data, the vertical tail will not be reduced at this time.

The static lateral stability is not directly tied to the vertical tail sizing, but Raymer suggests that the value should be negative at one half the magnitude of directional stability²⁹.

The lateral stability due to dihedral and the lateral stability of the wing can be calculated as shown in Eqs. (12.22) and (12.23)³⁵:

$$C_{l_{\beta r}} = -0.25 C_{L_{\alpha}} \Gamma \left(\frac{2(1+2\lambda)}{3(1+\lambda)} \right) \quad (12.22)$$

$$C_{l_{\beta wing}} = C_{l_{\beta basic}} + C_{l_{\beta \Delta}} + C_{l_{\beta r}} \quad (12.23)$$

The static lateral stability of the wing due to dihedral and the lateral stability of the wing were found to be -0.02 and -0.07 respectively, with a wing-fuselage static lateral stability of approximately -0.0344. The vertical tail and total lateral stability can be found as shown in Eqs. (12.24) and (12.25)³⁵:

$$C_{l_{\beta VT}} = -C_{L_{\alpha VT}} \left(1 + \frac{d\sigma}{d\beta} \right) \frac{q_{VT}}{q} \frac{S_{VT}}{S_{ref}} \frac{z_v}{b_w} \quad (12.24)$$

$$C_{l_{\beta}} = C_{l_{\beta wing}} + C_{l_{\beta VT}} + C_{l_{\beta wf}} \quad (12.25)$$

The vertical tail and total static lateral stability were found to be -0.07 and -0.17 respectively. The total static lateral stability is a little more than twice as large as Raymer recommends. Again, without any wind tunnel data or flight data, there will be no changes to the vertical design. With the stability and control analysis concluded, it is now possible to conduct performance analysis.

13. PERFORMANCE AND FLIGHT MECHANICS

13.1 STEADY LEVEL FLIGHT

Steady Level flight analysis is especially important for this mission due to the pesticide spraying during a cruise segment. Steady level flight analysis will include minimum

thrust and minimum power calculations and comparisons. The steady level flight performance will be analyzed using the 40 mph cruise conditions used when spraying pesticide. When analyzing steady level flight, it is important to note that the thrust should equal the drag, and lift should equal the weight, as shown in Eqs. (13.1) and (13.2)²⁹:

$$T = D = q S_w (C_{D_0} + K C_L^2) \quad (13.1)$$

$$L = W = q S_w C_L \quad (13.2)$$

The thrust and drag were found to be 40.2 lb., and the lift was found to be 653.1 lb. As the lift value is approximately one-third of the weight, the aircraft is not producing enough lift.

The rest of the performance analysis will be conducted before the redesign for comparison purposes and to see if there are other issues. The velocity and thrust-to-weight ratio for steady level flight are shown in Eqs. (13.3) and (13.4)²⁹:

$$V = \sqrt{\frac{2 W}{\rho C_L S}} \quad (13.3)$$

$$\frac{T}{W} = \frac{1}{L/D} = \frac{q C_{D_0}}{W/S} + \frac{W}{S} \frac{K}{q} \quad (13.4)$$

The velocity and thrust-to-weight ratio are 92.2 fps and 0.13 respectively. The velocity is about 34 fps higher than the current flight conditions, meaning the aircraft is not flying fast enough. A redesign would be needed as the steady level flight velocity is larger than the maximum velocity used to size the wing. This thrust to weight ratio is not dissimilar to T/W ratios calculated previously for level flight.

The minimum thrust for level flight conditions are the same conditions that will maximize the lift-to-drag ratio²⁹. This is due to the relationship between thrust and drag

during steady level flight. The velocity, lift coefficient, and drag can be found as shown in Eqs. (13.5)-(13.7)²⁹:

$$V_{min_T} = \sqrt{\frac{2W}{\rho S} \sqrt{\frac{K}{C_{D_0}}}} \quad (13.5)$$

$$C_{L_{min_T}} = \sqrt{\frac{C_{D_0}}{K}} \quad (13.6)$$

$$D_{min_T} = q S_w (2 C_{D_0}) \quad (13.7)$$

The velocity, lift coefficient, and drag at minimum thrust are 29.8 fps, 0.5977, and 39.1 lb. respectively. The minimum lift coefficient is the optimal lift coefficient and is only dependent on aerodynamic parameters²⁹. This means that the aircraft can fly at the optimal lift coefficient by varying the velocity or air density.

When analyzing the minimum power during steady level flight, it is important to note that the minimum power and minimum thrust conditions are not the same. This is due to power being drag times velocity instead of just drag. Power can be calculated as shown in Eq. (13.8)²⁹:

$$P = DV \quad (13.8)$$

The power was found to be 22 hp. The velocity, lift coefficient, and drag can be calculated as shown in Eqs. (13.9)-(13.11)²⁹:

$$V_{min_P} = \sqrt{\frac{2W}{\rho S} \sqrt{\frac{K}{3C_{D_0}}}} \quad (13.9)$$

$$C_{L_{min_P}} = \sqrt{\frac{3C_{D_0}}{K}} \quad (13.10)$$

$$D_{min_p} = q S_w (4 C_{D_0}) \quad (13.11)$$

The minimum power velocity, lift coefficient, and drag were found to be 22.7 fps, 1.04, and 78.3 lb. respectively. The level turning flight turn rate can be calculated as shown in Eq.

(13.12)²⁹:

$$\dot{\phi} = \frac{g \sqrt{N_e^2 - 1}}{V} 57.3 \quad (13.12)$$

The turn rate was found to be vary between 0 and 17.2°, depending on the load factor.

Before moving on from steady level flight, flight performance with respect to range will be discussed. Typically when trying to maximize range, the lift coefficient will stay the same throughout cruise with other flight parameters changing to allow for a constant lift coefficient. This is not possible for this mission as the cruise velocities will be held constant. This means that the dynamic pressure must decrease due to a decrease in air density resulting from an increase in altitude, if range maximization is important. This type of maneuver is not possible due to the objectives of this mission. This means that range will not be optimized.

13.2 STEADY CLIMB AND DESCENDING

There are two different climb conditions that must be calculated to properly assess the climb characteristics of an aircraft. The best rate of climb provides the maximum vertical velocity while the best angle of climb maximizes the angle of climb by slightly reducing the vertical velocity by increasing the horizontal distance²⁹. The two different best of cases are related and can be found by first calculating the best rate of climb vertical velocity as shown in Eq. (13.13)²⁹:

$$V_{v_{rate}} = \frac{550 \text{ bhp } \eta_P}{W} - \frac{DV}{W} \quad (13.13)$$

The vertical velocity was found to be 25.5 fps. The best angle of climb has a vertical velocity of approximately 90 percent of the best rate of climb²⁹. The climb velocity must be calculated, typically 1.2 times the stall velocity, to find the best angle of climb. The climb velocity and best angle of climb can be calculated as shown in Eqs. (13.14) and (13.15)²⁹:

$$V_{climb} = 1.2 \sqrt{\frac{2Wg}{\rho S C_{L_{stall}}}} \quad (13.14)$$

$$\gamma_{angle} = \sin^{-1} \left(\frac{0.9 V_{v_{rate}}}{V_{climb}} \right) \quad (13.15)$$

The climb velocity and best angle of climb were found to be 64.0 fps and 21.1°. During the calculation of the best climb velocity, the stall velocity was found to be 53.3 fps, which is smaller than the steady level flight velocity.

13.3 GLIDING FLIGHT

The gliding flight analysis presented below is not intended to maximize gliding range, but is intended to determine the maximum gliding distance if the engine were to fail. The glide ratio has the direction reversed from the climb angle and can be calculated as shown in Eq. (13.16)²⁹:

$$\frac{L}{D} = \frac{1}{\tan \gamma} \quad (13.16)$$

The glide ratio was found to be 2.6. The minimum sink rate lift-to-drag ratio, velocity, lift coefficient, and drag coefficient can be calculated as shown in Eqs. (13.17)-(13.20)²⁹:

$$\left(\frac{L}{D}\right)_{min} = \sqrt{\frac{3\pi A R e}{16 C_{D_0}}} \quad (13.17)$$

$$V_{min_{sink}} = \sqrt{\frac{2}{\rho} \frac{W}{S} \sqrt{\frac{K}{3 C_{D_0}}}} \quad (13.18)$$

$$C_{L_{min_{sink}}} = \sqrt{\frac{3 C_{D_0}}{K}} \quad (13.19)$$

$$C_{D_{min_{sink}}} = \frac{C_{L_{min_{sink}}}}{\left(\frac{L}{D}\right)_{min}} \quad (13.20)$$

The lift-to-drag ratio, velocity, and lift coefficient were found to be 14.1, 22.8 fps, 1.04, and 0.07. With the minimum sink lift-to-drag ratio and lift coefficient, the vertical velocity can be calculated, as shown in Eq. (13.21)²⁹:

$$V_{v_{glide}} = \sqrt{\frac{W}{S} \frac{2}{\rho (C_L^3 / C_D^2)}} \quad (13.21)$$

The vertical velocity was found to be 1.6 fps, which corresponds to a glide time of 188 s. from a cruise of 300 ft. This means the minimum sink vertical velocity will produce a glide distance of 12375 ft. if flying at the cruise maximum of 45 mph.

13.4 TAKEOFF ANALYSIS

Takeoff analysis is divided into four different components: ground roll, rotate, transition to climb, and climb. To calculate the ground roll distance, the thrust and aerodynamic components must be found first in Eqs. (13.22) and (13.23) and then used as shown in Eq. (13.24)²⁹:

$$K_T = \frac{T}{W} - \mu_r \quad (13.22)$$

$$K_A = \frac{\rho}{2(W/S)} (\mu_r C_L - C_{D_0} - K C_L^2) \quad (13.23)$$

$$D_G = \frac{1}{2g K_A} \ln \left(\frac{K_T + K_A V_f^2}{K_T + K_A V_i^2} \right) \quad (13.24)$$

The thrust and aerodynamic components were found to be 0.53 and -2.2E-4. The takeoff distance requirement is 500 ft. and the ground roll distance was found to be 132.1 ft., meaning the calculated ground roll distance is much low than should be expected. As this is a small aircraft, Raymer states that the rotate distance is approximately the same as the takeoff velocity, which is 1.1 times the stall velocity. This corresponds to a rotate segment distance of 53.3 ft. The radius of the transition arc must be calculated to find the transition distance as shown in Eq. (13.25)²⁹:

$$R_T = \frac{V_{TR}^2}{0.2g} \quad (13.25)$$

The transition arc radius was found to be 583.4ft. With the transition arc radius and climb angle, it is possible to calculate the height of the transition takeoff segment, as shown in Eq. (13.26)²⁹:

$$h_{TR} = R_T (1 - \cos \gamma_{climb}) \quad (13.26)$$

The height of the aircraft was found to be 40.2, which is less than the 50 ft. clearance height needed for civil aircraft. This radius can be used to find the horizontal distance of the transition segment, as shown in Eq. (13.27)²⁹:

$$D_{TR} = R_T \sin(\gamma_{climb}) \quad (13.27)$$

The transition segment distance was found to be 212.9 ft. As the obstacle was not able to clear the obstacle during the transition segment, the horizontal distance for climb must be found as shown in Eq. (13.28)²⁹:

$$D_C = \frac{h_{obstacle} - h_{TR}}{\tan(\gamma_{climb})} \quad (13.28)$$

The horizontal climb distance was found to be 25.0 ft. The total takeoff distance is shown in Eq. (13.29)²⁹:

$$D_i = D_G + D_R + D_{TR} + D_C \quad (13.29)$$

The total takeoff distance was found to be 466.2 ft.

13.5 LANDING ANALYSIS

Landing analysis is very similar to takeoff analysis except in reverse, however, unlike with the takeoff analysis, only the ground roll distance will be calculated. The requirements state that the ground roll distance must be less than 1,000 ft. The landing ground roll distance can be calculated by using Eq. (13.24) and modifying it so that the final velocity is 0, instead of the initial. The landing ground roll distance was found to be 157.6 ft. This distance is about 600 ft. smaller than the distance predicted by the landing wing loading, similarly to the takeoff landing distance.

14. DESIGN REVIEW

As the current design cannot satisfy its current requirements, due to a lack of lift, a redesign should be conducted. The current design flaws seem too large to solve with just trade studies, so the design requirements, maximum speed in particular, will be altered to see if there is a plausible design for the given requirements. The cruise speeds will be doubled, to 80 and 90 mph, in an attempt to find a design that can more effectively satisfy the requirements. This large jump is used instead of a smaller increment because it will be more prudent to find a design that works and then consider reducing the cruise speeds than making smaller incremental iterations in an attempt to reach a cruise speed that will satisfy the requirements. If the requirements are satisfied, trade studies will be performed in an attempt to improve the design.

15. REDESIGN INITIAL SIZING

15.1 THRUST-TO-WEIGHT RATIO

The redesign analysis will start with the thrust-to-weight ratio as it is the first analysis that will have an impact on the final design. The maximum speed has been increased to 90 mph, and is the velocity that will be used in analysis. The process will be the same as the previous section and a comparison will be done between the old and new values presented in Table 27.

Table 27. Thrust-to-weight ratio

	Old Values	New Values
T/W	0.566	0.448
hp/W	0.063	0.0796

The power-to-weight ratio of the new design is larger than the old design, which is to be expected. The power-to-weight ratio is also much closer to the typical agricultural power-to-

weight ratio, which is 0.09 hp/lb. The new T/W is lower than the previous value, which is due to the fact that increasing velocity decreases thrust.

15.2 WING LOADING

Before discussing the changes in wing loading values, it is important to remember the previous design considered cruise wing loadings to be aerodynamic optimizations, whereas the other values are mandatory minimums. Unlike the previous design, this design will consider the all wing loading values to be mandatory minimums.

Table 28. Wing Loading

Wing Loadings	Old Values (lb./ft ²)	New Values (lb./ft ²)
Stall	5.42	10.5
Takeoff	7.90	10.2
Spraying Cruise	2.55	10.2
Maximum Cruise	3.2	12.4
Climb	26.3	42.0
Landing	6.03	9.94
Wing Loading Used	5.42	9.94

The landing wing loading is the lowest with 9.94 lb./ft². This is more in line with home built aircraft, with typical wing loadings around 11, whereas the previous wing loading was similar to that of sailplanes, with typical wing loadings around 6¹. The wing loading is still lower than the general aviation wing loading of 17. The velocities for each stage of flight are presented in Table 29.

Table 29. Velocities

	Old Values (fps)	New Values (fps)
Stall	50.8	70
Takeoff	56.1	77
Spraying Cruise	58.7	117.3

Maximum Cruise	66	132
Climb	61.2	84
Approach Speed	82.7	100

As Table 29 shows, the approach speed is no longer the largest velocity, which should help generate more lift during cruise.

15.3 WEIGHT ESTIMATION

With changes to the power-to-weight ratio, wing loading, and maximum velocity, the estimated weight will change. Before analysis is done, it is impossible to say how it will change. The results are presented in Table 30.

Table 30. Weight Estimate

	Old Values	New Values
Weight (lb.)	1450.0	1487.1
Horsepower Needed (hp.)	92	119

The weight has not changed very much between the two designs. This is due to a smaller wing loading negating the increase in weight due to a larger maximum velocity and thrust-to-weight ratio. The lack of a large weight difference means the fuselage will have approximately the same length, allowing for the layout to stay about the same. This will be discussed further in Section 15.5.

15.4 INITIAL SIZING

With the large changes to the wing loading, the wing area will be close to half of the initial design, which means smaller vertical and horizontal tails. This will have a large effect on subsequent analysis including the center of gravity, parasitic drag, performance, etc. The taper ratios, tail volume coefficients, initial tail moment arms will all be the same as the first

initial sizing values. These effects will be discussed later on. The changes for initial sizing are presented in Table 31.

Table 31. Initial Sizing

	Old Values	New Values
Fuselage Length (ft.)	21.6	21.7
Tail Moment Arm	13.0	13.0
Wing Area (ft ² .)	267.8	149.6
Wing Span (ft.)	44.8	33.5
Wing Chord (ft.)	6.0	4.5
Horizontal Tail Area (ft ² .)	61.9	25.7
Horizontal Tail Span (ft.)	15.7	10.1
Horizontal Tail Chord (ft.)	3.9	2.5
Vertical Tail Area (ft ² .)	37.1	15.4
Vertical Tail Span (ft.)	7.5	4.8
Vertical Tail Root Chord (ft.)	7.1	4.6
Vertical Tail Tip Chord (ft.)	2.8	1.8
Vertical Tail \bar{C} (ft.)	5.3	3.4
Vertical Tail \bar{Y} (ft.)	3.2	2.1

As can be expected, a minor estimated weight change and a large increase in minimum wing loading causes the wing area to reduce significantly. This reduction in wing area also causes the tail areas to be reduced significantly as well. This is a positive development as the previous design had an issue with structural weight, and a reduction in wing and tail areas will lead to less structural weight. Furthermore, the reduction in wing and tail areas mean the control surfaces will be reduced, as will be shown in Section 16.3.

15.5 PROPULSION AND FUEL SYSTEM

Based on the horsepower needed from Table 3, the Lycoming O-235-F will be the selected engine. This engine has a maximum horsepower of 125, which may mean a more powerful engine will be needed once the weight analysis is conducted. This will not affect the layout very much as the Lycoming O-320-A has proximately the same dimensions and an additional 25 hp., while only being about 25 pounds heavier. The propeller will have to be

resized to account for the increase in maximum speed, and the results are presented in Table 32.

Table 32. Propeller Sizing

	Old Values	O-235-F	O-320-A
Diameter (ft.)	4.7	4.7	4.9
V_{tip_s} (fps)	695	687	687
V_{tip_n} (fps)	700	700	700

Table 32 shows that there is no change in the diameter of the propeller, which is not unexpected as the maximum velocity of the aircraft only increased by 50 fps while the tip of the propeller is traveling well over 650 fps. If the Lycoming O-320-A needed to be used instead, the propeller diameter would increase to 4.9, due the O-320-A have fewer rotations per minute.

15.6 WETTED AREAS

The wetted areas of the new fuselage, tails, and wing are presented in Table 33.

Table 33. Wetted Areas

	Old Wetted Area (ft ² .)	New Wetted Area (ft ² .)
Fuselage	293.4	294.5
Horizontal Tail	118.2	36.9
Vertical Tail	86.6	31.2
Wing	551.4	308.0

1 ft³. was added to the internal volume of the fuselage for new design as it is approximately the same, which means the new internal volume is 294 ft³.

15.7 C.G. ANALYSIS

When performing the c.g. analysis, the detailed weight calculations will be used to create a much more accurate estimation of the weight. The locations of the internal components will be the same as the previous design as a result of having fuselage sizes that

are approximately the same. The weight of the sprayer was increased as a precaution, as the previous estimate seemed too low. The c.g. analysis is presented in Table 34.

Table 34. C.G. Analysis

Component	Weight (lb.)	Location (ft.)
Wing	161	7.5
Horizontal Tail	13.9	20
Vertical Tail	11.2	20
Fuselage	149.8	10.4
Main Landing Gear	47.7	11.575
Nose Landing Gear	47.7	4.575
Fuel System	8.7	3.8
Flight Controls	97.8	11
Hydraulics	1.4	11.8
Electrical	74.2	7.2
Engine	350	1.49
Avionics	30.2	5.8
Pesticide	417	3.8
Fuel	96.2	5.5
Weight of Sprayer	100	9
Propeller	9.2	-0.33333333
Cameras	3	3.75
Sum	1619.0	
Aft C.G.		6.94
Center of Lift		6.375

As Table 34 shows, the initial c.g. is ahead the center of gravity, like the previous design. As the aerodynamic and stability analysis has not been conducted yet, the center of gravity will

not prompt a change in design. Unfortunately, the increase in weight means the current engine no longer provides enough horsepower, as the Lycoming O-235-F provides 125 hp. and the aircraft requires 124 hp. This means the engine will be switched to the Lycoming O320-A.

Table 35. Aircraft changes due to Engine Alteration

	Lycoming O-235-F	Lycoming O-320-A
Engine Weight	350	385
Total Weight	1619.0	1654.0
Aft C.G.	6.94	6.78

As expected, a heavier engine moved the aft c.g. forward. Once the aerodynamic and stability analysis has been conducted, the center of gravity will be readdressed. The center of gravity for each segment is in Appendix G.

15.8 LANDING GEAR

With an accurate c.g. analysis presented in the previous section, it is possible to select and analyze the tires and landing gear. The results are presented in Table 36.

Table 36. Landing Gear

	Old Values	New Values
Selected Tire	Goodyear type III 5.00-4	Goodyear type III 5.00-4
Tire Diameter (in.)	12.5	12.6
Tire Width (in.)	4.9	4.9
Maximum Tire Load (lb.)	213.1	241
Pavement Contact Area (in ²)	18.9	20.1
Tire Pressure (psi)	10.7	10.3
Kinetic Energy Braking (ft. lb./s)	4033.6	7865.5
Wheel Rim Diameter Range (in.)	7.5 to 9	7.5 to 9

The two designs have similar landing gear values, the same selected tires, and the same tire problems. The values are similar due to the similar weights. The selected tires weren't changed for the same reason, however, the selected tire does not fit the wheel rim diameter

range provided by Raymer, meaning more analysis must be done. It may also be necessary to design a tire from scratch to fit all of the necessary requirements.

16. REDESIGN ANALYSIS

16.1 AERODYNAMICS

With the initial design complete, the in-depth analysis of the design can begin, starting with the aerodynamics. The results presented below will only compare the spray cruise results as there is a minimal difference between the spray results and the maximum cruise results. The comparison between the designs is presented in Table 37.

Table 37. Redesign Aerodynamics

	Old Values	New Values
Wing Lift-Curve Slope	4.56	4.57
Horizontal Tail Lift-Curve Slope	3.35	3.71
Vertical Tail Lift-Curve Slope	2.78	2.78
Fuselage Parasitic Drag	0.0048	0.0078
Horizontal Tail Parasitic Drag	0.0019	0.0011
Vertical Tail Parasitic Drag	0.0012	0.0009
Wing Parasitic Drag	0.0095	0.01
Total Parasitic Drag	0.0183	0.021

Table 37 shows these aerodynamic values to be similar with the exception of the fuselage and horizontal tail parasitic drag. The large fuselage parasitic drag difference is due to the velocity increasing by a large amount with no other changes to offset the increase in velocity. The wing and tails are also experiencing a greater velocity with the new design, however, they also have large area reductions that offset the increase in velocity. This large offset in area is shown with the horizontal tail parasitic drag. The Oswald efficiency and drag due to lift factor are the same as the previous design due to their dependence only on wing

characteristics which have not changed from the previous design. A drag polar comparison is presented below.

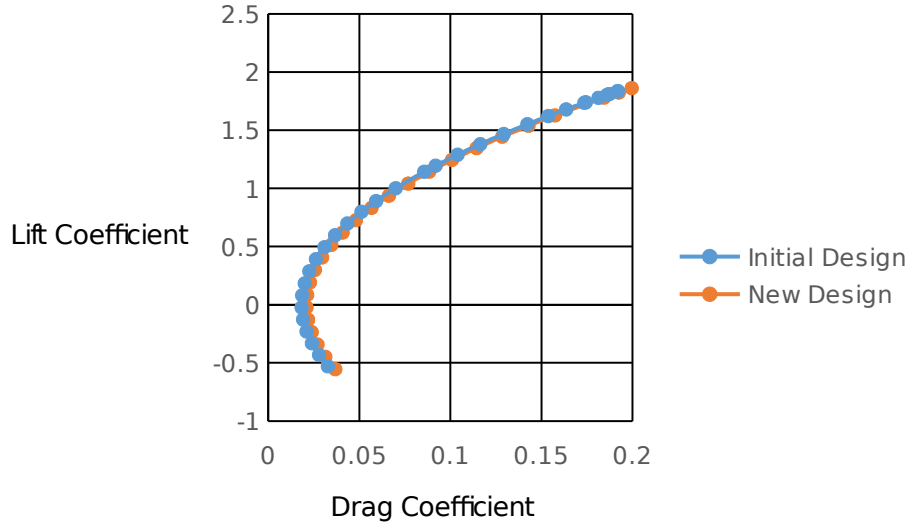


Figure 12. Drag Polar Comparison

Figure 12 shows the drag polar for the two designs being fairly similar, with slightly more drag for the new design, which is to be expected with a larger parasitic drag and the same drag due to lift factor.

16.2 PROPULSION

The propulsion analysis will be conducted in the same manner as the first design. The comparison between the results is presented below.

Table 38. Propulsion Comparison

	Old Values	New Values
Advance Ratio	0.446	0.975
Power Coefficient	0.377	0.103
Thrust Coefficient	0.719	0.0897
Speed Power Coefficient	21105	2171400
Forward Thrust	434	260
Static Thrust	412	247

The larger advance ratio means that the new design will move farther with one turn of the propeller. The much larger speed power coefficient is related to the larger advance ratio. The thrust coefficient to power coefficient ratio decreased with the new design, from 2 to 0.87. This ratio is about half of the value expected by Raymer, whereas the previous design was about 4 times the expected ratio²⁹. The propeller efficiency is assumed to 0.85, just like it was for the previous design.

16.3 STABILITY AND CONTROL ANALYSIS

The stability and control analysis will use the same methods as discussed previously. The initial design the static margin was found to be 0.053 and a static pitch stability of -0.24, both of which show that the aircraft has static pitch stability. As the aircraft is stable during the last segments of the mission, no change in design is required. The trim plot and comparisons to previous design are provided below.

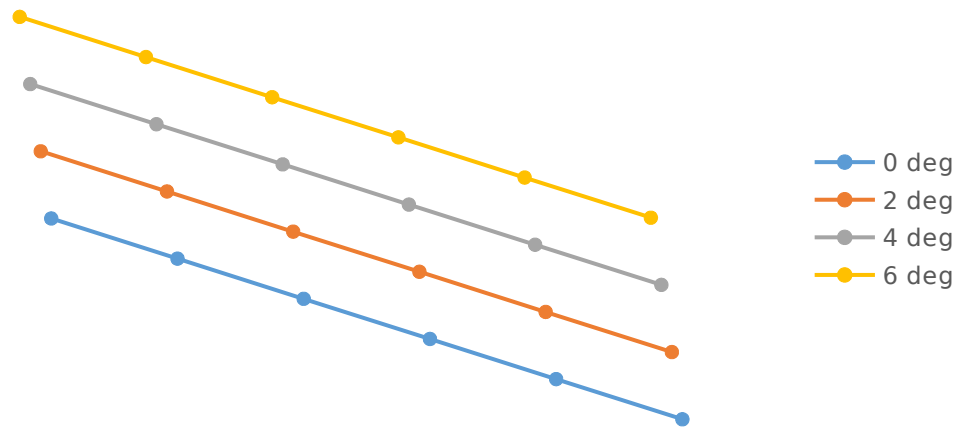


Figure 13. Redesign Trim Plot

Table 39. Stability and Control Analysis

	Old Values	New Values
Power Off Neutral Point Static Margin	0.019	0.12
Power Off Neutral Point Static Pitch Stability	-0.086	-0.55
Stick Free Power Off Neutral Point Static Margin	-0.0015	0.07

Stick Free Power Off Neutral Point Static Pitch Stability	0.007	-0.032
Trim Lift Coefficient	.614	0.623
Trim Elevator Deflection	3.7°	4.1
Static Directional Stability	0.14	0.086
Static Lateral Stability	-0.17	-0.15

The new stability and control values show the new design maintaining static pitch stability even when performing stick free analysis. The trim lift coefficients are fairly similar, and the new design has a smaller trim elevator deflection. The new design has a static directional stability value closer to the value recommended by Raymer and Nicolai, however, the static lateral stability is about four times the recommended value. With the stability and control analysis showing a stable aircraft, the size of the control surfaces is provided below.

Table 40. Control Surface Sizing

	Old Values	New Values
Aileron Area (ft ² .)	29.1	16.3
Elevator Area (ft ² .)	32.1	11.6
Rudder Area (ft ² .)	17.1	6.2

The elevator and rudder both span the entire distance of the horizontal and vertical tails. As can be expected, the control surface sizes for the new design are much smaller.

16.4 PERFORMANCE

With the stability and control analysis done, the performance of the aircraft can be calculated to see if the changes to the design have rectified the lack of lift. Before presenting all of the performance numbers for this design, it is important to note that the design was not able to generate enough lift at 80 mph (117.3 fps), resulting in the spray cruise velocity being increased to 84.5 mph (124 fps) to generate enough lift. The performance comparisons are presented below.

Table 41. Performance Comparison

	Old Values	New Values

Lift (lb.)	653.1	1662.3
Thrust (lb.)	40.2	109.4
Stall Velocity(fps)	53.3	72.2
Steady Level Flight Velocity (fps)	92.2	124
Thrust-to-Weight Ratio	0.13	0.33
Minimum Thrust Velocity (fps)	29.8	39.1
Minimum Thrust Lift Coefficient	0.6	0.64
Power (hp.)	22	81
Turning Rate	0-17.2°	0-42.2°
Best Rate of Climb (fps)	25.5	76.9
Best Angle of Climb (°)	21.1	14.1
Glide Vertical Velocity (fps)	1.6	2.3
Takeoff Distance (ft.)	465.9	734.6
Landing Ground Roll Distance (ft.)	157.6	400.1

The new design produces enough for the aircraft to fly during the level cruise portions of the mission. The thrust-to-weight ratio is much larger for the new design. Both the best rate of climb and best angle of climb values decreased with the design changes. As expected the glide vertical velocity is much larger, reducing the distance that the aircraft is able to glide. The total takeoff and landing ground roll distance also increased, which is to be expected with a larger stall velocity. As the aircraft was able to satisfy the requirements, a computer-aided design (CAD) model is presented in Appendix H.

17. COST ANALYSIS

Cost analysis must be performed in an attempt to quantify the cost of developing and manufacturing a new design to determine if the design is viable. Just because the design fulfills all of the mission requirements does not mean that it should be built. It does not matter how well the aircraft performs if it is too expensive to build. A worst case scenario will be analyzed in an attempt to account for any issues that occur during design and production. The analysis will be done using a modified Development and Procurement Costs of Aircraft (DAPCA) IV cost model, where the cost equations are given in 2012 dollars²⁹.

DAPCA tends to overestimate the hours and cost of general aviation, and some claim the results to be reasonable when dividing by 4²⁹. The hours and cost will be cut in half to account for the overestimation. The number of engineering, tooling, manufacturing, and quality control hours are provided in Eqs. (17.1)-(17.4)²⁹:

$$H_E = \frac{1.8 \left(4.86 W_{empty}^{0.777} V_{max}^{0.894} Q^{0.163} \right)}{2} \quad (17.1)$$

$$H_T = \frac{1.8 \left(6.99 W_{empty}^{0.777} V_{max}^{0.696} Q^{0.263} \right)}{2} \quad (17.2)$$

$$H_M = \frac{1.8 \left(7.37 W_{empty}^{0.82} V_{max}^{0.484} Q^{0.641} \right)}{2} \quad (17.3)$$

$$H_Q = \frac{1.8 \left(0.133 H_M \right)}{2} \quad (17.4)$$

Part of the worst case scenario involves using the maximum hour fudge factor when dealing with carbon fiber, which is shown by the factor of 1.8. Also, when these hours were calculated, it was assumed there would be 50 of these aircraft produced. The hours needed for each segment of work is provided below.

Table 42. Hours Analysis

Type of Work	Hours
Engineering	96785
Tooling	74410
Manufacturing	215760
Quality Control	25826

The results show this program requiring a large amount of hours to produce, which should be expected. The next step in cost analysis is determining the cost of development support, flight testing, and manufacturing materials cost, as shown in Eqs. (17.5)-(17.7)²⁹:

$$C_{DS} = \frac{91.3 W_{empty}^{0.63} V_{max}^{1.3}}{2} \quad (17.5)$$

$$C_{FT} = \frac{2498 W_{empty}^{0.325} V_{max}^{0.822} FTA^{1.21}}{2} \quad (17.6)$$

$$C_{MM} = \frac{22.1 W_{empty}^{0.921} V_{max}^{0.621} Q^{0.799}}{2} \quad (17.7)$$

It was assumed there would be six flight test aircraft, the largest typical value provided by Raymer¹. The engine was found to be approximately \$44,000.00 per engine³⁶. The cost of avionics can be approximated as \$8,000.00 per pound²⁹. The costs of these items are provided below.

Table 43. Cost Analysis

Types of Costs	Costs (\$)
Development Support	9,488,400.00
Flight Test	3,872,300.00
Manufacturing Materials	2,467,200.00
Engine per aircraft	44,000.00
Avionics per aircraft	241,600.00
Electrostatic Sprayer per Aircraft ³⁷	40,000.00

The total cost can be calculated as shown in Eq. (17.8)²⁹:

$$Cost = 115 H_E + 118 H_T + 98 H_M + 108 H_Q + C_{DS} + C_{FT} + C_{MM} + C_{Eng} Q + C_{Av} Q + C_{ES} Q \quad (17.8)$$

The total cost was found to be \$75,908,000.00 for the program. With a production quantity of 50, this means the cost per aircraft is \$1,518,160.00, about 7 times larger than a simple cost estimation of \$200.00 per pound of empty weight. This overestimation is most likely due to the avionics and composite costs. In an attempt to compare the DAPCA cost of the UAV and Thrush 510G, some values of the 510G will have to be assumed. The empty

weight of the Thrush 510G is 4,700 lb., the avionics will be assumed to be one percent of that at \$3000.00 per pound, the engine will be assumed to be twice as expensive, 100 aircraft will be produced with 6 flight tests, and the aircraft will have a maximum speed of 163.4 kt²¹. The cost was found to be \$320,270,000.00 for the program and \$3,202,700.00 per aircraft.

This cost analysis has some flaws. The first of which appears to be an overestimation of the costs of the manned crop duster. Air Tractor agricultural aircraft, similar Thrush aircraft, started at around \$550,000.00 in 2009³⁷. This means that the Thrush aircraft cost estimate was much higher than it should have been. This means the cost estimation may also be higher for the UAV. The low cost of the manned agricultural aircraft also raises a practicality concern. If the UAV has a higher cost than the manned crop dusters, the potential market niche for the UAV would seem smaller than it otherwise would be. This will be discussed more in Section 19.

18. TRADE STUDIES

In an attempt to analyze and improve the design, three trade studies will be conducted. The first two trade studies will use the maximum cruise wing loading as the baseline wing loading when calculating lift. However, the design wing loading, 9.94, will stay the same when calculating the initial dimensions of the aircraft. The maximum cruise wing loading will alter the maximum velocity, causing some slight changes to the weight. The first trade study is presented in Table 44.

Table 44. Maximum Cruise Wing Loading-Aspect Ratio Trade Study

$\frac{W}{S}$ - AR		Maximum Cruise Wing Loading					
		9.95		12.43		14.92	
Aspect Ratio	6.0	W=1619 L=1427	$\frac{L}{W}=0.88$	W=1631 L=1837	$\frac{L}{W}=1.13$	W=1642 L=2262	$\frac{L}{W}=1.38$

	7.5	W=164 1 L=1443	$\frac{L}{W}=0.88$	W=1654 L=1857	$\frac{L}{W}=1.12$	W=166 6 L=2287	$\frac{L}{W}=1.37$
	9.0	W=166 3 L=1456	$\frac{L}{W}=0.88$	W=1676 L=1874	$\frac{L}{W}=1.12$	W=168 9 L=2310	$\frac{L}{W}=1.37$

Table 44 shows that the aspect ratio does not have a large effect on the lift-to-weight ratio, however, the cruise wing loading does. The wing loading appears to have a greater effect on the lift-to-weight ratio as the wing loading increases. The aspect ratio seems to have a marginal effect on the weight, with the lift-to-weight ratio decreasing as the aspect ratio increases. This is effect of the aspect ratio on weight will be explored more in Figure 14.



Figure 14. Effect of Aspect Ratio on Weight

Figure 14 shows that no matter the velocity, there is a similar pattern between the aspect ratio and the weight. It shows that the weight increases between the aspect ratio decreases as the aspect ratio increases. It also shows a fairly linear increase in weight as the velocity increases for all aspect ratios. The analysis shown was conducted using only the refined weight estimate. The results may vary if the more in-depth weight analysis were to be used.

The second trade study involves comparing the lift-to-weight ratio produced by varying the maximum cruise wing loading and the power-to-weight ratio. This was done by comparing the velocities required for the maximum cruise wing loading and power-to-weight ratio and selecting the smaller velocity as the design maximum, and then using that velocity to find the weight of the aircraft and the lift generated. The minimum velocity was used because a wing loading of 14.92 is going to require a much larger velocity than a power to weight ratio of 0.0637, and so one of the design factors had to be set as the limit. The results are provided in Table 45.

Table 45. Maximum Cruise Wing Loading-Power-to-Weight Trade Study

$\frac{W}{S}$ - $\frac{hp}{W}$		Maximum Cruise Wing Loading					
		9.95		12.43		14.92	
Power-to-Weight Ratio	0.063 7	W=160 7 L=685	$\frac{L}{W}=0.43$	W=160 7 L=685	$\frac{L}{W}=0.43$	W=160 7 L=685	$\frac{L}{W}=0.43$
	0.079 6	W=164 5 L=1457	$\frac{L}{W}=0.89$	W=165 5 L=1858	$\frac{L}{W}=1.12$	W=165 5 L=1877	$\frac{L}{W}=1.13$
	0.095 5	W=165 8 L=1503	$\frac{L}{W}=0.91$	W=166 8 L=1919	$\frac{L}{W}=1.15$	W=167 7 L=2347	$\frac{L}{W}=1.40$

Table 45 shows that it may not be possible to go much lower than a power-to-weight ratio of 0.0796, unless a wing is used that is larger than the initial sizing suggests. This is because the aircraft is having difficulty producing enough lift if the cruise velocity is lower than 75 to 80 mph. It would be possible to increase the wing size at a lower velocity, however, more analysis would need to be conducted to see if the weight increase from a larger wing negates any benefits to the amount of lift produced by the larger wing. It would be easier to increase the wing size as the velocity approached 75 or 80 mph as the weight and drag penalty would

be reduced. This smaller penalty would be a result of a smaller wing area increase to produce enough lift.

The final trade study is a simple comparison between the minimum cruise velocity and wing area. The purpose of this trade study is to attempt to find the most lift that can be generated at the smallest velocity possible. With that in mind, the design minimum cruise velocity will be set as the maximum in the trade study, and will be compared to velocities that are 20 and 10 percent smaller. To compensate for smaller velocities, the design wing area will be the smallest, and will be compared to wing areas 10 and 20 percent larger. The previous trade studies have shown that a weight range of 1600 to 1650 lb. is a reasonable estimate, meaning a lift less than 1600 lb. will not be considered as a plausible value. The trade study results are presented below.

Table 46. Minimum Cruise Velocity Wing Area Trade Study

Velocity-Wing Area		Minimum Cruise Velocity (fps)		
		99.2	111.6	124
Wing Area (ft.)	149.6	1063.5	1346	1661.7
	164.6	1170.1	1480	1828.3
	179.5	1276.1	1615	1993.8

Table 46 shows that 111.6 fps, 76.1 mph, may be either the minimum or close to the minimum cruise velocity needed to generate enough lift without having to drastically increase wing area. This is not really a design issue, however, it may be a practicality issue due to strict FAA regulations. The practicality issue is discussed further in Section 19.

19. FEASIBILITY VS. PRACTICALITY

As the redesign shows it is possible to design an aircraft that satisfies the design requirements once the maximum cruise velocity was increased. However, just because a design is feasible, it does not mean the design is practical. The practicality concern is

somewhat connected to the reluctance of the FAA to certify crop dusting UAVs. The maximum velocity of this aircraft will be twice as much as the Yamaha RMAX, with a much larger payload. This raises some uncertainty as to whether the FAA would certify the aircraft. Another issue with the practicality is the comparison to manned crop duster. The UAV will fly at the lower end of operating speeds for manned crop dusters, with a payload potentially ranging from at least 8 to 10 times smaller than modern manned crop dusters. This may limit the potential market to smaller farms, which might not have the capital necessary to warrant spending over a million dollars on a UAV, or paying a large sum to a team to spray their farms with this crop dusters.

The potential higher cost of the UAV will also limit the potential market due to the number of available pilots and the ability of said pilots to pay for the UAV. The UAV would have to be piloted by an expert, with the largest likely available pool of pilots coming from the military, and it seems unlikely that many would have the available capital to pay for the UAV. This means the most likely scenario for a business would be someone with enough capital to buy a UAV, pay a pilot and potentially 3 other people, while carrying a much smaller payload compared to the manned a manned crop duster. This does not seem practical unless the UAV is cheaper than the manned aircraft, which may not happen. This report shows the UAV design having the potential to fill a niche in the market, nevertheless, more research and analysis must be done to determine if this UAV fills the niche effectively.

20. CONCLUSION

With the current advancements in UAV technologies, the possibility of a new UAV crop duster was introduced. The initial aircraft was designed around the design requirements of a 50 gallon pesticide payload, maximum cruise velocity of 45 mph, takeoff distance of 500

ft., and a landing distance of 1,000 ft. The initial design requirement restricted the design too much to produce a viable aircraft, which required increasing the maximum cruise velocity to 90 mph. The redesigned UAV was capable of fulfilling all of the design requirements. The UAV has a gross takeoff weight of 1654.0 lb., fuselage length of 21.7 ft., and wing area of 149.6 ft². The aircraft was shown to be statically stable. Cost analysis was conducted, with the cost per aircraft approaching approximately \$1,518,160.00. This was a little less than half the estimated cost of the Thrush 510G, which showed a potential opening in the crop dusting market. This aircraft has proven it has the performance to potentially compete in the crop dusting industry.

References

- ¹Downs, E., and Lemmer, G., "Origins of Aerial Crop Dusting," *Agricultural History*, Vol. 39, No. 3, 1965, pp. 123-35.
- ²McConnell, R., Antón, F., and Magnotti, R., "Crop Duster Aviation Mechanics: High Risk for Pesticide Poisoning," *American Journal of Public Health*, Vol. 80, No. 10 1990, pp. 1236-239.
- ³Barnhart, R., Hottman, S., Marshall, D., and Shappee, E., *Introduction to Unmanned Aircraft Systems*, 1st ed., CRC Press Group, Boca Raton, FL 2011.
- ⁴Huang, Y., Thomson, S., Hoffmann, C., Lan, Y., and Fritz, B., "Development and Prospect of Unmanned Aerial Vehicle Technologies for Agricultural Production Management," *International Journal of Agricultural and Biological Engineering*, Vol. 6, No. 3, 2013, pp. 1-10.
- ⁵"Yamaha Precision Agriculture, Yamaha Helicopters," *Yamaha Precision Agriculture, Yamaha Helicopters*, Yamaha Motor Corporation, 2014.
[<http://www.yamahaprecisionagriculture.com/rmax.aspx>. Accessed 8/20/15]
- ⁶Wong, KC. "Survey of Regional Developments: Civil Applications." U. of Sydney, 2001.
- ⁷Gardisser, D., "Aerial-Fixed Wing Application and Drift," *North American Conference on Pesticide Spray Drift Management*, Portland, ME, 1998, pp. 86-87.

- ⁸Kirk, I. "Managing Spray Drift from Aerial Fixed-Wing Applications," *North American Conference on Pesticide Spray Drift Management*, Portland, ME, 1998, pp. 88-100.
- ⁹Hewitt, A. J., Johnson, D. R., Fish, J. D., Hermansky, C. G., Valcore, D. L. "Development of the Spray Drift Task Force Database for Aerial Applications," *Environmental Toxicology and Chemistry*, Vol. 21, No. 3, 2002, pp. 648-58.
- ¹⁰Bird, S. L., Perry, S. G., Ray, S. L., and Teske, M. E., "Evaluation of the AgDISP Aerial Spray Algorithms in the AgDRIFT Model," *Environmental Toxicology and Chemistry*, Vol. 21, No. 3, 2002, pp. 672-81.
- ¹¹Frank, R., Ripley, B. D., Lampman, W., Morrow, D., Collins, H., Gammond, G. R., Mccubbin, P., "Comparative Spray Drift Studies of Aerial and Ground Applications 1983-1985," *Environmental Monitoring and Assessment*, Vol. 29, 1994, pp. 167-81.
- ¹²Nuyttens, D., Schamphelre, M. D., Verboven, P., Brusselman, E., and Dekeyser, D., "Droplet Size and Velocity Characteristics of Agricultural Sprays," *Transactions of the ASABE*, Vol. 52, No. 5, 2009, pp. 1471-480.
- ¹³Huang, Y., Hoffmann, W. C., Lan, Y., Wu, W., and Fritz, B. K., "Development of a Spray System for an Unmanned Aerial Vehicle Platform," *Applied Engineering in Agriculture*, Vol. 25, No. 6, 2009, pp. 803-09.
- ¹⁴Law, S. E., "Agricultural Electrostatic Spray Application: A Review of Significant Research and Development during the 20th Century," *Journal of Electrostatics*, Vol. 51, No. 52, 2001, pp. 25-42.
- ¹⁵Giles, D., and Blewett, T., "Effects of Conventional and Reduced-Volume, Charged-Spray Application Techniques on Dislodgeable Foliar Residue of Captan on Strawberries," *Journal of Agricultural and Food Chemistry*, Vol. 39, 1996, pp. 1646-651.
- ¹⁶Kirk, I. W., Hoffmann, W. C., and Carlton, J. B., "Aerial Electrostatic Spray System Performance," *Transactions of the ASAE*, Vol. 44, No. 5, 2001, pp. 1089-092.
- ¹⁷Wilde, M., "Dusting crops a boon, necessity for farmers," *Waterloo-Cedar Falls Courier*, 2010.
- ¹⁸Toscano, M., "Unmanned Aircraft Systems Roadmap to the Future," *Kansas UAS Conference*, Manhattan, KS, (2013).
- ¹⁹Toscano, M., "Civilian Applications of UAVs-A California Perspective, a Policy Symposium," *The American Institute of Aeronautics and Astronautics*, Westlake Village, CA, (2013).
- ²⁰"AT-401B Air Tractor," *AT-401B Air Tractor*, Air Tractor, 2015.
[<http://www.airtractor.com/aircraft/401b>. Accessed 4/11/15.]
- ²¹"510G Thrush Aircraft," *510G Thrush Aircraft*, Thrush, 2011.
[<http://www.thrushaircraft.com/en/aircraft/510g.html>. Accessed 4/11/15.]

- ²²"General Description Dromader," *PZL MIELEC*. PZL MIELEC, 2009.
[<http://www.pzlmielec.com.pl/en/offer/products/m18-dromader/general-description/>.
Accessed 4/11/15.]
- ²³ Jackson, P., *Jane's All the World's Aircraft, 2003-2004*, Jane's Information Group, Coulson, Surrey, UK, 94th ed., 2003.
- ²⁴"CRESCO – DESCRIPTION," *Pacific Aerospace: Cresco*, Pacific Aerospace, 2015.
[<http://www.aerospace.co.nz/aircraft/cresco/description>. Accessed 4/11/2015]
- ²⁵Jackson, P., *Jane's All the World's Aircraft, 1988-1989*, Jane's Information Group, Coulson, Surrey, UK, 79th ed., 1988.
- ²⁶"Aeronave Ipanema." *Inovadora E Eficiente*. Embraer SA, 2012.
[<http://www.embraeragricola.com.br/pt-BR/Aeronave-Ipanema/Paginas/Inovadora-e-Eficiente.aspx>. Accessed 4/11/15.]
- ²⁷"SR 200 UAV," *Rotomotion SR200*, Rotomotion.
[http://www.rotomotion.com/datasheets/sr200_uav_sheet.pdf. Accessed 8/24/15.]
- ²⁸"AG-RHCD-01 Agriculture UAV Crop Duster Sprayers Helicopter UAV," *AG-RHCD-01 Agriculture UAV Crop Duster Sprayers Helicopter UAV*, HSE - Unmanned Aerial Vehicles (UAV), 2013.
[http://www.uavcropdustersprayers.com/agriculture_helicopter_uav_crop_duster_or_80_1.htm. Accessed 8/20/15.]
- ²⁹ Raymer, D. P., *Aircraft Design: A Conceptual Approach*, Washington, D.C.: American Institute of Aeronautics and Astronautics, 2012.
- ³⁰"Rotax 912 ULS DCDI 100HP," *Rotax 914 UL specifications, performance, weights and documentation*, Rotax
[http://www.rotaxservice.com/rotax_engines/rotax_912ULSs.htm. Accessed 10/15/15.]
- ³¹"LYCOMING," *Lycoming > PRODUCTS > Engines > Certified > 235 Series > Engine Data*, Avro Corporation, 2015
[<http://www.lycoming.com/lycoming/products/engines/certified/235series/engineadata.aspx>. Accessed 10/15/15.]
- ³² "Sprayer Tutorial," — *Virginia Tech Pesticide Programs (VTPP)*, Virginia Tech, 2014
[http://vtpp.ext.vt.edu/pesticide-safety-education-program/pesticide-application-equipment?force_toc:int=1. Accessed 11/12/15.]
- ³³ Moir, I., and Seabridge, A. G., *Aircraft systems: Mechanical, Electrical, and Avionics Subsystems Integration*, 3rd ed., Chichester, West Sussex, England: Wiley, 2008.
- ³⁴"The Aircraft Tire DataBook," *Tire Databook* Available:
[<https://www.goodyearaviation.com/resources/tiredatabook.html>. Accessed 02/12/2016]
- ³⁵ Nicolai, L. M., and Carichner, G. E., *Fundamentals of Aircraft and Airship Design*, Reston, VA: American Institute of Aeronautics and Astronautics, 2010

³⁶“Aviation Factory Engines & Aircraft Parts For Cessna Airplanes & More - Air Power, Inc.,” *Aviation Factory Engines & Aircraft Parts For Cessna Airplanes & More - Air Power, Inc.*, Air Power Inc, 2016[<http://www.airpowerinc.com/productcart/pc/engines.asp?searchparm=o320>. Accessed 4/1/16.]

³⁷Madden, D., “Aerial Applicators Now Hitting The ‘Bull’s Eye,’” *The Land*, Jun. 2009.

³⁸“eCFR — Code of Federal Regulations,” *eCFR — Code of Federal Regulations*, Federal Aviation Administration, 2014 [http://www.ecfr.gov/cgi-bin/text-idx?c=ecfr&tpl=/ecfrbrowse/title14/14tab_02.tpl. Accessed 8/24/15]

³⁹“Exemption No. 11448 – Yamaha RMAX,” *Federal Aviation Administration - Section 333*, Federal Aviation Administration, 2015 [https://www.faa.gov/uas/legislative_programs/section_333/333_authorizations/media/yamaha_11448.pdf. Accessed 8/24/15]

Appendices

Appendix A – FAA Regulations

§91.313 Restricted category civil aircraft: Operating limitations.³⁸

(a) No person may operate a restricted category civil aircraft—

(1) For other than the special purpose for which it is certificated; or

(2) In an operation other than one necessary to accomplish the work activity directly associated with that special purpose.

(b) For the purpose of paragraph (a) of this section, operating a restricted category civil aircraft to provide flight crewmember training in a special purpose operation for which the aircraft is certificated is considered to be an operation for that special purpose.

(c) No person may operate a restricted category civil aircraft carrying persons or property for compensation or hire. For the purposes of this paragraph, a special purpose operation involving the carriage of persons or material necessary to accomplish that operation, such as crop dusting, seeding, spraying, and banner towing (including the carrying of required persons or material to the location of that operation), and operation for the purpose of providing flight crewmember training in a special purpose operation, are not considered to be the carriage of persons or property for compensation or hire.

(d) No person may be carried on a restricted category civil aircraft unless that person—

(1) Is a flight crewmember;

(2) Is a flight crewmember trainee;

(3) Performs an essential function in connection with a special purpose operation for which the aircraft is certificated; or

(4) Is necessary to accomplish the work activity directly associated with that special purpose.

(e) Except when operating in accordance with the terms and conditions of a certificate of waiver or special operating limitations issued by the Administrator, no person may operate a restricted category civil aircraft within the United States—

(1) Over a densely populated area;

(2) In a congested airway; or

(3) Near a busy airport where passenger transport operations are conducted.

(f) This section does not apply to nonpassenger-carrying civil rotorcraft external-load operations conducted under part 133 of this chapter.

(g) No person may operate a small restricted-category civil airplane manufactured after July 18, 1978, unless an approved shoulder harness is installed for each front seat. The shoulder harness must be designed to protect each occupant from serious head injury when the occupant experiences the ultimate inertia forces specified in §23.561(b)(2) of this chapter. The shoulder harness installation at each flight crewmember station must permit the crewmember, when seated and with the safety belt and shoulder harness fastened, to perform all functions necessary for flight operation. For purposes of this paragraph—

(1) The date of manufacture of an airplane is the date the inspection acceptance records reflect that the airplane is complete and meets the FAA-approved type design data; and

(2) A front seat is a seat located at a flight crewmember station or any seat located alongside such a seat.

§137.51 Operation over congested areas: General.³⁸

(a) Notwithstanding part 91 of this chapter, an aircraft may be operated over a congested area at altitudes required for the proper accomplishment of the agricultural aircraft operation if the operation is conducted—

(1) With the maximum safety to persons and property on the surface, consistent with the operation; and

(2) In accordance with the requirements of paragraph (b) of this section.

(b) No person may operate an aircraft over a congested area except in accordance with the requirements of this paragraph.

(1) Prior written approval must be obtained from the appropriate official or governing body of the political subdivision over which the operations are conducted.

(2) Notice of the intended operation must be given to the public by some effective means, such as daily newspapers, radio, television, or door-to-door notice.

(3) A plan for each complete operation must be submitted to, and approved by appropriate personnel of the FAA Flight Standards District Office having jurisdiction over the area where the operation is to be conducted. The plan must include consideration of obstructions to flight; the emergency landing capabilities of the aircraft to be used; and any necessary coordination with air traffic control.

(4) Single engine aircraft must be operated as follows:

(i) Except for helicopters, no person may take off a loaded aircraft, or make a turnaround over a congested area.

(ii) No person may operate an aircraft over a congested area below the altitudes prescribed in part 91 of this chapter except during the actual dispensing operation, including the approaches and departures necessary for that operation.

(iii) No person may operate an aircraft over a congested area during the actual dispensing operation, including the approaches and departures for that operation, unless it is operated in a pattern and at such an altitude that the aircraft can land, in an emergency, without endangering persons or property on the surface.

(5) Multiengine aircraft must be operated as follows:

(i) No person may take off a multiengine airplane over a congested area except under conditions that will allow the airplane to be brought to a safe stop within the effective length of the runway from any point on takeoff up to the time of attaining, with all engines operating at normal takeoff power, 105 percent of the minimum control speed with the critical engine inoperative in the takeoff configuration or 115 percent of the power-off stall speed in the takeoff configuration, whichever is greater, as shown by the accelerate stop distance data. In applying this requirement, takeoff data is based upon still-air conditions, and no correction is made for any uphill gradient of 1 percent or less when the percentage is measured as the difference between elevation at the end points of the runway divided by the total length. For uphill gradients greater than 1 percent, the effective takeoff length of the runway is reduced 20 percent for each 1-percent grade.

(ii) No person may operate a multiengine airplane at a weight greater than the weight that, with the critical engine inoperative, would permit a rate of climb of at least 50 feet per

minute at an altitude of at least 1,000 feet above the elevation of the highest ground or obstruction within the area to be worked or at an altitude of 5,000 feet, whichever is higher. For the purposes of this subdivision, it is assumed that the propeller of the inoperative engine is in the minimum drag position; that the wing flaps and landing gear are in the most favorable positions; and that the remaining engine or engines are operating at the maximum continuous power available.

(iii) No person may operate any multiengine aircraft over a congested area below the altitudes prescribed in part 91 of this chapter except during the actual dispensing operation, including the approaches, departures, and turnarounds necessary for that operation.

Appendix B – Yamaha Exemptions

Exemption No. 11448³⁹

UNITED STATES OF AMERICA
DEPARTMENT OF TRANSPORTATION
FEDERAL AVIATION ADMINISTRATION
WASHINGTON, DC 20591

In the matter of the petition of

**YAMAHA MOTOR CORPORATION,
U.S.A.**

for an exemption from parts 21, 27; and §§ 45.23(b); 61.113(a) & (b); 91.7(a); 91.9(b)(2); 91.103; 91.109; 91.119; 91.121; 91.151(b); 91.203(a) & (b); 91.405(a); 91.407(a)(1); 409(a)(2); 91.417(a) & (b); 91.1501; 137.19(d); 137.19(e)(2)(ii), (iii), and (v); 137.31(a) & (b); 137.33(a); and 137.42 of Title 14, Code of Federal Regulations

Regulatory Docket No. FAA-2014-0397

GRANT OF EXEMPTION

By letter posted to the public docket on June 13, 2014,¹ Mr. David P. Murray, Willkie Farr & Gallagher, LLP, Counsel for Yamaha Motor Corporation, U.S.A., 1875 K Street, N.W., Washington, DC 20006 petitioned the Federal Aviation Administration (FAA) on behalf of Yamaha Motor Corporation, U.S.A. (Yamaha) for an exemption from parts 21, 27, and §§ 45.23(b), 61.113(a) & (b), 91.7(a), 91.9(b)(2), 91.103, 91.109, 91.119, 91.121, 91.151(b), 91.203(a) & (b), 91.405(a), 91.407(a)(1), 91.409(a)(2), 91.417(a) & (b), 91.1501, 137.19(d), 137.19(e)(2)(ii), (iii), and (v), 137.31(a) & (b), 137.33(a), and 137.42 of Title 14, Code of Federal Regulations (14 CFR). Yamaha petitioned for an exemption to operate the Yamaha RMAX for the purpose of providing commercial agricultural-related services.

The petitioner requests relief from the following regulations:

Part 21 prescribes, in pertinent part, the procedural requirements for issuing and changing design approvals, productions approvals, airworthiness certificates, and airworthiness approvals.

¹ By letter dated November 6, 2014, the petitioner responded to the FAA's request for information.

Part 27 prescribes, in pertinent part, the airworthiness standards for the issuance of type certificates for normal category rotorcraft with maximum weights of 7,000 pounds or less and nine or less passenger seats.

Section 45.23(b) prescribes, in pertinent part, that when marks include only the Roman capital letter “N” and the registration number is displayed on limited, restricted or light-sport category aircraft or experimental or provisionally certificated aircraft, the operator must also display on that aircraft near each entrance to the cabin, cockpit, or pilot station, in letters not less than 2 inches nor more than 6 inches high, the words “limited,” “restricted,” “light-sport,” “experimental,” or “provisional,” as applicable.

Sections 61.113(a) and (b) prescribe that—

- (a) no person who holds a private pilot certificate may act as a pilot in command of an aircraft that is carrying passengers or property for compensation or hire; nor may that person, for compensation or hire, act as pilot in command of an aircraft.
- (b) a private pilot may, for compensation or hire, act as pilot in command of an aircraft in connection with any business or employment if:

- (1) The flight is only incidental to that business or employment; and
- (2) The aircraft does not carry passengers or property for compensation or hire.

Section 91.7(a) prescribes, in pertinent part, that no person may operate a civil aircraft unless it is in an airworthy condition.

Section 91.9(b)(2) prohibits operation of U.S.-registered civil aircraft unless there is available in the aircraft a current approved Airplane or Rotorcraft Flight Manual, approved manual material, markings, and placards, or any combination thereof.

Section 91.103 prescribes, in pertinent part, that each pilot in command shall, before beginning a flight, become familiar with all available information concerning that flight, to include—

- (a) For a flight under IFR or a flight not in the vicinity of an airport, weather reports and forecasts, fuel requirements, alternatives available if the planned flight cannot be completed, and any known traffic delays of which the pilot in command has been advised by ATC;
- (b) For any flight, runway lengths at airports of intended use, and the following takeoff and landing distance information:
 - (1) For civil aircraft for which an approved Airplane or Rotorcraft Flight Manual containing takeoff and landing distance data is required, the takeoff and landing distance data contained therein; and

- (2) For civil aircraft other than those specified in paragraph (b)(1) of this section, other reliable information appropriate to the aircraft, relating to aircraft performance under expected values of airport elevation and runway slope, aircraft gross weight, and wind and temperature.

Section 91.109 prescribes, in pertinent part, that no person may operate a civil aircraft (except a manned free balloon) that is being used for flight instruction unless that aircraft has fully functioning dual controls.

Section 91.119 prescribes, in pertinent part, that, except when necessary for takeoff or landing, no person may operate an aircraft below the following altitudes:

- (a) *Anywhere*. An altitude allowing, if a power unit fails, an emergency landing without undue hazard to persons or property on the surface.
- (b) *Over congested areas*. Over any congested area of a city, town, or settlement, or over any open air assembly of persons, an altitude of 1,000 feet above the highest obstacle within a horizontal radius of 2,000 feet of the aircraft.
- (c) *Over other than congested areas*. An altitude of 500 feet above the surface, except over open water or sparsely populated areas. In those cases, the aircraft may not be operated closer than 500 feet to any person, vessel, vehicle, or structure.
- (d) *Helicopters, powered parachutes, and weight-shift-control aircraft*. If the operation is conducted without hazard to persons or property on the surface
 - (1) A helicopter may be operated at less than the minimums prescribed in paragraph (b) or (c) of this section, provided each person operating the helicopter complies with any routes or altitudes specifically prescribed for helicopters by the FAA;

Section 91.121 requires, in pertinent part, each person operating an aircraft to maintain cruising altitude by reference to an altimeter that is set "...to the elevation of the departure airport or an appropriate altimeter setting available before departure."

Section 91.151(b) prescribes, in pertinent part, that no person may begin a flight in a rotorcraft under VFR conditions unless (considering wind and forecast weather conditions) there is enough fuel to fly to the first point of intended landing and, assuming normal cruising speed, to fly after that for at least 20 minutes.

Section 91.203(a) prohibits, in pertinent part, any person from operating a civil aircraft unless it has within it (1) an appropriate and current airworthiness certificate; and (2) an effective U.S. registration certificate issued to its owner or, for operation within the United States, the second copy of the Aircraft registration Application as provided for in § 47.31(c).

Section 91.203(b) prescribes, in pertinent part, that no person may operate a civil aircraft unless the airworthiness certificate or a special flight authorization issued under § 91.715 is displayed at the cabin or cockpit entrance so that it is legible to passengers or crew.

Section 91.405(a) requires, in pertinent part, that an aircraft owner or operator shall have that aircraft inspected as prescribed in subpart E of the same part and shall, between required inspections, except as provided in paragraph (c) of the same section, have discrepancies repaired as prescribed in part 43 of the chapter.

Section 91.407(a)(1) prohibits, in pertinent part, any person from operating an aircraft that has undergone maintenance, preventive maintenance, rebuilding, or alteration unless it has been approved for return to service by a person authorized under § 43.7 of the same chapter.

Section 91.409(a)(2) prescribes, in pertinent part, that no person may operate an aircraft unless, within the preceding 12 calendar months, it has had an inspection for the issuance of an airworthiness certificate in accordance with part 21 of this chapter.

Section 91.417(a) and (b) prescribe, in pertinent part, that—

(a) Each registered owner or operator shall keep the following records for the periods specified in paragraph (b) of this section:

(1) Records of the maintenance, preventive maintenance, and alteration and records of the 100-hour, annual, progressive, and other required or approved inspections, as appropriate, for each aircraft (including the airframe) and each engine, propeller, rotor, and appliance of an aircraft. The records must include—

(b) The owner or operator shall retain the following records for the periods prescribed:

(1) The records specified in paragraph (a)(1) of this section shall be retained until the work is repeated or superseded by other work or for 1 year after the work is performed.

(2) The records specified in paragraph (a)(2) of this section shall be retained and transferred with the aircraft at the time the aircraft is sold.

(3) A list of defects furnished to a registered owner or operator under § 43.11 of this chapter shall be retained until the defects are repaired and the aircraft is approved for return to service.

Section 91.1501 requires, in pertinent part, that operators support the continued airworthiness of each airplane including revising the inspection program, incorporating design changes, and incorporating revisions to Instructions for Continued Airworthiness.

Section 137.19(d) prescribes, in pertinent part, that the applicant for an agricultural aircraft operator certificate must have at least one certificated and airworthy aircraft, equipped for agricultural operation.

Sections 137.19(e)(2)(ii), (iii), and (v) prescribe, in pertinent part, the tests of skill for agricultural aircraft operations that must be demonstrated by the applicant in the areas of (ii) approaches to the working area, (iii) flare-outs, and (v) pullups and turnarounds.

Section 137.31(a) prescribes, in pertinent part, that no person may operate an aircraft unless that aircraft meets the requirements of Sec. 137.19(d).

Section 137.31(b) prescribes, in pertinent part, that no person may operate and aircraft unless that aircraft is equipped with a suitable and properly installed shoulder harness for use by each pilot.

Section 137.33(a) prescribes, in pertinent part, that no person may operate an aircraft unless a facsimile of the agricultural aircraft operator certificate, under which the operation is conducted, is carried on that aircraft.

Section 137.42 prescribes, in pertinent part, that no person may operate an aircraft in operations required to be conducted under part 137 without a safety belt and shoulder harness properly secured about that person.

The petitioner supports its request with the following information:

The petitioner proposes to operate the RMAX UAS to conduct commercial agricultural-related services in the United States. The petitioner also intends to conduct commercial agricultural aircraft operations as described in 14 CFR, part 137. The RMAX is capable of providing a wide array of essential agricultural spraying services, including watering, fertilizers, pesticides, and herbicides. The RMAX can also be equipped with sensors and equipment to detect and monitor agricultural areas that require irrigation, fertilization, or other treatments.

The petitioner has provided the following information along with its petition to support its request for an exemption, which includes proprietary and/or confidential supporting documents:

- 1) RMAX training program;
- 2) Yamaha RMAX Ground Theory Manual;
- 3) Yamaha RMAX Operations Manual; and
- 4) Yamaha RMAX Agricultural Guidebook

Documents 1 through 4 above are hereinafter collectively referred to as the operating documents.

The FAA has organized the petitioner's information into four sections: (1) the Unmanned Aircraft System (UAS), (2) the UAS Pilot in Command (PIC), (3) the UAS operating parameters, and (4) the public interest.

Unmanned Aircraft System (UAS)

The Yamaha RMAX is a remotely-piloted rotorcraft. It is 9 feet long and 3 feet 6 inches tall, has an empty weight of 141 lbs. and a load capacity of about 61 pounds for both liquid and granular applications. The main rotor is about 10 feet in diameter and extends 4 feet from either side of the RMAX and less than 3 feet from its front. The RMAX usually flies at a speed of no more than 12 mph (with a maximum speed of 45 mph). It is powered by a 2-cylinder, 246 cc engine that uses regular unleaded fuel with 2-stroke engine oil with a maximum output of 21 horsepower.

The petitioner states that the RMAX carries neither a pilot nor passenger and will operate within visual line of sight (VLOS) of a trained pilot and visual observer (spotter) only over uninhabited areas (e.g. fields, groves and orchards) and away from airports (i.e. three nautical miles or more) and populated areas.

The petitioner further cites the well-established performance and safety record of the RMAX with its 20 year history of use in Japan and its recent approved use in Australia and South Korea. The RMAX has also been flown in the United States as a public aircraft for research and development purposes. The petitioner states that the RMAX has logged over 2 million flight hours, treating more than 2.4 million acres of farmland each year in Japan alone. During the this two decade period, there have been no injuries due to problems with the aircraft in Japan, Australia or South Korea and in the limited instances where a problem with the aircraft has occurred, the RMAX has either been safely landed and shut down by the pilot or fallen to the ground without personal injury. There have been no collisions with other aircraft.

The petitioner also states that the RMAX has a host of onboard safety systems, including: a self-monitor function (diagnostic before takeoff); altitude control system (YACS); global positioning system (GPS) flight control system; lost link safety default (hover and land); YACS and GPS warning/indicator lights; speed indicator light; and rotor brake (propellers tilt upon shut down to allow air resistance to quickly bring the propellers to full stop.

UAS Pilot in Command (PIC)

The petitioner states that § 61.113(a) limits private pilots to being in command of non-commercial flights (i.e., not for compensation or hire); while § 61.113(b) provides an exception that allows a private pilot to command an aircraft without passengers or property, in connection with business or employment if "[t]he flight is only incidental to that business or employment.

Yamaha states that the PIC of a RMAX would not meet the conditions of § 61.113(b) because the operation of the RMAX would not be incidental to the proposed agricultural-related services, but rather essential to it.

Yamaha is requesting an exemption from the limitation in § 61.113(a) that prohibits the holder

of a private pilot certificate from acting as a PIC for compensation or hire. Alternatively, Yamaha is requesting an exemption from § 61.113(b) that would allow the holder of a private pilot certificate to act as PIC for compensation or hire even if the flight is not incidental to the business or employment of the PIC. Either of these requests, if granted, would allow a person holding a private pilot certificate to act as PIC of an RMAX operation for compensation or hire.

The petitioner states that it has integrated safety elements into the operation of the RMAX including comprehensive pilot and visual observer (spotter) training and certification requirements. These requirements, developed in cooperation with Australia's Civil Aviation Safety Authority (CASA) include: a comprehensive UAV training course which includes theory and practical components, a pilot theory exam, supervised flight training including agricultural spraying, completion of Yamaha's training program requirements including examination; and continued periodic training even after certification.

Completion and satisfaction of Yamaha training and certification requirements would be a condition for pilots and spotters operating the RMAX for agricultural purposes in the United States. In addition, for agricultural-related operations that involve chemical applications, the pilot operating the RMAX would also be certified under the FAA's rules governing Agricultural Aircraft Operations, 14 CFR part 137.

UAS Operating Parameters

The petitioner states the following conditions will be observed in support of its ability to provide at least an equal level of safety or no adverse safety effect to persons or property in the air or on the ground:

- a. The petitioner states that the RMAX will be operated within visual line of sight (VLOS) of the PIC.
- b. The PIC is always accompanied by a trained "spotter" who is positioned at the opposite side of the agricultural area and is in constant radio communication with the pilot. The spotter ensures that the RMAX is always within line-of-sight and helps identify and alert the PIC to any potential obstacles on the ground or in the air.
- c. Both the PIC and spotter will have completed a comprehensive training and certification program established by Yamaha prior to operation of the RMAX.
- d. The PIC will take all preflight actions as set forth in its flight manual, which includes a comprehensive preflight checklist.
- e. The RMAX will only be flown during daylight hours and in good weather.
- f. The PIC and spotter will maintain a safe distance from the RMAX when it is operating as set forth in its flight manual.

- g. UAS flights will be limited to a maximum altitude of 400 feet above ground level (AGL), and will normally be flown at altitudes of 20 feet AGL or less over a field or other agricultural area.
- h. UAS flights will only be flown over uninhabited areas (e.g. fields, groves, and orchards) and away from airports (i.e. three nautical miles or more) or populated areas.
- i. The maximum flight time for each UAS operation will be 60 minutes, with most agricultural flights lasting approximately 30 minutes.
- j. Operations of the RMAX that meet the definition of an “agricultural aircraft operation” will be conducted in accordance with 14 CFR part 137.

The petitioner states that although the RMAX has sufficient fuel capacity to provide for one hour of flight time, flight times for agricultural -related purposes are typically only 30 minutes due to the RMAX’s load capacity for spraying and other applications. The petitioner notes that the RMAX is typically refueled while it refills its payload, and thus is likely to comply with the 20-minute requirement from § 91.151(b), *Fuel requirements for flight in VFR conditions*, most of the time. Regardless of the potential for compliance, such a requirement is not necessary for the RMAX because it only operates 20 feet above an empty field, so the risk or danger associated with failing to reach a safe landing place is not present.

For the agricultural-related operations being requested, the petitioner intends to apply for an agricultural aircraft operator certificate issued under 14 CFR part 137. The petitioner has identified several sections of part 137 from which it seeks relief. Section 137.19(d) requires that an applicant for an agricultural aircraft operation has at least one certificated and airworthy aircraft. Section 137.31(a) prohibits agricultural operations in aircraft that do not meet § 137.19(d). The petitioner is requesting to conduct agricultural aircraft operations with RMAX aircraft that are not certificated, but are otherwise airworthy.

The petitioner requests relief from §§ 137.31(b) and 137.42 which require installation and use of a safety belt and shoulder harness by the pilot during agricultural aircraft operations. The petitioner states that since the RMAX is an unmanned aircraft (UA), these requirements are inapplicable. The petitioner states that an equivalent level of safety will be maintained by requiring the pilot and visual observer to maintain appropriate distances from the RMAX during operations to ensure their safety.

The petitioner also requests relief from certain requirements in section § 137.19(e)(2) that describe skill areas for maneuvers that are inapplicable to the RMAX when performing agricultural services. These include the demonstration of skill for the following maneuvers: (ii) approaches to the working area, (iii) flare-outs, and (v) pullups and turnarounds. Yamaha states that demonstrated compliance with the remaining applicable skills requirements of § 137.19(e)(2), along with the knowledge requirements of § 137.19(e)(1), will provide an adequate level of safety for operation of the RMAX.

The petitioner also requests relief from § 137.33(a) which requires that a facsimile of the

agricultural aircraft operator certificate be carried on the aircraft. Similar to relief granted in Exemption 11062, because the RMAX is an unmanned aircraft, this requirement is not necessary. Yamaha proposes that RMAX pilots will have copies of the required certificates with them and available for inspection at all locations where and while the RMAX is being used to perform agricultural chemical spray application and dispensing services.

The FAA's analysis is as follows:

The FAA has organized its analysis into five sections: (1) the UAS, (2) the UAS PIC, (3) the UAS operating parameters, (4) the UAS operating certificate, and (5) the public interest.

UAS

The petitioner requested relief from 14 CFR part 21, *Certification Procedures for Products and Parts*, and 14 CFR part 27, *Airworthiness Standards: Normal Category Rotorcraft*. In accordance with the statutory criteria provided in Section 333 of P.L. 112-95 in reference to 49 USC § 44704, and in consideration of the size, weight, speed, operational capabilities, design safety features, and limited operating area associated with the aircraft and its operation, the Secretary of Transportation has determined that this aircraft meets the conditions of Section 333. Because of the size, method of operation, and speed of the RMAX, operation of the RMAX under the conditions and limitations below will not adversely impact safety. An engineering review of the data supplied to the FAA during its evaluation supports this finding. Therefore, the FAA finds that the requested relief from 14 CFR parts 21 and 27, and any associated noise certification and testing requirements of part 36, are not necessary.

The RMAX is larger and heavier than UAS previously approved to operate under Section 333. The FAA reviewed engineering data supplied by the petitioner to assess whether the increase in size and weight would adversely impact safety. Our evaluation considered risk mitigating factors such as RMAX service history, pilot and spotter training requirements, system safety features, the intended low-altitude and remote area of operations, and other operating limitations.

The RMAX UAS has been in operation since 1997 and logged more than two million flight hours. There are approximately 2,600 RMAX UAS in use worldwide. Yamaha has developed production, certification, operation, and maintenance requirements for the RMAX. Yamaha provided data that demonstrates the RMAX historical safety record for the types of agricultural service operations being requested in its petition.

Manned aircraft conducting agricultural operations can weigh thousands of pounds and carry hundreds of gallons of fuel and payload. The RMAX weighs approximately 200 lbs. and carries about 2 gallons of fuel and 4 gallons of payload. Manned aircraft are operated by an onboard pilot and may carry other onboard crewmembers. The RMAX pilot and crew will be remotely located from the aircraft and will remain outside a designated safety zone when the RMAX is operating, ensuring that the pilot and observer are never so close to the RMAX to pose a hazard to the crew. The risk to an onboard pilot and crew during an incident or accident is eliminated with the use of a UAS for the proposed operation.

Manned aircraft are at risk of fuel spillage and fire in the event of an incident or accident. The RMAX carries much less fuel and would impact the surface with less energy than a manned aircraft and therefore lowers the potential risk and severity of fire following an incident or accident due to fuel or payload spillage.

The petitioner's UAS has on-board safety features that ensure the UAS can operate safely under both normal and contingency operating conditions. These features include automation to increase safety and reduce pilot workload. Some examples are the self-monitoring function (pre-takeoff diagnostics), an altitude control system (YACS), and a GPS flight control system. The lost-link safety default feature allows the RMAX to automatically hover and land in response to a lost-link event. Safety features such as the YACS and GPS warning/indicator lights and speed indicator light provide critical system status information to the pilot. When concluding a flight, the rotor brake feature causes the propellers to tilt upon shut down to allow air resistance to quickly bring the propellers to full stop. These safety features ensure that these operations will not adversely impact safety compared to a manned aircraft performing a similar operation and address ALPA's comments on mitigating risk of command and control link failures.

UAS PIC

The FAA has analyzed the petitioner's proposed operation and has determined that it does not differ significantly from the situation described in Grant of Exemption No. 11213 to Aeryon Labs, Inc. (Docket No. FAA-2014-0642). Therefore, the FAA finds that a PIC conducting operations under this grant of exemption may operate the UAS for compensation or hire, or in furtherance of a business, with any of the following pilot certificates: sport, recreational, private, commercial, or airline transport. Additionally, a PIC must hold and possess either a medical certificate issued under 14 CFR part 67 or a U.S. issued driver's license irrespective of the pilot certificate held. In addition, PICs must comply with 14 CFR § 61.53, *Prohibition on operations during medical deficiency*.

Operating Parameters of the UAS

The petitioner's operating documents describe operational procedures and limitations developed for the RMAX to provide mitigate potential safety risk to persons and property. The FAA considered these procedures and limitations in determining the proposed operations can be conducted safely.

The petitioner has requested relief from 14 CFR § 91.7(a), *Civil aircraft airworthiness*. While the petitioner's UAS will not require an airworthiness certificate, the FAA has determined that for the purposes of this exemption the pilot may determine the aircraft is in an airworthy condition prior to flight. The FAA's regulations state that the PIC of a civil aircraft is responsible for determining whether the aircraft is in a condition for safe flight. Therefore, relief from § 91.7(a) is granted and relief from § 91.7(b) is not necessary.

The petitioner requested relief from 14 CFR § 91.9(b)(2), *Civil aircraft flight manual, marking, and placard requirements* and § 91.203(a) and (b): *Civil aircraft: Certifications required*. The FAA has previously determined that relief from these sections is not necessary. See Exemption

No. 11062. Relevant materials may be kept in a location accessible to the PIC in compliance with the regulations.

The petitioner requested relief from 14 CFR § 91.103 *Preflight Action*. The PIC will take all actions including reviewing weather, flight battery requirements, landings, and takeoff distances and aircraft performance data before initiation of flight. The FAA has imposed stricter requirements with regard to visibility and distance from clouds; this is to both keep the UA from departing the VLOS and to preclude the UA from operating so close to a cloud as to create a hazard to other aircraft operating in the NAS. The FAA also notes the risks associated with sun glare; the FAA believes that the PIC's and VO's ability to still see other air traffic, combined with the PIC's ability to initiate a return-to-home sequence, are sufficient mitigations in this respect. The PIC will also account for all relevant site-specific conditions in his or her preflight procedures. Therefore, the FAA is not granting relief from § 91.103.

While the petitioner requested relief from 14 CFR § 91.109 *Flight instruction; Simulated instrument flight and certain flight tests*, the petition did not describe training scenarios in which a dual set of controls would be utilized or required, i.e. dual flight instruction, provided by a certificated flight instructor or other company-designated individual, which would require that individual to have fully functioning dual controls. The FAA is requiring that the petitioner's PICs possess at least a sport pilot certificate. This exemption will also require that training operations only be conducted during dedicated training sessions. As such, the FAA finds that the petitioner can conduct its operations without the requested relief from § 91.109.

Regarding the petitioner's requested relief from 14 CFR § 91.119, *Minimum safe altitudes: General*, the petitioner states that the RMAX will be operated at altitudes below 500 feet AGL and closer than 500 feet to persons, primarily the PIC and visual observer, although the PIC and VO will always maintain a safe distance from the RMAX as required by the operating documents. The RMAX will only be flown over uninhabited areas. Therefore, regarding the relief requested, the FAA finds that:

- a. Relief from § 91.119(a), which requires operating at an altitude that allows a safe emergency landing if a power unit fails, is not granted. The FAA expects the petitioner to be able to perform an emergency landing without undue hazard to persons or property on the surface if a power unit fails.
- b. Relief from § 91.119(b), operation over congested areas, is not applicable, because this grant of exemption prohibits operations over congested or densely populated areas.
- c. Relief from § 91.119(c) is necessary because the aircraft will be operated at altitudes below 500 feet AGL. Section 91.119(c) states that no person may operate an aircraft below the following altitudes: *over other than congested areas*, an altitude of 500 feet above the surface, except over open water or sparsely populated areas. The FAA finds operations conducted in compliance with the conditions and limitations in this grant of exemption warrant relief from § 91.119(c).
- d. Relief from § 91.119(d) is not applicable.

Regarding the petitioner's requested relief from 14 CFR § 91.121, *Altimeter settings*, when the UA is equipped with a barometric altimeter, relief from § 91.121 is not necessary. When the UA is not equipped with a barometric altimeter, an alternate means for measuring and reporting UA altitude is necessary, such as GPS. As stated in the conditions and limitations below, the FAA requires altitude

be reported in feet AGL. The petitioner may choose to set the altitude indicator to zero feet AGL rather than local barometric pressure or field altitude before flight. Considering the limited altitude of the proposed operations, relief from 14 CFR § 91.121 is granted to the extent necessary to comply with the applicable conditions and limitations stated below.

Regarding petitioner's requested relief from 14 CFR § 91.151(b), *Fuel requirements for flight in VFR conditions*, prior UAS specific relief has been granted in Exemption Nos. 8811, 10808, and 10673 for daytime, Visual Flight Rules (VFR) conditions. The conditions and limitations below prohibit the PIC from beginning a UAS flight unless (considering wind and forecast weather conditions) there is enough available fuel for UAS to operate for the intended operational time and to operate after that for at least five minutes or with the reserve fuel recommended by the manufacturer if greater. The FAA finds that this provides sufficient reason to grant the relief from 14 CFR § 91.151.

The petitioner requested relief from 14 CFR § 91.1501, *Continued Airworthiness and Safety Improvements – Purpose and definition*. This regulation requires operators to support the continued airworthiness of each airplane. While under this grant of exemption petitioner is permitted to operate without an airworthiness certificate, the PIC is still required to ensure the aircraft is in a condition for safe flight prior to each operation. Therefore, relief from § 91.1501 is not applicable.

UAS Operating Certificate

The petitioner did not request relief from § 137.19(c), *Certification requirements*, which requires the applicant for a commercial agricultural aircraft operator certificate to have available the services of at least one person who holds a current U.S. commercial or airline transport pilot certificate and who is properly rated for the aircraft to be used. The petitioner requests to conduct commercial agricultural aircraft operations under 14 CFR part 137, *Agricultural Aircraft Operations*, with persons holding a private pilot certificate. The FAA has determined that relief from § 137.19(c) is necessary to the extent necessary to permit persons holding a sport, recreational, or private pilot certificate to act as PIC for commercial agricultural aircraft operations. The basis for this relief is the same as discussed in the UAS PIC section above. The PIC must still comply with the additional knowledge and applicable skill requirements in part 137 as well as the petitioner's training requirements in the operating documents. Lastly, because of the relief provided to § 137.19(c), we also provide relief to the pilot certificate requirements of § 137.41(c), *Personnel*.

Regarding the requested relief from §§ 137.19(d), *Certification requirements*, and 137.31(a), *Aircraft requirements*, Yamaha states that it will retain custody of the RMAX UAS and the agricultural related services would be under the direction, supervision, and control of Yamaha. As stated in the analysis above, and consistent with the Secretary's determination that airworthiness certification is not necessary, the FAA finds that relief from 14 CFR parts 21 and 27 is not necessary.

The FAA has determined that based on Yamaha's safe operating history of the RMAX, and the RMAX design safety features, operations conducted under the requirements of this exemption will not adversely impact safety. Thus, although the RMAX is not certificated, the FAA finds that relief from §§ 137.19(d) and 137.31(a) is warranted to the extent necessary to permit the RMAX to be operated in commercial agricultural aircraft operations. Although relief from the

requirement for the aircraft to be certificated is granted, prior to operating, the aircraft must be in a condition for safe flight in accordance with § 91.7(b).

Regarding the requested relief from § 137.19(e)(2)(ii), (iii), and (v), *Certification requirements*, the FAA has determined that demonstration of the skills described in these paragraphs is not necessary because they are not compatible or applicable to the operation of the RMAX during agricultural aircraft operations as described in the petitioner's operating documents. Yamaha's RMAX training and certification program provides the PIC with the necessary skills to safely operate the RMAX. Granting relief from a demonstration of the skills described in § 137.19(e)(2)(ii), (iii), and (v) does not adversely impact safety, therefore relief is warranted. Skill requirements in the other sections of § 137.19(e)(2) not exempted must be demonstrated as required for certification as a agricultural aircraft operator under 14 CFR part 137. If the operating procedures of the RMAX ever change or evolve to require the PIC to perform any of the skills described in 137.19(e)(2)(ii), (iii), and (v), Yamaha must petition for amendment to this grant. Lastly, because of the relief provided to § 137.19(e)(2)(ii), (iii), and (v), the FAA also grants relief from those portions of the associated knowledge and skill test requirements of § 137.41(c),

Regarding the petitioner's requested relief from §§ 137.31(b), *Aircraft requirements*, and § 137.42, *fastening of safety belts and shoulder harnesses*, the FAA finds that an exemption from these requirements related to the installation and use of a shoulder harness and safety belt is warranted because the RMAX is an unmanned aircraft with no onboard pilot. These requirements are intended to ensure the safety of the onboard pilot during manned agricultural aircraft operations and thus, relief from §§ 137.31(b) and 137.42 does not adversely impact safety.

Regarding the petitioner's requested relief from § 137.33(a), *Carrying of certificate*, which requires that a facsimile of the agricultural aircraft operator certificate be carried on the aircraft, the FAA finds that relief is necessary and warranted. The FAA has previously determined that relief from §§ 91.9(b)(2) and 91.203(a) and (b) for the carriage of the aircraft flight manual and aircraft registration onboard the aircraft is not necessary. The FAA finds that this analysis is applicable to the requirements of § 137.33(a). These documents may be kept in a location accessible to the PIC. Therefore, a facsimile of the agricultural aircraft operator certificate may also be kept in a location accessible to the PIC.

The FAA's Decision:

In consideration of the foregoing, I find that a grant of exemption is in the public interest. Therefore, pursuant to the authority contained in 49 U.S.C. §§ 106(f), 40113, and 44701, delegated to me by the Administrator, Yamaha Motor Corporation, U.S.A. is granted an exemption from 14 CFR §§ 61.23(a) and (c); 61.101(e)(4) and (5); 61.113(a); 91.7(a); 91.119(c); 91.121; 91.151; 91.405(a); 91.407(a)(1); 91.409(a)(1) and (2); 91.417(a) and (b); 137.19(c) and (d);, 137.19(e)(2)(ii), (iii), and (v); 137.31(a) and (b); 137.33(a); and 137.42 to the extent necessary to allow the petitioner to operate the RMAX UAS for the purpose of agricultural-related services operations. This exemption is subject to the conditions and limitations listed below.

Conditions and Limitations:

In this grant of exemption, Yamaha Motor Corporation, U.S.A., is hereafter referred to as the operator.

Failure to comply with any of the conditions and limitations of this grant of exemption will be grounds for the immediate suspension or rescission of this exemption.

1. Operations authorized by this grant of exemption are limited to the Yamaha RMAX Type II G UAS as described in the operating documents with a maximum take-off weight not to exceed 99 kg (218) pounds. Proposed operations of any other aircraft will require a new petition or a petition to amend this exemption.
2. The UA may not be operated at an airspeed exceeding 45 miles per hour. In no case will the UA be operated at airspeeds greater than the maximum UA operating airspeed recommended by the aircraft manufacturer.
3. The UA must be operated at an altitude of no more than 400 feet above ground level (AGL). Altitude must be reported in feet AGL.
4. The UA must be operated within visual line of sight (VLOS) of the PIC at all times. This requires the PIC to be able to use human vision unaided by any device other than corrective lenses, as specified on the PIC's FAA-issued airman medical certificate or U.S. driver's license.
5. All operations must utilize a visual observer (VO). The UA must be operated within the visual line of sight (VLOS) of the PIC and VO at all times. The VO may be used to satisfy the VLOS requirement as long as the PIC always maintains VLOS capability. The VO and PIC must be able to communicate verbally at all times; electronic messaging or texting is not permitted during flight operations. The PIC must be designated before the flight and cannot transfer his or her designation for the duration of the flight. The PIC must ensure that the VO can perform the duties required of the VO.
6. This exemption and all documents needed to operate the UAS and conduct its operations in accordance with the conditions and limitations stated in this grant of exemption, are hereinafter referred to as the operating documents. The operating documents must be accessible during UAS operations and made available to the Administrator upon request. If a discrepancy exists between the conditions and limitations in this exemption and the procedures outlined in the operating documents, the conditions and limitations herein take precedence and must be followed. Otherwise, the operator must follow the procedures as outlined in its operating documents. The operator may update or revise its operating documents. It is the operator's responsibility to track such revisions and present updated and revised documents to the Administrator or any law enforcement official upon request. The operator must also present updated and revised documents if it petitions for extension or amendment to this grant of exemption. If the operator determines that any update or revision would affect the basis upon which the FAA granted this exemption, then the operator must petition for an amendment to its grant of exemption. The FAA's UAS Integration Office

(AFS-80) may be contacted if questions arise regarding updates or revisions to the operating documents.

7. Any UAS that has undergone maintenance or alterations that affect the UAS operation or flight characteristics, e.g. replacement of a flight critical component, must undergo a functional test flight prior to conducting further operations under this exemption. Functional test flights may only be conducted by a PIC with a VO and must remain at least 500 feet from other people. The functional test flight must be conducted in such a manner so as to not pose an undue hazard to persons and property.
8. The operator is responsible for maintaining and inspecting the UAS to ensure that it is in a condition for safe operation.
9. Prior to each flight, the PIC must conduct a pre-flight inspection and determine the UAS is in a condition for safe flight. The pre-flight inspection must account for all potential discrepancies, e.g. inoperable components, items, or equipment. If the inspection reveals a condition that affects the safe operation of the UAS, the aircraft is prohibited from operating until the necessary maintenance has been performed and the UAS is found to be in a condition for safe flight.
10. The operator must follow the U manufacturer's maintenance, overhaul, replacement, inspection, and life limit requirements for the aircraft and aircraft components.
11. Each UAS operated under this exemption must comply with all manufacturer safety bulletins.
12. Under this grant of exemption, a PIC must hold either an airline transport, commercial, private, recreational, or sport pilot certificate. The PIC must also hold a current FAA airman medical certificate or a valid U.S. driver's license issued by a state, the District of Columbia, Puerto Rico, a territory, a possession, or the Federal government. The PIC must also meet the flight review requirements specified in 14 CFR § 61.56 in an aircraft in which the PIC is rated on his or her pilot certificate.
13. The PIC and VO must be trained and qualified in accordance with the operating documents.
14. The operator may not permit any PIC to operate unless the PIC demonstrates the ability to safely operate the UAS in a manner consistent with how the UAS will be operated under this exemption, including evasive and emergency maneuvers and maintaining appropriate distances from persons, vessels, vehicles and structures. PIC qualification flight hours and currency must be logged in a manner consistent with 14 CFR § 61.51(b). Flights for the purposes of training the operator's PICs and VOs (training, proficiency, and experience-building) and determining the PIC's ability to safely operate the UAS in a manner consistent with how the UAS will be operated under this exemption are permitted under the terms of this exemption. However, training operations may only be conducted during dedicated training sessions. During training, proficiency, and experience-building flights, all persons not essential for flight operations are considered nonparticipants, and the PIC must operate

the UA with appropriate distance from nonparticipants in accordance with 14 CFR § 91.119.

15. UAS operations may not be conducted during night, as defined in 14 CFR § 1.1. All operations must be conducted under visual meteorological conditions (VMC). Flights under special visual flight rules (SVFR) are not authorized.
16. The UA may not operate within 5 nautical miles of an airport reference point (ARP) as denoted in the current FAA Airport/Facility Directory (AFD) or for airports not denoted with an ARP, the center of the airport symbol as denoted on the current FAA-published aeronautical chart, unless a letter of agreement with that airport's management is obtained or otherwise permitted by a COA issued to the exemption holder. The letter of agreement with the airport management must be made available to the Administrator or any law enforcement official upon request.
17. The UA may not be operated less than 500 feet below or less than 2,000 feet horizontally from a cloud or when visibility is less than 3 statute miles from the PIC.
18. If the UAS loses communications or loses its GPS signal, the UA must return to a pre-determined location within the private or controlled-access property.
19. The PIC must abort the flight in the event of unpredicted obstacles or emergencies.
20. The PIC is prohibited from beginning a flight unless (considering wind and forecast weather conditions) there is enough available fuel for the UA to conduct the intended operation and to operate after that for at least five minutes or with the reserve fuel recommended by the manufacturer if greater.
21. Air Traffic Organization (ATO) Certificate of Waiver or Authorization (COA). All operations shall be conducted in accordance with an ATO-issued COA. The exemption holder may apply for a new or amended COA if it intends to conduct operations that cannot be conducted under the terms of the attached COA.
22. All aircraft operated in accordance with this exemption must be identified by serial number, registered in accordance with 14 CFR part 47, and have identification (N-Number) markings in accordance with 14 CFR part 45, Subpart C. Markings must be as large as practicable.
23. Documents used by the operator to ensure the safe operation and flight of the UAS and any documents required under 14 CFR §§ 91.9, 91.203, and 137.33(a), must be available to the PIC at the Ground Control Station of the UAS any time the aircraft is operating. These documents must be made available to the Administrator or any law enforcement official upon request.
24. The UA must remain clear and give way to all manned aviation operations and activities at all times.
25. The UAS may not be operated by the PIC from any moving device or vehicle.

26. All Flight operations must be conducted at least 500 feet from all nonparticipating persons, vessels, vehicles, and structures unless:
- a. Barriers or structures are present that sufficiently protect nonparticipating persons from the UA and/or debris in the event of an accident. The operator must ensure that nonparticipating persons remain under such protection. If a situation arises where nonparticipating persons leave such protection and are within 500 feet of the UA, flight operations must cease immediately in a manner ensuring the safety of nonparticipating persons; and,
 - b. The owner/controller of any vessels, vehicles or structures has granted permission for operating closer to those objects and the PIC has made a safety assessment of the risk of operating closer to those objects and determined that it does not present an undue hazard.

The PIC, VO, operator trainees or essential persons are considered participating persons under this exemption.

27. All operations shall be conducted over private or controlled-access property with permission from the property owner/controller or authorized representative. Permission from property owner/controller or authorized representative will be obtained for each flight to be conducted.
28. Any incident, accident, or flight operation that transgresses the lateral or vertical boundaries of the operational area as defined by the applicable COA must be reported to the FAA's UAS Integration Office (AFS-80) within 24 hours. Accidents must be reported to the National Transportation Safety Board (NTSB) per instructions contained on the NTSB Web site: www.nts.gov.

Unless otherwise specified in this grant of exemption, the unmanned aircraft system (UAS), pilot in command (PIC), and operator must comply with all applicable parts of 14 CFR including, but not limited to, parts 45, 47, 61, 91, and 137.

This exemption terminates on May 31, 2017, unless sooner superseded or rescinded.

Issued in Washington, DC, on May 1, 2015.

/s/

John Barbagallo
Acting Director, Flight Standards Service

Appendix C – AgDRIFT Study

AgDRIFT was used to find the most efficient aerial application airspeed. Unfortunately, AgDRIFT has a minimum airspeed requirement of 40 mph. AgDRIFT can still be used below 40 mph, but the potential inaccuracy of the results would limit how meaningful those results actually are. With that in mind, 6 aircraft were chosen for this experiment, and were flown at airspeeds from 40 to 150 mph in 10 mph intervals. The aircraft chosen were the Air Tractor 401, Ag Husky, Piper PA-18-150 Super Cub, Stearman N2S-3, M-18 B Dromader, and Ipanema 202. One region was then selected for a more in-depth analysis of the aerial application efficiency at these varying speeds. After all this was done, 40 mph was selected. The results from this experiment and analysis of the results is presented below. The settings used during the testing are presented below with the use of screenshots.

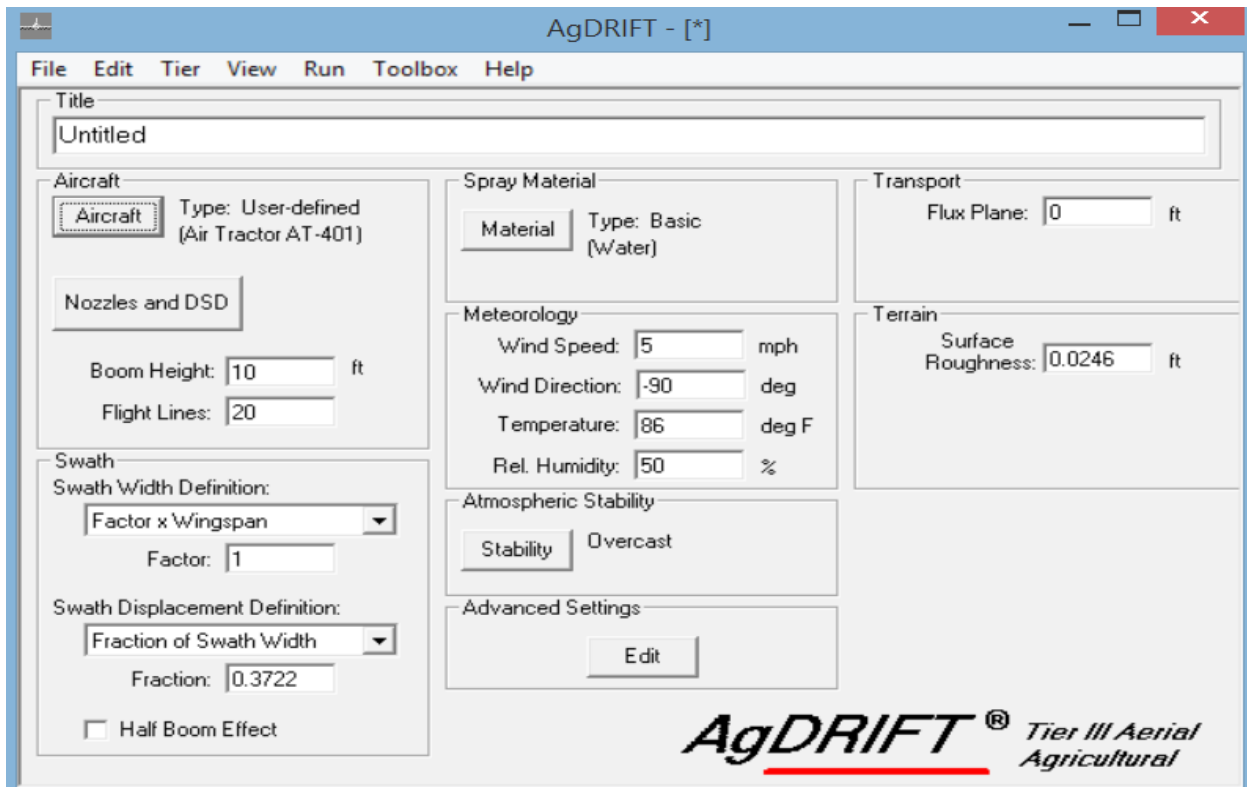


Figure 15. Tier 3 AgDRIFT Interface

This is the main interface of the Tier III Aerial Agricultural testing. The Atmospheric Stability, Advanced Settings, Transport, and Terrain variables were all kept at the default values. The variables that were changed under Swath were the Swath Width Definition and Factor. This was done to make the swath produced by the spray the same width as the wingspan of the aircraft. This way, any pesticide past the wingspan counted as drift. The Wind Speed was lowered from 10 to 5, so the drift produced due to wind was lessened while still using a wind speed that would be encountered often during aerial spraying. All other Meteorology variables were left as defaults.

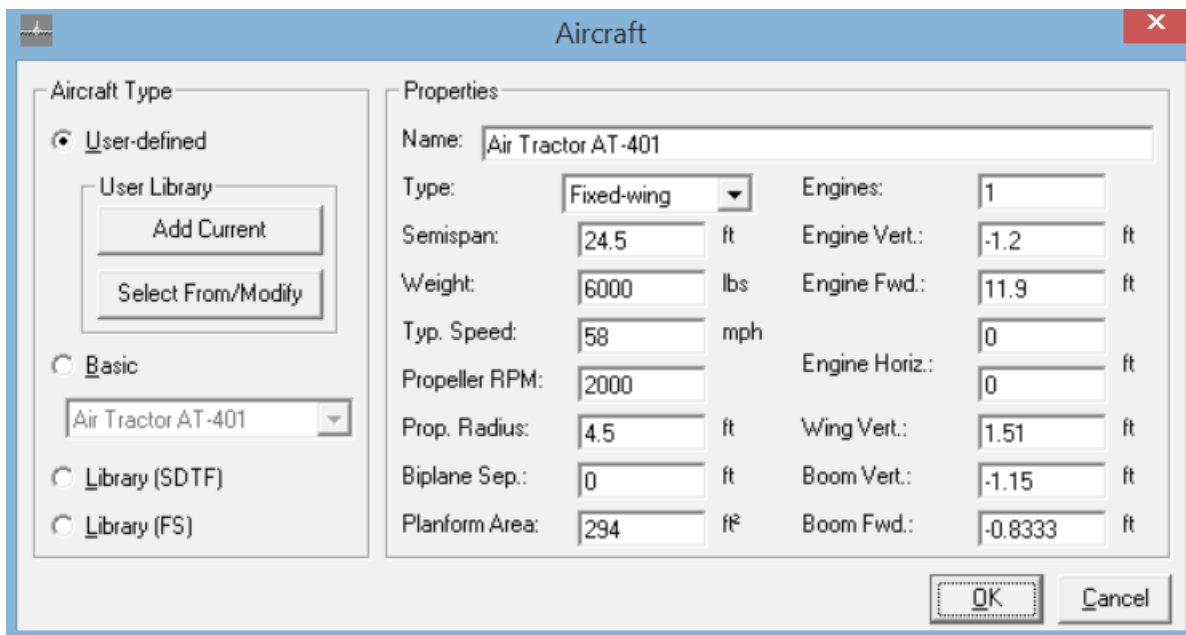


Figure 16. Tier 3 AgDRIFT Aircraft Interface

The only variable that was changed from defaults for the aircraft was the airspeed of the aircraft. Once the airspeed was inputted, AgDRIFT would ask if the nozzles should go to 65% of the semi span wing length on both sides, and this option was always chosen.

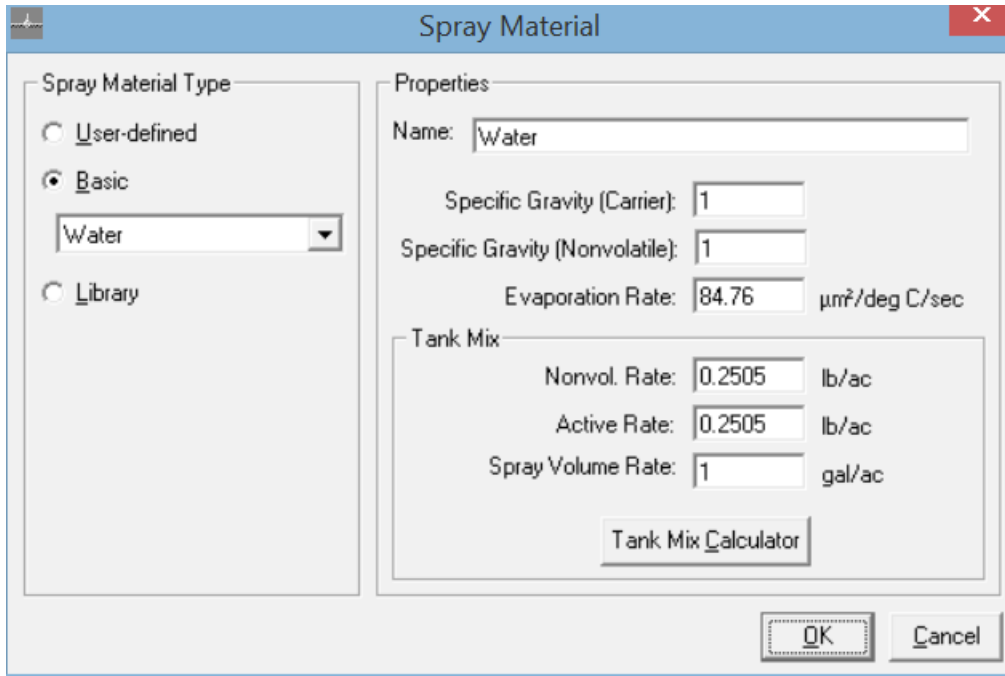


Figure 17. Tier 3 AgDRIFT Spray Interface

The Tank Mix Calculator was used to keep the default tank mix percentages while using Spray Volume Rates of 1 and 4 gallons per acre. All of the other variables were left constant. Once the simulation was run, the Application Efficiency, Downwind Drift, and Airborne Drift were recorded.

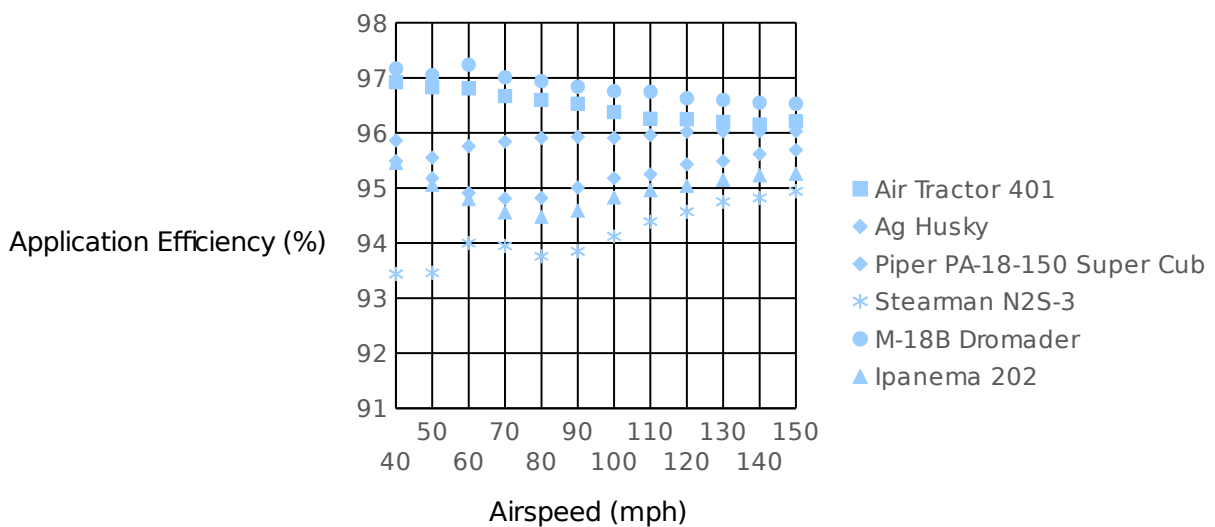


Figure 18. Application Efficiency vs Airspeed

The results from the simulations show the most efficient airspeed is dependent on multiple factors. The most efficient application airspeed regions appear to be around 40 and 140 mph. The 140 mph region would introduce problems with the ability to control the UAV at such a fast speed so close to the ground. Due to this potential problem the 40 to 60 mph region was expanded.

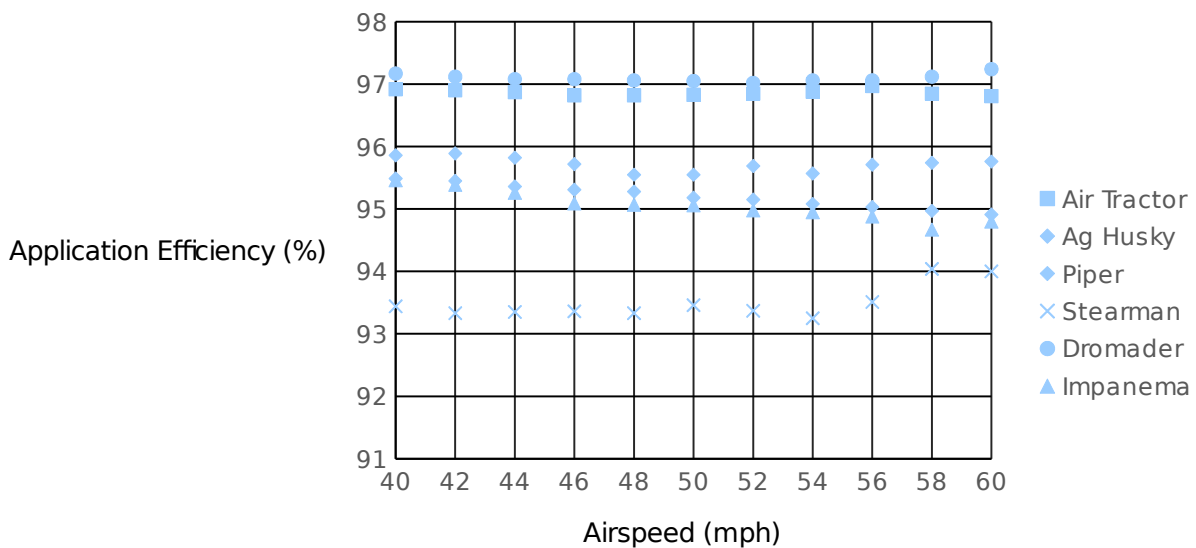


Figure 19. Application Efficiency vs Airspeed, 40 to 60 mph

Within this smaller airspeed region, the Air Tractor and Dromader efficiency stay relatively constant during the selected airspeed region. The Piper is most efficient at 42 mph and fluctuates throughout the airspeed range. The Ag Husky and Impanema are both most efficient at 40 mph, and then decrease throughout the airspeed range. The Stearman efficiency fluctuates until the airspeed reaches 54 mph and then starts to increase. Based on the simulations, only the Stearman doesn't have either a maximum at 40 mph, or have a maximum value that is roughly the same as the value that occurs at 40 mph. This means that most of the aircraft have high relative efficiencies at 40 mph, making 40 mph the choice for application airspeed.

The following two figures show the downwind drift and airborne drift vary between the aircraft at different airspeeds. This helps to show drift does not behave uniformly for each aircraft.

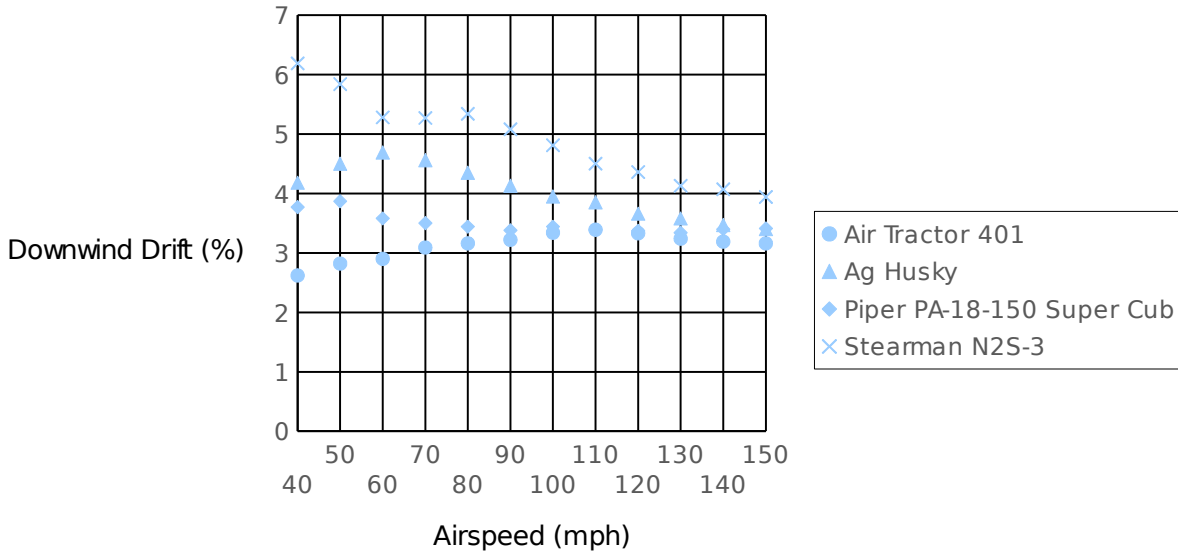


Figure 20. Downwind Drift vs Airspeed

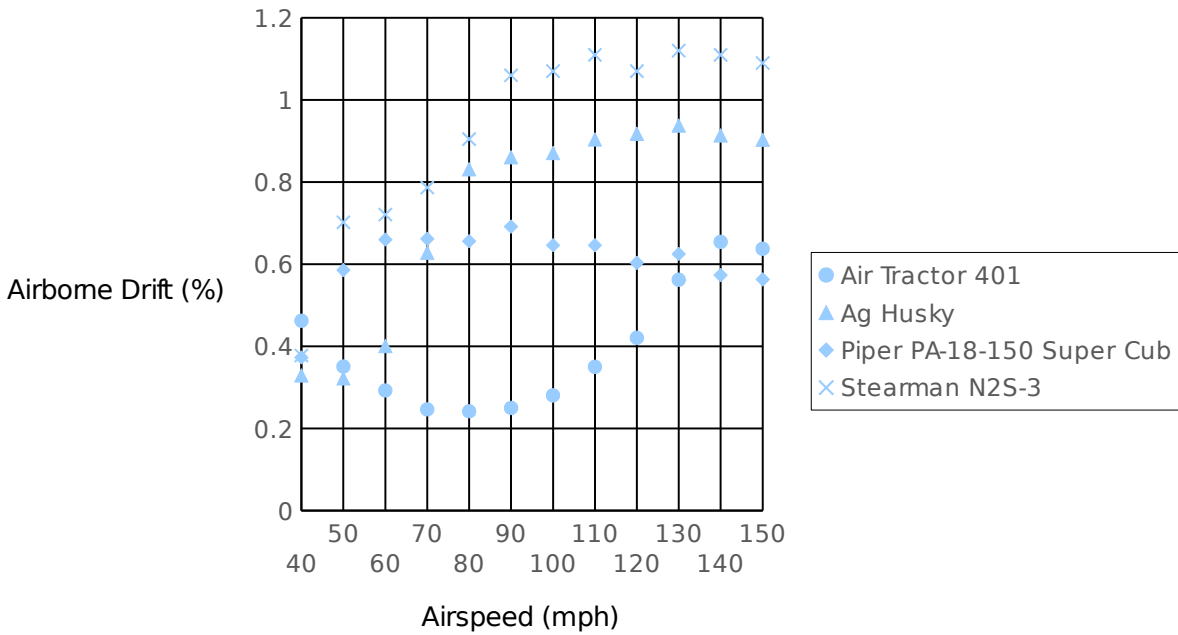


Figure 21. Airborne Drift vs Airspeed

Since crop dusters can apply pesticides at different rates per acre, it is important to test the application efficiency at different application rates. This was done with the Air Tractor and Ag Husky at 1 gal/acre and 4 gal/acre. The results show there are minimal application efficiency changes with an increased application rate.

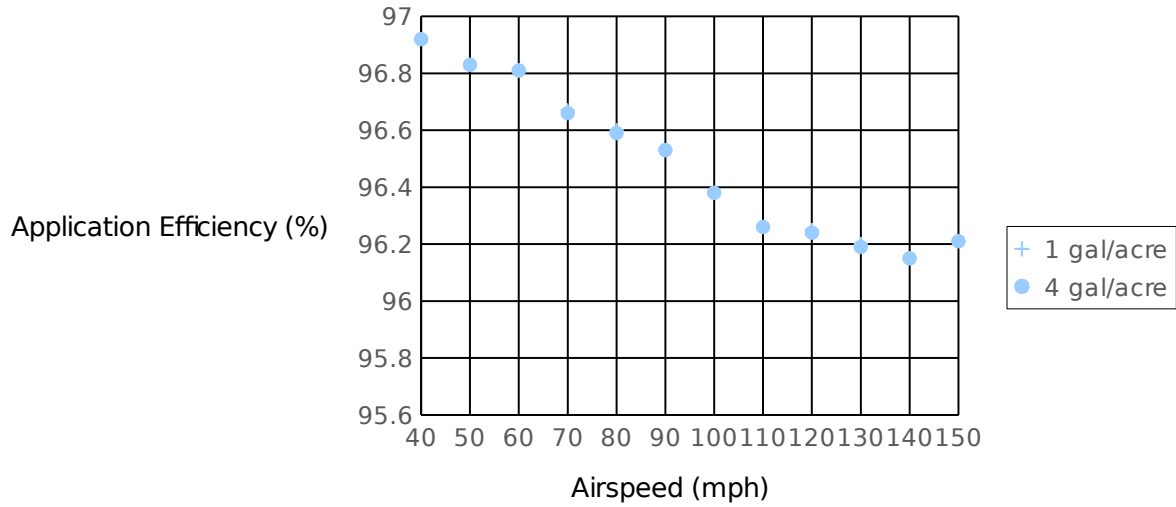


Figure 22. Air Tractor Variable Rate Application Efficiency

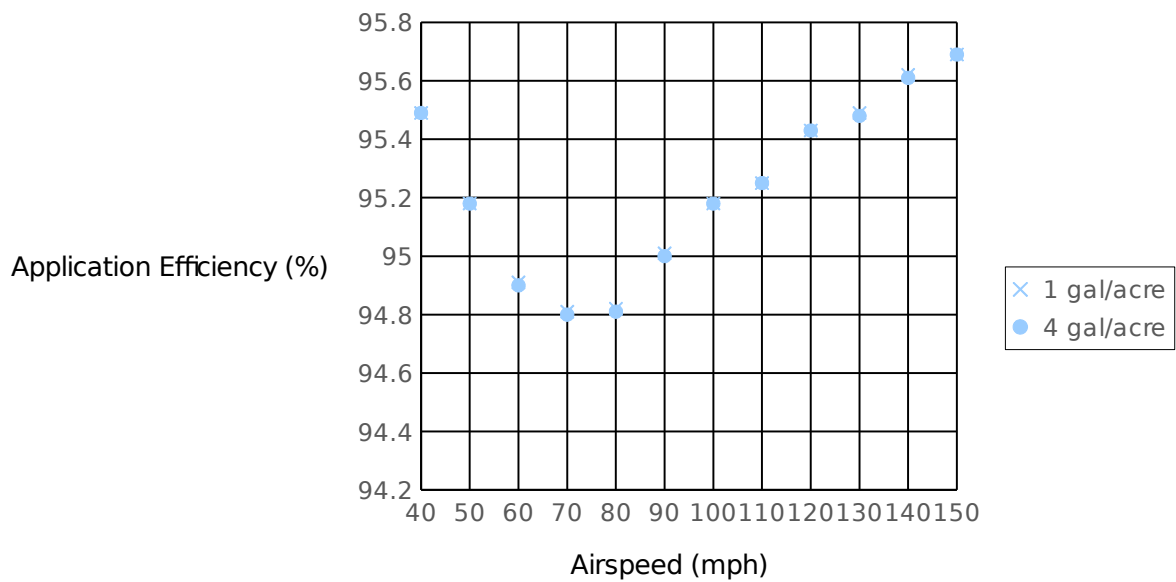


Figure 23. Ag Husky Variable Rate Application Efficiency

Appendix D – XFOIL results

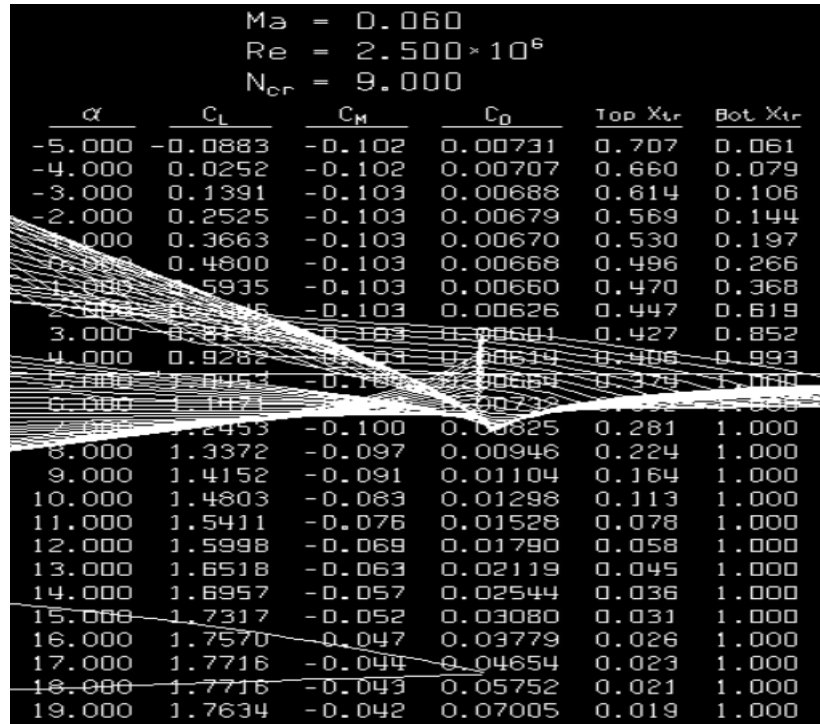


Figure 24. NACA 4415 Xfoil Results



Figure 25. Eppler 1210 Xfoil Results

$Ma = 0.060$
 $Re = 2.500 \times 10^6$
 $N_{cr} = 9.000$

α	C_L	C_M	C_D	Top X_{tr}	Bot. X_{tr}
-5.000	-0.0412	-0.104	0.00808	0.598	0.028
-4.000	0.0660	-0.102	0.00799	0.480	0.029
-3.000	0.1747	-0.100	0.00812	0.379	0.032
-2.000	0.2860	-0.099	0.00805	0.331	0.040
-1.000	0.3976	-0.098	0.00795	0.298	0.080
0.000	0.5089	-0.097	0.00773	0.276	0.185
1.000	0.6198	-0.096	0.00771	0.253	0.288
2.000	0.7268	-0.095	0.00745	0.237	0.538
3.000	0.8285	-0.093	0.00755	0.224	0.679
4.000	0.9483	-0.092	0.00787	0.213	0.737
5.000	1.0565	-0.090	0.00830	0.201	0.740
6.000	1.1636	-0.089	0.00868	0.194	0.818
7.000	1.2707	-0.088	0.00890	0.186	1.000
8.000	1.3818	-0.087	0.00947	0.180	1.000
9.000	1.4833	-0.085	0.01015	0.173	1.000
10.000	1.5833	-0.083	0.01081	0.167	1.000
11.000	1.6783	-0.080	0.01161	0.158	1.000
12.000	1.7660	-0.076	0.01259	0.145	1.000
13.000	1.8291	-0.068	0.01413	0.121	1.000
14.000	1.8552	-0.055	0.01752	0.081	1.000
15.000	1.9025	-0.048	0.02029	0.073	1.000
16.000	1.9354	-0.041	0.02462	0.062	1.000
17.000	1.9162	-0.036	0.03497	0.037	1.000
18.000	1.8582	-0.037	0.05203	0.025	1.000

Figure 26. USA 40B Xfoil Results

Appendix E – Refined Weight Estimate Table

Refined Weight Estimate	W0, guesses	Wf	We	W0	Wf								
	1450.0	93.4	939.6	1450.0									
	Fuel Ratio	Fuel Spent	New Weight		We/W0	a	b	c1	c2	c3	c4	c5	
Segment 1	1.0	14.5	1435.5		0.648	0	1.67	-0.14	0.07	0.1	-0.1	0.11	
Segment 2	1.0	21.5	1414.0										
Segment 3	1.0	0.6	1413.4										
Segment 4	1.0	10.6	1402.8		W/S	S	AR	b	One-row	Acre	# of rows	R	Safety factor
Segment 5	1.0	1.3	1401.4		5.4	267.8	7.5	44.8	140293.6	3.2	15.5	48602.0	1.2
Segment 6	1.0	21.0	1380.4										
Segment 7	1.0	0.6	1379.8		40 mph	q	W/S	AR	e	CD0	Part 1	Part 2	L/D

Segment 8	1.0	10.3	1369. 4			3.93 74	2.41 76	7.5	0.8	0.02	0.0325 7	0.0325 6	15.34 99
Segment 9	1.0	7.5	1361. 9										
Segment Sum	0.9	88.1			45 mph	q	W/S	AR	e	CD0	Part 1	Part 2	L/D
Total Fuel Weight		93.4				4.98 33	3.05 97	7.5	0.8	0.02	0.0325 7	0.0325 7	15.34 99

Appendix F – Aircraft C.G.

Table 47. Fore and Aft C.G. Rotax Engine

Segment Number	Beginning C.G. (ft.)	End C.G. (ft.)
1	6.59	6.60
2	6.60	6.61
3	6.61	6.61
4	6.61	6.62
5	6.62	6.74
5	6.74	6.86
5	6.86	6.99
5	6.99	7.12
5	7.12	7.25
5	7.25	7.39
5	7.39	7.53
5	7.53	7.68
5	7.68	7.72
6	7.72	7.76
7	7.76	7.76
8	7.76	7.78
9	7.78	7.80

To see how using a heavier engine would affect the c.g., the engine was changed to the Lycoming O-235-F.

Table 48. Fore and Aft C.G. Lycoming Engine

Segment Number	Beginning C.G. (ft.)	End C.G. (ft.)
1	6.02	6.02
2	6.02	6.03
3	6.03	6.03
4	6.03	6.03
5	6.03	6.11
5	6.11	6.20
5	6.20	6.28
5	6.28	6.37
5	6.37	6.45
5	6.45	6.53
5	6.53	6.61
5	6.61	6.69
5	6.69	6.71
6	6.71	6.73
7	6.73	6.73
8	6.73	6.73
9	6.73	6.74

Table 49. Fore and Aft C.G. Lycoming Engine, New Moment Arm

Segment Number	Beginning C.G. (ft.)	End C.G. (ft.)
1	6.28	6.29
2	6.29	6.29
3	6.29	6.29
4	6.29	6.30
5	6.30	6.39
5	6.39	6.49
5	6.49	6.58
5	6.58	6.68
5	6.68	6.77
5	6.77	6.87
5	6.87	6.96
5	6.96	7.05
5	7.05	7.08
6	7.08	7.10
7	7.10	7.10
8	7.10	7.11
9	7.11	7.12

The increase in tail sizing, using a horizontal and vertical tail coefficient of .52, increases the parasitic drag to 0.0183 and 0.0184 for 40 mph and 45 mph respectively.

Appendix G – Redesign Aircraft C.G.

Table 50. Fore and Aft C.G. Lycoming O-235-F

Segment Number	Beginning C.G. (ft.)	End C.G. (ft.)
1	6.15	6.16
2	6.16	6.16
3	6.16	6.16
4	6.16	6.16
5	6.16	6.26
5	6.26	6.35
5	6.35	6.44
5	6.44	6.53
5	6.53	6.61
5	6.61	6.70
5	6.70	6.79
5	6.79	6.88
5	6.88	6.90
6	6.90	6.92
7	6.92	6.92
8	6.92	6.93
9	6.93	6.94

Table 51. Fore and Aft C.G. Lycoming O-320-A

Segment Number	Beginning C.G. (ft.)	End C.G. (ft.)
1	6.06	6.07
2	6.07	6.07
3	6.07	6.07
4	6.07	6.07
5	6.07	6.16
5	6.16	6.24
5	6.24	6.32
5	6.32	6.41
5	6.41	6.49
5	6.49	6.57
5	6.57	6.65
5	6.65	6.73
5	6.73	6.75
6	6.75	6.77
7	6.77	6.77
8	6.77	6.77
9	6.77	6.78

Appendix H – CAD MODEL

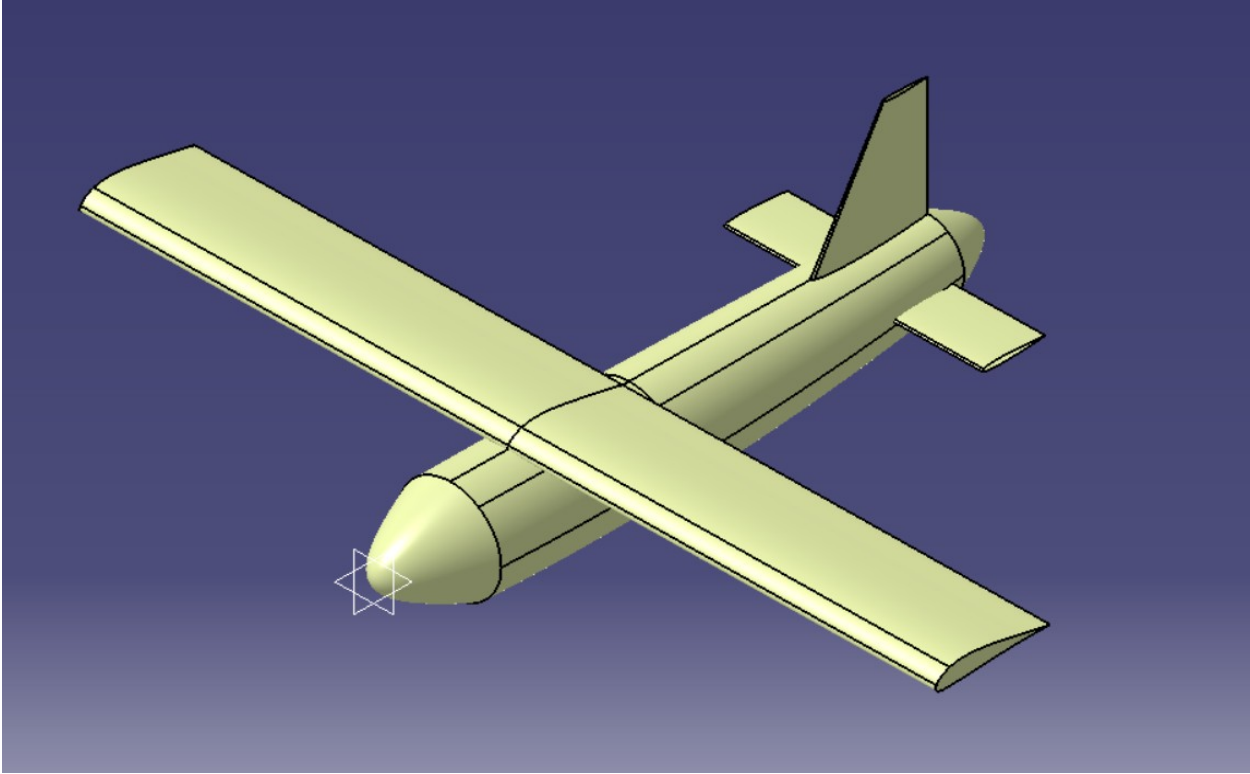


Figure 27. CAD Model of UAV

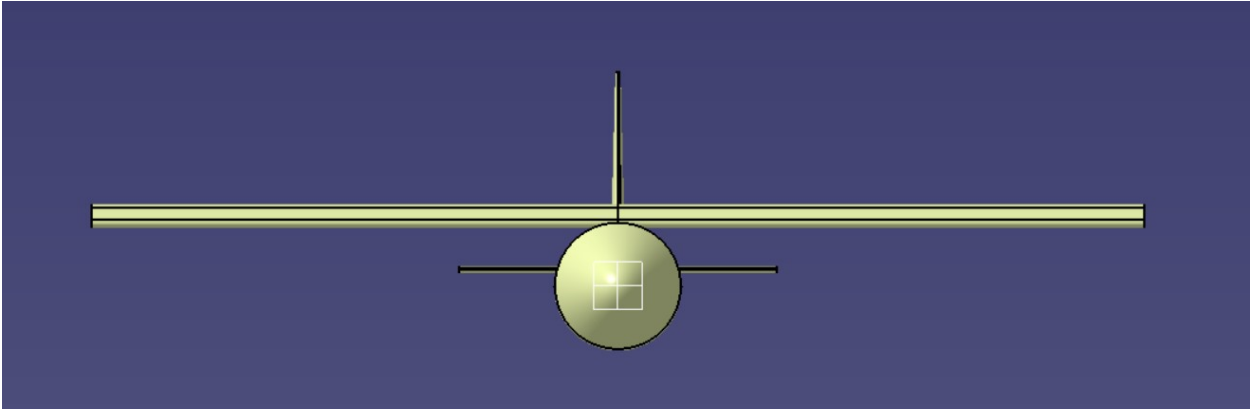


Figure 28. Front View of UAV

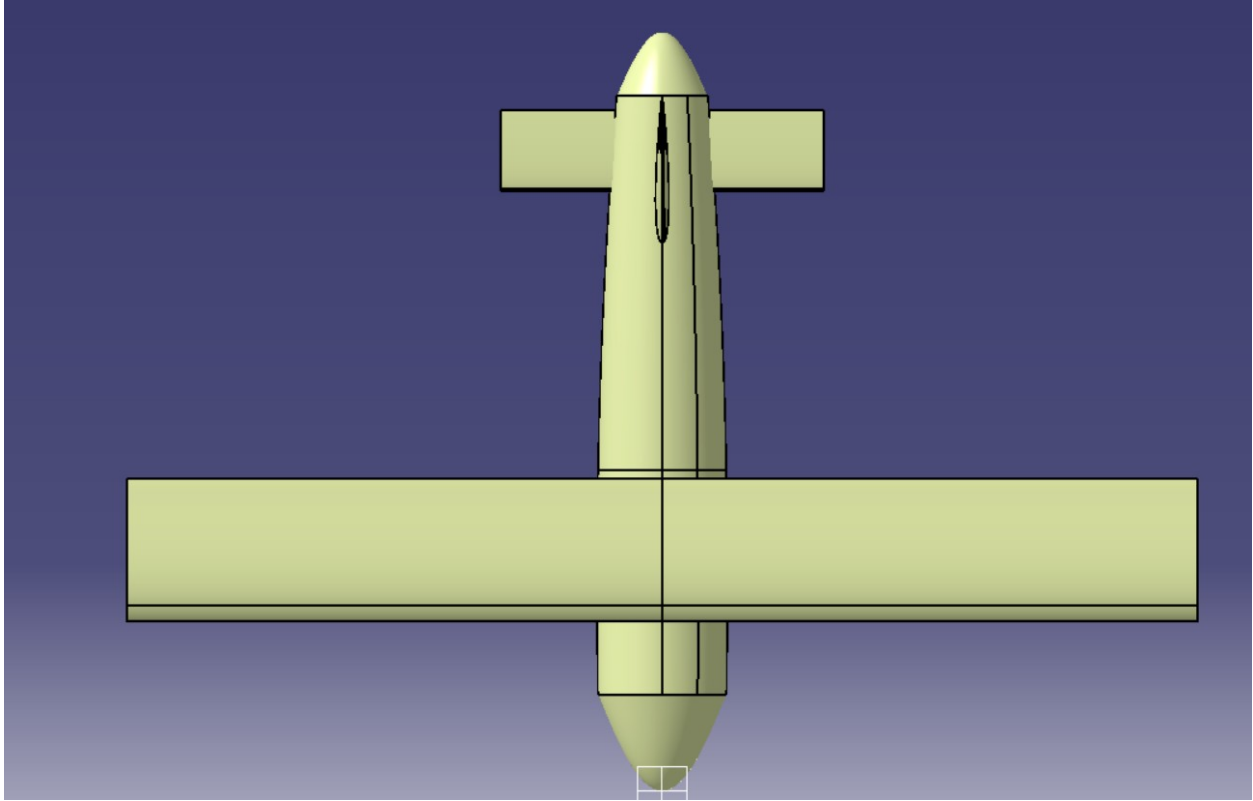


Figure 29. Top View of UAV

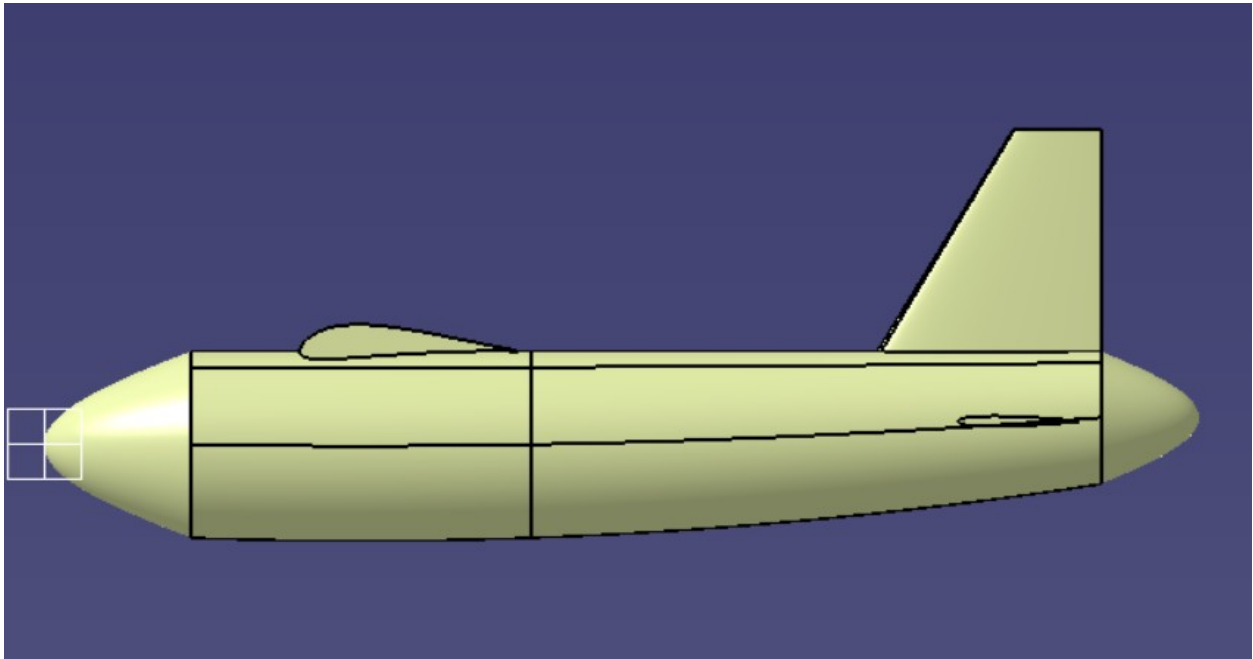


Figure 30. Side View of UAV

Appendix I – Matlab Code

Matlab Code

Wing Loading

```
cl=2.0406;
CL=0.9*cl;
V_S=50.769;
TOP=85.8;
CL_TO=CL/1.21;
density_c=0.002288;
density_TO=0.002308;
sigma=density_c/.0023769
AR=7.5;
e=0.8;
cd_0=0.02;
alpha=0.009;
C=0.5;
%Wing Loading
W_S_S=0.5*density_c*V_S^2*CL
V_TO=1.1*V_S;
W_S_TO=TOP*sigma*CL_TO*alpha*(49)^C
q_c_40=0.5*density_c*58.667^2;
W_C_40=q_c_40*sqrt(pi()*AR*0.8*0.02)
q_c_45=0.5*density_c*66^2;
W_C_45=q_c_45*sqrt(pi()*AR*0.8*0.02)
% q_L=0.5*density_c*66^2;
% W_L=q_L*sqrt(pi()*AR*0.8*0.02)
V_climb=1.2*V_S;
q_climb=0.5*density_TO*V_climb^2;
V_v=15;
G=V_v/V_climb;
V_max=V_climb*0.592484;
PW=alpha*(49)^C
TW=((550*0.8)/(49))*PW
TW_m=((1/11.5)+G)*1.00874*0.97
PW_m=TW_m/((550*0.8)/(V_max));
x=TW_m-(G+2*sqrt(cd_0/(pi()*AR*e)));
% syms TW G AR q_climb e cd_0
W_S_G_1=(TW-G+sqrt((TW-G)^2-(4*cd_0/(pi()*AR*e))))/(2/(q_climb*pi()*AR*e))
W_S_G_2=(TW-G-sqrt((TW-G)^2-(4*cd_0/(pi()*AR*e))))/(2/(q_climb*pi()*AR*e))
W_S=W_S_G_1/0.97
% % pretty(W_S_G_1)
% % pretty(W_S_G_2)
%Landing Distance
%S_Land=80*(5.45)*(1/(sigma*CL))+450
W_S_L=(720.3-450)/(80*(1/(sigma*CL)))
```

Fuselage, Wing, and Tail Sizing

```
%Fuselage
a=4.04;
C=0.23;
W_0=1450;
l=a*W_0^C
```

```

%Wing Variables
lambda=0;
AR=7.5;
S=267.8;
b=44.8;
c=S/b
CSW_b=0.32*b
CSW_c=0.34*c
% Horizontal Tail Variables
lambda_H=0;
AR_H=4;
c_H=0.5;
L_H=0.6*1;
S_H=(c_H*c*S)/L_H
b_H=sqrt(S_H*AR_H)
cH=S_H/b_H
CSHT_c=0.45*cH
% Vertical Tail Variables
lambda_T=0.4;
AR_T=1.5;
c_T=0.04;
L_T=0.6*1;
S_T=(c_T*b*S)/L_T
b_T=sqrt(S_T*AR_T)
c_root_T=(2*S_T)/(b_T*(1+lambda_T))
c_tip_T=lambda_T*c_root_T
C_bar_T=(2/3)*c_root_T*((1+lambda_T+lambda_T^2)/(1+lambda_T))
Y_bar_T=2*(b_T/6)*((1+2*lambda_T)/(1+lambda_T))
CSVT_c=0.45*c_H

```

Landing Gear

```

%Variables
W=1607.9;
W_w=W/8; %Weight per wheel
A_D=1.51;
B_D=0.349;
A_W=0.715;
B_W=0.312;
L_T=7; %Distance between tires
Fore_CG=6.3;
Aft_CG=7.15;
N_f=Fore_CG-3;
N_a=Aft_CG-3;
M_f=10-Fore_CG;
M_a=10-Aft_CG;
H=3.15; %Height of rear wheels
R_r=5.2;
W_land=W;
g=32.2;
V_S=50.769;
%Tire Sizing
D=A_D*(W_w^B_D) %Diameter
Wi=A_W*(W_w^B_W) %Width
w=(Wi*1.3)
d=(D*1.3)

```

```

%Loads
MSL=(W*(N_a/L_T))/8
MSL_N=(W*(M_f/L_T))/4
MSL_n=(W*(M_a/L_T))/4
DBL=((10*H*W)/(g*L_T))/4
%Tire Pressure
A_p=2.3*sqrt(w*d)*((d/2)-R_r)
P=W_w/A_p
KE_brake=0.5*(W_land/(4*g))*V_S^2

```

Aerodynamics Analysis

```

%Variables
AR=7.5;
eida=0.95; %airfoil efficiency
M_40=0.052; % 40 mph Mach number
M_45=0.0586; % 45 mph Mach number
density_40=0.002308;
density_45=0.002288;
dyn_vis_40=3.715*10^-7;
dyn_vis_45=3.7094*10^-7;
v_40=58.67;
v_45=66;
wing_tc=0.158;
tail_tc=0.09;
S_fuse_top=86.29;
S_fuse_side=86.29;
l_wing=6;
l_fuse=21.6;
l_HT=3.9;
l_VT=5.3;
wing_xc=.211;
tail_xc=.309;
k=0.7*10^-5;
%Reference, Exposed, and Wetted Surface Areas
S_ref_wing=267.8;
S_ref_fuse=71.4;
S_ref_HT=65.2;
S_ref_VT=42.8;
S_exp_wing=267.8;
S_exp_fuse=222.7;
S_exp_HT=60;
S_exp_VT=42.8;
S_wet_wing=S_exp_wing*(1.977+0.52*wing_tc)
S_wet_fuse=3.4*(S_fuse_top+S_fuse_side)/2
S_wet_HT=S_exp_HT*(1.977+0.52*tail_tc)
S_wet_VT=S_exp_VT*(1.977+0.52*tail_tc)
%Subsonic Lift-Curve Slope
Beta=sqrt(1-M_40^2)
F=1.07*(1+4/44.8)^2
check=F*(S_exp_wing/S_ref_wing);
%syms AR Beta eida S_exp S_ref F
C_L_alpha_40=(2*pi()*AR)/(2+sqrt(4+((AR^2*Beta^2)/(eida)^2)*(1+tan(0)^2/Beta^2)))*0.98
%pretty(C_L_alpha)
Beta=sqrt(1-M_45^2);
C_L_alpha_45=(2*pi()*AR)/(2+sqrt(4+((AR^2*Beta^2)/(eida)^2)*(1+tan(0)^2/Beta^2)))*0.98

```

```

%Parasitic Drag 40 mph
%Wing
R_wing=(density_40*v_40*l_wing)/dyn_vis_40
R_cwing=38.21*(l_wing/k)^1.053
if R_wing<R_cwing
    Cf_wing=0.455/(log10(R_wing)^2.58*(1+0.144*M_40^2)^0.65)
else
    Cf_wing=0.455/(log10(R_cwing)^2.58*(1+0.144*M_40^2)^0.65)
end
FF_wing=(1+(0.6/(wing_xc)*wing_tc)+100*(wing_tc)^4)*(1.34*M_40^0.18)
CD0_wing=Cf_wing*FF_wing*(S_wet_wing/S_ref_wing)
%Fuselage
R_fuse=(density_40*v_40*l_fuse)/dyn_vis_40;
R_cfuse=38.21*(l_fuse/k)^1.053;
if R_fuse<R_cfuse
    Cf_fuse=0.455/(log10(R_fuse)^2.58*(1+0.144*M_40^2)^0.65)
else
    Cf_fuse=0.455/(log10(R_cfuse)^2.58*(1+0.144*M_40^2)^0.65)
end
f_fuse=l_fuse/4
FF_fuse=1+60/(f_fuse^3)+f_fuse/400
CD0_fuse=Cf_fuse*FF_fuse*(S_wet_fuse/S_ref_wing)
%Horizontal Tail
R_HT=(density_40*v_40*l_HT)/dyn_vis_40;
R_cHT=38.21*(l_HT/k)^1.053;
if R_HT<R_cHT
    Cf_HT=0.455/(log10(R_HT)^2.58*(1+0.144*M_40^2)^0.65)
else
    Cf_HT=0.455/(log10(R_cHT)^2.58*(1+0.144*M_40^2)^0.65)
end
FF_HT=(1+(0.6/(tail_xc)*tail_tc)+100*(tail_tc)^4)*(1.34*M_40^0.18);
CD0_HT=(Cf_HT*FF_HT*(S_wet_HT/S_ref_wing))*1.1
%Vertical Tail
R_VT=(density_40*v_40*l_VT)/dyn_vis_40;
R_cVT=38.21*(l_VT/k)^1.053;
if R_VT<R_cVT
    Cf_VT=0.455/(log10(R_VT)^2.58*(1+0.144*M_40^2)^0.65)
else
    Cf_VT=0.455/(log10(R_cVT)^2.58*(1+0.144*M_40^2)^0.65)
end
FF_VT=(1+(0.6/(tail_xc*l_VT)*tail_tc)+100*(tail_tc)^4)*(1.34*M_40^0.18);
CD0_VT=(Cf_VT*FF_VT*(S_wet_VT/S_ref_wing))*1.1
%Total Parasitic Drag
CD0_total_40=1.05*(CD0_wing+CD0_fuse+CD0_HT+CD0_VT)+6.8708e-05
%Parasitic Drag 45 mph
%Wing
R_wing=(density_45*v_45*l_wing)/dyn_vis_45;
R_cwing=38.21*(l_wing/k)^1.053;
if R_wing<R_cwing
    Cf_wing=0.455/(log10(R_wing)^2.58*(1+0.144*M_45^2)^0.65)
else
    Cf_wing=0.455/(log10(R_cwing)^2.58*(1+0.144*M_45^2)^0.65)
end
FF_wing=(1+(0.6/(wing_xc)*wing_tc)+100*(wing_tc)^4)*(1.34*M_45^0.18);
CD0_wing=Cf_wing*FF_wing*(S_wet_wing/S_ref_wing)
%Fuselage

```

```

R_fuse=(density_45*v_45*l_fuse)/dyn_vis_45;
R_cfuse=38.21*(l_fuse/k)^1.053;
if R_fuse<R_cfuse
    Cf_fuse=0.455/(log10(R_fuse)^2.58*(1+0.144*M_45^2)^0.65)
else
    Cf_fuse=0.455/(log10(R_fuse)^2.58*(1+0.144*M_45^2)^0.65)
end
f_fuse=l_fuse/4;
FF_fuse=1+60/(f_fuse^3)+f_fuse/400;
CD0_fuse=Cf_fuse*FF_fuse*(S_wet_fuse/S_ref_wing)
%Horizontal Tail
R_HT=(density_45*v_45*l_HT)/dyn_vis_45;
R_cHT=38.21*(l_HT/k)^1.053;
if R_HT<R_cHT
    Cf_HT=0.455/(log10(R_HT)^2.58*(1+0.144*M_45^2)^0.65)
else
    Cf_HT=0.455/(log10(R_HT)^2.58*(1+0.144*M_45^2)^0.65)
end
FF_HT=(1+(0.6/(tail_xc)*tail_tc)+100*(tail_tc)^4)*(1.34*M_45^0.18);
CD0_HT=(Cf_HT*FF_HT*(S_wet_HT/S_ref_wing))*1.1
%Vertical Tail
R_VT=(density_45*v_45*l_VT)/dyn_vis_45;
R_cVT=38.21*(l_VT/k)^1.053;
if R_VT<R_cVT
    Cf_VT=0.455/(log10(R_VT)^2.58*(1+0.144*M_45^2)^0.65)
else
    Cf_VT=0.455/(log10(R_VT)^2.58*(1+0.144*M_45^2)^0.65)
end
FF_VT=(1+(0.6/(tail_xc)*tail_tc)+100*(tail_tc)^4)*(1.34*M_45^0.18);
CD0_VT=(Cf_VT*FF_VT*(S_wet_VT/S_ref_wing))*1.1
%Total Parasitic Drag
CD0_total_45=1.05*(CD0_wing+CD0_fuse+CD0_HT+CD0_VT)+6.8708e-05
%Induced Drag
e=1.78*(1-0.045*AR^0.68)-0.64
K=1/(pi()*AR*e)
K_GE=K*(33*(15/44.8)^1.5)/(1+(33*(15/44.8)^1.5))

```

Propulsion Analysis

```

%Variables
rho=0.002308;
D=2.3;
n=5800/60;
V=58.667*1.689
bhp=92;
P=550*bhp
%Advanced Ratio
J=V/(n*D)
%Power Coefficient
C_P=P/(rho*n^3*D^5)
%Thrust Coefficient
T=(550*.85*bhp)/V
C_T=T/(rho*n^2*D^4)
%Speed Power Coefficient
C_S=V^5*sqrt(rho/(P*n^2))
%Propeller Efficiency

```

```

n_p=(T*V)/(550*bhp)
%Thrust
forward_T=(550*bhp*n_p)/V
static_T=((C_T*550*bhp)/(C_P*n*D))*0.95

```

Raymer Weight Analysis

```

%Variables
S_w=267.8;
AR=7.5;
q=3.9374; %3.9374 for 40 mph, 4.9833 for 45 mph
t_c=0.158;
N_z=4.5;
W_dg=1450;
S_ht=71.4;
ht_t_c=0.09;
AR_ht=4;
S_vt=42.8;
vt_t_c=0.09;
AR_vt=1.5;
lambda_vt=0.4;
S_f=247.81;
L_t=11.88;
L=21.6;
h=4;
N_l=4.5;
W_l=1450;
L_m=3.15;
L_n=3.15;
W_eng=124.7;
V_t=2.1;
N_t=1;
N_en=1;
B_w=44.8;
K_h=0.12;
W=80;
M=0.0735;
W_av=28.2;
%Wing Weight
W_wing=0.9*(0.036*S_w^0.758*AR^0.6*q^0.006*(100*t_c)^-0.3*(N_z*W_dg)^0.49)
%Horizontal Tail Weight
W_HT=0.88*(0.016*(N_z*W_dg)^0.419*q^0.168*S_ht^0.896*(100*ht_t_c)^-0.12*AR_ht^0.043)
%Vertical Tail Weight
W_VT=0.88*(0.073*(N_z*W_dg)^0.376*q^0.122*S_vt^0.873*(100*vt_t_c)^-0.49*AR_vt^0.357*lambda_vt^-0.039)
%Fuselage Weight
W_fuse=0.95*(0.052*S_f^1.086*(N_z*W_dg)^0.177*L_t^-0.051*(L/h)^-0.072*q^0.241)
%Main Landing Gear Weight
W_main=0.095*(N_l*W_l)^0.768*(L_m/12)^0.409
%Fuel System Weight
W_fs=2.49*V_t^0.726*1^0.363*N_t^0.242*N_en^0.157
%Flight Control Weight
W_fc=0.053*L^1.536*B_w^0.371*(N_z*W_dg*10^-4)^0.8
%Hydraulic Weight
W_h=K_h*W^0.8*M^0.5
%Electrical Weight

```

```

W_elec=12.57*(W_fs+W_av)^0.51
W_sum=W_wing+W_HT+W_VT+W_fuse+W_main*2+W_fs+W_fc+W_h+W_elec+140.6+28.2+50

```

Nicolai Weight Analysis

```
%Variables
```

```

W_0=1450;
N=4.5;
AR=7.5;
S_w=267.8;
t_c=0.158;
V_e=(0.002308/.0023769)*34.759;
L=21.6;
W=4;
D=4;
S_h=61.9;
l_t=12.96;
b_h=15.7;
t_hr=3.9*0.09*12;
S_v=37.1;
b_v=7.5;
t_vr=7.1*0.09*12;
L_lg=3.06667*12;
W_land=1450;
N_land=4.5;
F_g=15.6;
W_av=28.2;

```

```
%Wing Weight
```

```
W_w=0.8*(96.948*(((W_0*N)/10^5)^0.65*AR^0.57*(S_w/100)^0.61*(2/(2*t_c))^0.36*(1+V_e/500)^0.5)^.993)
```

```
%Fuselage Weight
```

```
W_f=0.825*(200*(((W_0*N)/10^5)^0.286*(L/10)^.857*((W+D)/10)*(V_e/100)^.358)^1.1)
```

```
%Horizontal Tail Weight
```

```
W_ht=0.75*(127*(((W_0*N)/10^5)^0.87*(S_h/100)^1.2*(l_t/10)^0.483*(b_h/t_hr)^0.5)^0.458)
```

```
%Vertical Tail Weight
```

```
W_vt=0.75*(98.5*(((W_0*N)/10^5)^0.87*(S_v/100)^1.2*(b_v/t_vr)^0.5))
```

```
%Landing Gear Weight
```

```
W_lg=.92*(0.054*(L_lg)^0.501*(W_land*N_land)^0.684)
```

```
%Fuel System Weight
```

```
W_fs=2.49*(F_g)^0.6
```

```
%Surface Control Weight
```

```
W_sc=1.08*(W_0)^0.7
```

```
%Electrical Systems Weight
```

```
W_es=12.57*((W_fs+W_av)/1000)^0.51
```

Stability and Control

```
%Variables
```

```

aft_cg=7.12*12;
c_bar=72;
ac=6.728*12;
K_fus=.0075;
W_f=48;
L_f=21.6*12;
L_t=11.232;
c=72;
S_w=267.8;
ac_h=ac+L_t*12;

```

```

eda_h=0.9;
CL_alpha=4.5572;
S_h=71.4;
a_h_a=0.6;
CLh_alpha=3.3548;
Cmw=-0.097;
vol=293;
S_ref=267.8;
b=44.8;
AR=7.5;
C_L=.6;
S_vs=45.7;
z_w=2;
d=4;
CLt_alpha=2.7755;
V_vt=0.04;
gamma=1;
Gamma=0.0174533;
S_vt=42.8;
z_v=1.26+3.43;
C_l_wf=-0.0344;
C_l_basic=-0.05;
C_l_delta=0;
%Downwash
cg_bar=aft_cg/c_bar
acw_bar=ac/c_bar
Cm_alpha_fuse=((K_fus*W_f^2*L_f)/(c*S_w*144))*0.174533 %Radians
ach_bar=ac_h/c_bar
%Power-Off Neutral Point
Xnp_bar=(CL_alpha*acw_bar-Cm_alpha_fuse+eda_h*(S_h/S_w)*a_h_a*CLh_alpha*ach_bar)/
(CL_alpha+eda_h*(S_h/S_w)*CLh_alpha*a_h_a)
SM=(Xnp_bar*c_bar-aft_cg)/c_bar
Cm_alpha=-CL_alpha*SM
%Stick Free Power-Off Neutral Point
Xnp_bar_fs=(CL_alpha*acw_bar-Cm_alpha_fuse+.75*(eda_h*(S_h/S_w)*a_h_a*CLh_alpha*ach_bar))/
(CL_alpha+.75*(eda_h*(S_h/S_w)*CLh_alpha*a_h_a)
SM_fs=(Xnp_bar_fs*c_bar-aft_cg)/c_bar
Cm_alpha_fs=-CL_alpha*SM_fs
%Static Directional Stability
C_n_fuse=-1.3*(vol/(S_ref*b))
C_n_wing=C_L^2*(1/(4*pi()*AR))
q_vt_q=0.724+(3.06*(S_vs/S_w))+0.4*(z_w/d)+.009*AR
C_n_vt=V_vt*CLt_alpha*q_vt_q
C_n_Beta=C_n_fuse+C_n_wing+C_n_vt
%Static Lateral Stability
C_l_Gamma=-0.25*CL_alpha*Gamma*((2*(1+2*gamma))/(3*(1+gamma)))
C_l_wing=C_l_basic+C_l_delta+C_l_Gamma
C_l_vt=-CLt_alpha*q_vt_q*(S_vt/S_ref)*(z_v/b)
C_l_Beta=C_l_wing+C_l_vt+C_l_wf

```

Performance and Flight Controls

%Variables (Units are in SI for ease of analysis)

```

S=24.88;
CD_0=0.0184; %
K=0.0515;

```

```

CL=0.614;
rho=1.189494318;
q=0.5*rho*17.8816^2;
rho_2=1.1791867416;
W_S=2.4387*2.2/0.092903; %3.0597 for 45 mph, 26.3136 for glide
W=731.4;
g=9.81;
n=1:0.5:3;
bhp=0.063*1612.5;
eda_p=0.814;
V_v_1=0;
h2=91.44;
h1=0;
AR=7.5;
e=.825;
mu=0.04;
S_ref=41.276821;
C_L_stall=1.836;
C_L_0=0.49437;
T_W_TO=0.566;
%Stall Velocity
V_stall=sqrt((2*W*g)/(rho*S*C_L_stall)) %with density using slugs, no gravity term is used
V_v_2=1.2*V_stall
V_TD=1.3*V_stall;
%Steady Level Flight
T=q*S*(CD_0+K*CL^2) %T=D
D=T;
L=q*S*CL      %L=W
V=87.5;
V=sqrt((2*1612)/(267.8*0.002308*0.614))
X=D*V
T_W=(q*CD_0)/(W/S)+(W/S)*(K/q)
%Min Thrust
V_min_T=sqrt(((2*W/S)/rho)*sqrt(K/CD_0))
CL_min_T=sqrt(CD_0/K)
D_min_T=q*S*(CD_0*2)
%Min Power
V_min_P=sqrt(((2*W/S)/rho)*sqrt(K/(3*CD_0)))
CL_min_P=sqrt((3*CD_0)/K)
D_min_P=q*S*(4*CD_0)
%Turning flight
Psi_dot=((g*sqrt(n.^2-1))/V)*57.3
%Steady Climb
V_v=(550*bhp*eda_p)/1612.5-(40.2*92.2)/1612.5 %feet per second
gamma_angle=asind((0.9*V_v)/(V_v_2*3.28))
%Gliding Flight
gamma_glide=1/tand(gamma_angle)
L_D_max=0.5*sqrt((pi()*AR*e)/CD_0)
L_D_min=sqrt((3*pi()*AR*e)/(16*CD_0))
V_min_sink=sqrt(((2*W)/(rho_2*S))*sqrt(K/(3*CD_0)))
CL_min_sink=sqrt((3*CD_0)/K)
CD_min_sink=(2*((0.5*CL_min_sink*rho_2*V_min_sink^2*S)/L_D_min))/(rho_2*V_min_sink^2*S)
% CL_sink=(2*W*cosd(gamma_angle))/(rho_2*20.1^2*S)
% CD_sink=(2*D*sind(gamma_angle))/(rho_2*20.1^2*S_ref)
V_v_glide=sqrt(W/S*(2/(rho_2*(CL_min_sink^3/CD_min_sink^2))))
% %Takeoff Analysis

```

```

K_T=(T_W_TO)-mu
K_A=(rho/(2*W/S))*(mu*C_L_0-CD_0-K*C_L_0^2)
S_G=1/(2*g*K_A)*log((K_T+K_A*V_v_2^2)/(K_T))
S_G_L=1/(2*g*K_A)*log((K_T)/(K_T+K_A*V_TD^2))

Cost Analysis
%Variables
W_e=1140.7;
V=78.21;
Q=50;
FTA=6;
N_e=1;
%DAPCA Cost Model
H_E=1.8*(4.86*W_e^0.777*V^0.894*Q^0.163)*0.5
H_T=1.8*(5.99*W_e^0.777*V^0.696*Q^0.263)*0.5
H_M=1.8*(7.37*W_e^0.82*V^0.484*Q^0.641)*0.5
H_Q=1.8*0.133*H_M*0.5
C_D=91.3*W_e*0.63*V^1.3*0.5
C_F=2498*W_e^0.325*V^0.822*FTA^1.21*0.5
C_M=22.1*W_e^0.921*V^0.621*Q^0.799*0.5
C_Eng=44000;
C_Avionics=8000*30.2
C_ES=40000;
Cost=115*H_E+118*H_T+98*H_M+108*H_Q+C_D+C_F+C_M+C_Eng*Q+C_Avionics*Q+C_ES*50

```

Appendix J – Hand Calculations

$$W_0 = W_{crew} + W_{payload} + W_{fuel} + W_{empty} = 0 + 417 + 85.6 + 662.7 = 1165 \text{ lb.} \quad (4.1)$$

$$W_0 = \frac{W_{payload}}{1 - \frac{W_{fuel}}{W_0} - \frac{W_{empty}}{W_0}} = \frac{417}{1 - 0.0735 - 0.569} = 1165 \text{ lb} \quad (4.2)$$

$$\frac{W_{empty}}{W_0} = (0.95) 0.74 W_0^{-0.03} K_{VS} = (0.95) 0.74 (1165)^{-0.03} = 0.569 \quad (4.3)$$

$$C = C_{bhp} \frac{V}{550 \eta_p} = 0.4 \frac{45}{550 (0.8) (3600)} = 0.0000111 \quad (4.4)$$

$$\left(\frac{W_i}{W_{i-1}} \right)_{cruise} = e^{\frac{-RC_{bhp}}{550 * \eta_p \frac{L}{D}}} = e^{\frac{26400 (0.4)}{550 * 0.8 (16)}} = 0.999725 \approx 1 \quad (4.6)$$

$$\frac{T}{W} = \frac{\eta_p P}{V W} = \frac{550 \eta_p hp}{V W} = \frac{550 (0.8)}{49} 0.063 = 0.5657 \quad (5.1)$$

$$\frac{P}{W_0} = 0.009 V_{max}^{0.5} = 0.009 (49^{0.5}) = 0.063 \quad (5.2)$$

$$\left(\frac{T}{W} \right)_{cruise} = \frac{1}{\left(\frac{L}{D} \right)_{cruise}} = \frac{1}{11.5} = 0.087 \quad (5.3)$$

$$\left(\frac{T}{W} \right)_{climb} = \frac{1}{\left(\frac{L}{D} \right)_{cruise}} + \frac{V_{vertical}}{V} = \frac{1}{11.5} + \frac{15}{60.84} = 0.247 \quad (5.4)$$

$$\left(\frac{T}{W} \right)_{takeoff} = \left(\frac{T}{W} \right)_{cruise} \frac{W_{cruise}}{W_{takeoff}} \frac{T_{takeoff}}{T_{cruise}} = (0.087) (0.96) (1.0) = 0.084 \quad (5.5)$$

$$\left(\frac{T}{W} \right)_{takeoff} = \left(\frac{T}{W} \right)_{climb} \frac{W_{climb}}{W_{takeoff}} \frac{T_{takeoff}}{T_{climb}} = (0.333) (0.97) (1.0) = 0.326 \quad (5.6)$$

$$C_{L_{max}} = 0.9 C_{L_{max}} = 0.9 (2.0406) = 1.84 \quad (5.7)$$

$$C_{L_c} = \frac{C_{L_{max}}}{1.21} = \frac{1.84}{1.21} = 1.52 \quad (5.8)$$

$$\left(\frac{W}{S} \right)_{takeoff} = 85.8 \sigma C_{L_c} \frac{hp}{W} = 85.8 (0.9626) (1.52) 0.063 = 7.9 \quad (5.9)$$

$$\left(\frac{W}{S} \right)_{stall} = \frac{1}{2} \rho V_{stall}^2 C_{L_{max}} = \frac{1}{2} 0.002288 (50.7^2) 1.84 = 5.4 \quad (5.10)$$

$$G = \frac{V_{vertical}}{V} = \frac{15}{60.84} = 0.247 \quad (5.11)$$

$$q = \frac{1}{2} \rho V^2 = \frac{1}{2} 0.002308 (58.67^2) = 3.97 \quad (5.12)$$

$$\left(\frac{W}{S}\right)_{climb} = \frac{\frac{T}{W} - G \pm \sqrt{\left(\frac{T}{W} - G\right)^2 - \frac{4C_{D_0}}{\pi ARe}}}{2} = \frac{0.5657 - 0.247 \pm \sqrt{(0.5657 - 0.247)^2 - \frac{4(0.02)}{\pi 7.5(0.8)}}}{2} \quad (5.13)$$

$$\left(\frac{W}{S}\right)_{cruise} = q_{cruise} \sqrt{\pi ARe C_{D_0}} = 3.97 \sqrt{\pi 7.5(0.8) 0.02} = 2.44 \quad (5.14)$$

$$d_{landing} = 0.3 V_{app}^2 = 0.3 (49^2) = 720.3 \quad (5.15)$$

$$d_{landing} = 80 \left(\frac{W}{S}\right) \left(\frac{1}{\sigma C_{L_{max}}}\right) + 450 = 80 (5.97) \left(\frac{1}{0.9626(1.84)}\right) + 450 = 720.3 \quad (5.16)$$

$$S = \frac{W_0}{\left(\frac{W}{S}\right)_{min}} = \frac{1450}{5.4} = 267.8 \quad (5.17)$$

$$b = \sqrt{ARS} = \sqrt{7.5(267.8)} = 44.8 \quad (5.18)$$

$$c = \frac{S}{b} = \frac{267.8}{44.8} = 5.97768 \approx 6.0 \quad (5.19)$$

$$\frac{L}{D} = \frac{1}{\frac{q_{cruise} C_{D_0}}{\frac{W}{S_{cruise}}} + \frac{1}{q_{cruise} \pi ARe} \frac{W}{S_{cruise}}} = \frac{1}{\frac{3.94(0.02)}{2.4} + \frac{1}{3.94 \pi 7.5(0.8)} 2.4} = 15.3 \quad (5.20)$$

$$\frac{W_e}{W_0} = 1.67 W_0^{-0.14} AR^{0.07} \left(\frac{hp}{W_0}\right)^{0.1} \left(\frac{W_0}{S}\right)^{-0.1} V_{max}^{0.11} = 1.67 (1450^{-0.14}) AR^{0.07} (0.063)^{0.1} (5.4^{-0.1}) (4 \quad (5.21)$$

$$l_{fuselage} = 4.04 W_0^{0.23} = 4.04 (1450^{0.23}) = 21.6 \quad (5.22)$$

$$S_{HT} = \frac{c_{HT} \dot{C}_W S_W}{L_{HT}} = \frac{0.5(6)267.8}{12.96} = 61.9 \quad (5.23)$$

$$S_{VT} = \frac{c_{VT} b_W S_W}{L_{VT}} = \frac{0.6(44.8)267.8}{12.96} = 37.1 \quad (5.24)$$

$$c_{root} = \frac{2S}{b(1+\lambda)} = \frac{2(37.1)}{7.46(1+0.4)} = 7.1 \quad (5.25)$$

$$c_{tip} = \lambda c_{root} = 0.4(7.1) = 2.8 \quad (5.26)$$

$$\dot{C} = \frac{2}{3} c_{root} \frac{1+\lambda+\lambda^2}{1+\lambda} = \frac{2}{3} 7.1 \frac{1+0.4+0.4^2}{1+0.4} = 5.3 \quad (5.27)$$

$$\dot{Y} = \frac{b}{6} \frac{1+2\lambda}{1+\lambda} = \frac{7.46}{6} \frac{1+2(0.4)}{1+0.4} = 3.2 \quad (5.28)$$

$$D = K_p \sqrt[4]{hp} = 1.7 \sqrt[4]{92} = 5.3 \quad (6.1)$$

$$V_{tip_s} = \frac{\pi n D}{60} = \frac{\pi (2800) (5.3)}{60} = 1596 \quad (6.2)$$

$$V_{tip_h} = \sqrt{V_{tip_s}^2 + V^2} = \sqrt{1596^2 + 82.7^2} = 1598 \quad (6.3)$$

$$A_{cooling} = \frac{hp}{2.2 V_{climb}} = \frac{92}{2.2 (60.8)} = 0.69 \quad (6.4)$$

$$S_{wet} = S_{exp} \left[1.977 + 0.52 \left(\frac{t}{c} \right) \right] = 267.8 [1.977 + 0.52 (0.158)] = 551.4 \quad (6.5)$$

$$S_{wet_{fuse}} = 3.4 \left(\frac{A_{top} + A_{side}}{2} \right) = 3.4 \left(\frac{86.29 + 86.29}{2} \right) = 293.4 \quad (6.6)$$

$$\int \dot{i} = 3.4 \frac{A_{top} A_{side}}{4L} = 3.4 \frac{(86.29 * 86.29)}{4L} = 293.0 \quad (6.7)$$

$Vol_{\dot{i}}$

$$W_{fuse} = 0.95 (1.26 S_{exp_{fuse}}) = 0.95 (1.26 (222.7)) = 296.2 \quad (6.8)$$

$$W_{tail} = 0.88 (1.76 S_{exp_{tail}}) = 0.88 (1.76 (371.)) = \dot{i} \quad 65.3 \quad (6.9)$$

$$W_{wing} = 0.9 (2.25 S_{exp_{wing}}) = 0.9 (2.25 (267.8)) = \dot{i} \quad 602.6 \quad (6.10)$$

$$W_{lg} = 0.057 W_0 = 0.057 (1450) = \dot{i} \quad 82.3 \quad (6.11)$$

$$T_d = 1.51 W_w^{0.349} = 1.51 (181.25^{0.349}) = 9.6 \quad (7.1)$$

$$T_w = 0.715 W_w^{0.312} = 0.715 (181.25^{0.312}) = 3.7 \quad (7.2)$$

$$S_L = W_w \frac{N_a}{B} = 402 \frac{4.15}{7} = 119.2 \quad (7.3)$$

$$S_{L_n} = W_{nw} \frac{M_f}{B} = 201 \frac{3.7}{7} = 212.5 \quad (7.4)$$

$$S_{I_n} = W_{nw} \frac{M_a}{B} = 201 \frac{2.85}{7} = 163.7 \quad (7.5)$$

$$D_{t_n} = \frac{10 H W_{nw}}{g B} = \frac{10(3.15)(362.5)}{32.2(7)} = 56.2 \quad (7.6)$$

$$A_p = 2.3 \sqrt{w d} \left(\frac{d}{2} - R_r \right) = 2.3 \sqrt{(4.9)(12.5)} \left(\frac{12.5}{2} - 5.2 \right) = 18.8 \quad (7.7)$$

$$P_t = \frac{W_w}{A_p} = \frac{201}{18.8} = 10.7 \quad (7.8)$$

$$KE_{braking} = \frac{1}{2} \frac{W_{landing}}{g} V_{stall}^2 = \frac{1}{2} \frac{1612.5}{32.2} 50.8^2 = 19081 \quad (7.9)$$

$$\beta = \sqrt{1 - M^2} = \sqrt{1 - 0.052^2} = 0.9986 \quad (8.1)$$

$$F = 1.07 \left(1 + \frac{d}{b_w} \right)^2 = 1.07 \left(1 + \frac{4}{44.8} \right)^2 = 1.27 \quad (8.2)$$

$$C_{L_u} = \frac{2 \pi A R}{2 + \sqrt{4 + \frac{A R^2 \beta^2}{\eta_{af}^2}}} \left(\frac{S_{exp}}{S_{ref}} \right) F = \frac{2 \pi 7.5}{2 + \sqrt{4 + \frac{7.5^2 (0.9986^2)}{0.95^2}}} \left(\frac{267.8}{267.8} \right) 0.98 = 4.5572 \quad (8.3)$$

$$C_{D_0} = C_{f_e} \frac{S_{wet}}{S_{ref}} = 0.0055 \frac{551.4}{267.8} = 0.0113 \quad (8.4)$$

$$\Re = \frac{\rho V l}{\mu} = \frac{0.002308 (58.67) (6)}{3.715 * 10^{-7}} = 2.19 * 10^6 \quad (8.5)$$

$$\Re_{cutoff} = 38.21 \left(\frac{l}{k} \right)^{1.053} = 38.21 \left(\frac{6}{0.7 * 10^{-5}} \right)^{1.053} = 6.76 * 10^7 \quad (8.6)$$

$$C_f = \frac{0.455}{(\log_{10} \Re)^{2.58} (1 + 0.144 M^2)^{0.65}} = \frac{0.455}{(\log_{10} (2.187 * 10^6))^{2.58} (1 + 0.144 (0.052^2))^{0.65}} = 0.0039 \quad (8.7)$$

$$FF = \left[1 + \frac{0.6}{(x/c)_m} \frac{t}{c} + 100 \left(\frac{t}{c} \right)^4 \right] [1.34 M^{0.18}] = \left[1 + \frac{0.6}{0.211} + 100 (0.158)^4 \right] [1.34 (0.052^{0.18})] = 1. \quad (8.8)$$

$$f = \frac{l}{d} = \frac{21.6}{4} = 5.4 \quad (8.9)$$

$$FF_{fuse} = \left(1 + \frac{60}{f^3} + \frac{f}{400} \right) = \left(1 + \frac{60}{5.4^3} + \frac{5.4}{400} \right) = 1.4 \quad (8.10)$$

$$C_{D_0} = C_f FF \frac{S_{wet}}{S_{ref_w}} = 0.039 (1.19) \frac{551.4}{267.8} = 0.095 \quad (8.11)$$

$$e = 1.78 (1 - 0.045 A R^{0.68}) - 0.64 = 1.78 (1 - 0.045 (7.5^{0.68})) - 0.64 = 0.825 \quad (8.12)$$

$$K = \frac{1}{\pi A Re} = \frac{1}{\pi (7.5) 0.825} = 0.0515 \quad (8.13)$$

$$K_{effective} = \frac{33(h/b)^{1.5}}{1+33(h/b)^{1.5}} K = \frac{33(15/44.8)^{1.5}}{1+33(15/44.8)^{1.5}} 0.0515 = 0.0455 \quad (8.14)$$

$$C_D = C_{D_0} + K C_L^2 = 0.0183 + 0.0515 (-0.53)^2 = 0.033 \quad (8.15)$$

$$J = \frac{V}{n_{rs} D} = \frac{58.67(1.689)}{(5800/60)(2.3)} = 0.446 \quad (9.1)$$

$$C_P = \frac{550 \text{ bhp}}{\rho n_{rs}^3 D^5} = \frac{550}{0.002308 ((5800/60)^3)(2.3^5)} = 0.37 \quad (9.2)$$

$$C_T = \frac{T}{\rho n_{rs}^2 D^4} = \frac{434}{0.002308 ((5800/60)^2)(2.3^4)} = 0.72 \quad (9.3)$$

$$C_S = V^5 \sqrt{\frac{\rho}{P n_{rs}^2}} = (58.67(1.689))^5 \sqrt{\frac{0.002308}{50600 ((5800/60)^2)}} = 21105 \quad (9.4)$$

$$T_{ff} = \frac{550 \text{ bhp } \eta_p}{V} = \frac{550(92)0.85}{58.67(1.689)} = 434 \quad (9.5)$$

$$T_s = \frac{C_T}{C_P} \frac{550 \text{ bhp}}{n_{rs} D} = \frac{0.72}{0.37} \frac{550(92)}{(5800/60)(2.3)} \quad (9.6)$$

$$\left(\frac{D}{q}\right)_{misc} = (2 \times 10^{-4}) \frac{\text{bhp}}{S_{ref}} = (2 \times 10^{-4}) \frac{92}{267.8} = 6.9 \times 10^{-5} \quad (9.7)$$

$$W_{wing} = 0.9 \left(0.036 S_w^{0.758} AR^{0.6} q^{0.006} \lambda^{0.04} \left(\frac{100t}{c}\right)^{-0.3} (N_z W_{dg})^{0.49} \right) = 0.9 \left(0.036 (267.8)^{0.758} 7.5^c \right) \quad (11.1)$$

$$W_{HT} = 0.88 \left(0.016 (N_z W_{dg})^{0.419} q^{0.168} S_{HT}^{0.896} \left(\frac{100t}{c}\right)^{-0.12} AR_{HT}^{0.043} \right) = 0.88 \left(0.016 ((4.5) 1450)^{0.419} \right) \quad (11.2)$$

$$W_{VT} = 0.88 \left(0.073 (N_z W_{dg})^{0.376} q^{0.122} S_{VT}^{0.873} \left(\frac{100t}{c}\right)^{-0.49} AR_{VT}^{0.357} \lambda_{VT}^{0.039} \right) = 0.88 \left(0.073 (4.5 (1450) \right) \quad (11.3)$$

$$W_{fuse} = 0.95 \left(0.052 S_f^{1.086} (N_z W_{dg})^{0.177} I_t^{-0.051} \left(\frac{l}{d}\right)^{-0.072} q^{0.241} \right) = 0.95 \left(0.052 (247.81)^{1.086} ((4.5) \right) \quad (11.4)$$

$$W_{mlg} = 0.095 (N_l W_{landing})^{0.768} \left(\frac{L_m}{12}\right)^{0.409} = 0.095 ((1450))^{0.768} \left(\frac{3.15}{12}\right)^{0.409} = 46.7 \quad (11.5)$$

$$W_{fs} = 2.49 V_t^{0.726} N_t^{0.242} N_{en}^{0.157} = 2.49 (2.1^{0.726}) (1^{0.242}) (1^{0.157}) = 4.3 \quad (11.6)$$

$$W_{fc} = 0.053 l_f^{1.536} b_w^{0.371} (N_z W_{dg} 10^{-4})^{0.8} = 0.053 (21.6^{1.536}) (44.8^{0.371}) ((4.5) 1450 (10^{-4}))^{0.8} = 17 \quad (11.7)$$

$$W_h = 0.12 W_0^{0.8} M^{0.5} = 0.12 (1450^{0.8}) M^{0.5} = 1.1 \quad (11.8)$$

$$W_{elec} = 12.57 (W_{fs} + W_{av})^{0.51} = 12.57 (4.3 + 28.2)^{0.51} = 74.2 \quad (11.9)$$

$$V_e = \frac{\rho}{\rho_0} V = \frac{0.002308}{0.002377} 34.8 = 33.8 \quad (11.10)$$

$$W_{wing} = 0.8 \left(96.948 \left[\left(\frac{W_0 N_z}{10^5} \right)^{0.65} AR^{0.57} \left(\frac{S_w}{100} \right)^{0.61} \left(\frac{1+\lambda}{2 \frac{t}{c}} \right)^{0.36} \left(1 + \frac{V_e}{500} \right)^{0.5} \right]^{0.993} \right) = 0.8 \left(96.948 \left[\right. \right. \quad (11.11)$$

$$W_{HT} = 0.75 \left(127 \left[\left(\frac{W_0 N_z}{10^5} \right)^{0.87} \left(\frac{S_{HT}}{100} \right)^{1.2} \left(\frac{l_t}{10} \right)^{0.483} \left(\frac{b_{HT}}{t_{HR}} \right)^{0.5} \right]^{0.458} \right) = 0.75 \left(127 \left[\left(\frac{1450 (4.5)}{10^5} \right)^{0.87} \left(\right. \right. \quad (11.12)$$

$$W_{VT} = 0.75 \left(98.5 \left[\left(\frac{W_0 N_z}{10^5} \right)^{0.87} \left(\frac{S_{VT}}{100} \right)^{1.2} \left(\frac{b_{VT}}{t_{VR}} \right)^{0.5} \right] \right) = 0.75 \left(98.5 \left[\left(\frac{1450 (4.5)}{10^5} \right)^{0.87} \left(\frac{42.8}{100} \right)^{1.2} \left(\frac{7.}{7.} \right. \right. \quad (11.13)$$

$$W_{fuse} = 0.825 \left(200 \left[\left(\frac{W_0 N_z}{10^5} \right)^{0.286} \left(\frac{l_f}{10} \right)^{0.857} \left(\frac{2d}{10} \right) \left(\frac{V_e}{100} \right)^{0.358} \right]^{1.1} \right) = 0.825 \left(200 \left[\left(\frac{1450 (4.5)}{10^5} \right)^{0.286} \left(\right. \right. \quad (11.14)$$

$$W_{lg} = 0.92 (0.054 (L_m)^{0.501} (W_{landing} N_l)^{0.684}) = 0.92 (0.054 (3.15)^{0.501} (1450 (4.5))^{0.684}) = 123 \quad (11.15)$$

$$W_{fs} = 2.49 F_g^{0.6} N_t^{0.2} N_{en}^{0.13} = 2.49 (15.6^{0.6}) 1^{0.2} (1^{0.13}) = 13 \quad (11.16)$$

$$W_{sc} = 1.08 (W_0)^{0.7} = 1.08 (1450)^{0.7} = 176.4 \quad (11.17)$$

$$W_{elec} = 12.57 \left(\frac{W_{fs} + W_{av}}{1000} \right)^{0.51} = 12.57 \left(\frac{13 + 28.2}{1000} \right)^{0.51} = 2.5 \quad (11.18)$$

$$\dot{X}_{cg} = \frac{a_{cg}}{\dot{C}} = \frac{6.78}{4.5} = 1.5374 \quad (12.1)$$

$$\dot{X}_{ac_w} = \frac{w_{qc}}{\dot{C}} = \frac{6.375}{4.5} = 1.4456 \quad (12.2)$$

$$\dot{X}_{ac_h} = \frac{h_{qc}}{\dot{C}} = \frac{19.375}{4.5} = 4.3934 \quad (12.3)$$

$$C_{m_{afuse}} = \frac{K_{fuse} d^2 l_f}{c S_w} = \frac{0.0075 (4^2)}{(149.6)} = 7.06 E^{-5} \quad (12.4)$$

$$r = \frac{2l_t}{b_w} = \frac{2(13)}{33.5} = 0.78 \quad (12.5)$$

$$m = \frac{2z_t}{b_w} = \frac{2(1.42)}{33.5} = 0.085 \quad (12.6)$$

$$\frac{d\alpha_h}{d\alpha} = 1 - \frac{d\epsilon}{d\alpha} = 1 - 0.375 = 0.625 \quad (12.7)$$

$$\dot{X}_{np} = \frac{C_{L_\alpha} \dot{X}_{ac_w} - C_{m_{efuse}} + \eta_h \frac{S_{HT}}{S_w} C_{L_{ah}} \frac{d\alpha_h}{d\alpha} \dot{X}_{ac_h}}{C_{L_\alpha} + \eta_h \frac{S_{HT}}{S_w} C_{L_{ah}} \frac{d\alpha_h}{d\alpha}} = \frac{(4.5713)1.4456 - 7.06 E^{-5} + 0.9 \frac{25.7}{149.6} (3.709)}{4.5713 + 0.9 \frac{25.7}{149.6} (3.709) 0.6} \quad (12.8)$$

$$SM = -C_{L_\alpha} \left(\frac{\dot{X}_{np} \dot{C} - a_{cg}}{\dot{C}} \right) = -4.5713 \left(\frac{(1.657)4.5 - (6.375)}{4.5} \right) = 0.12 \quad (12.9)$$

$$C_{m_\alpha} = -C_{L_\alpha} SM = -4.5713(0.12) = -0.55 \quad (12.10)$$

$$\dot{X}_{np} = \frac{C_{L_\alpha} \dot{X}_{ac_w} - C_{m_{efuse}} + .75 \left(\eta_h \frac{S_{HT}}{S_w} C_{L_{ah}} \frac{d\alpha_h}{d\alpha} \dot{X}_{ac_h} \right)}{C_{L_\alpha} + .75 \left(\eta_h \frac{S_{HT}}{S_w} C_{L_{ah}} \frac{d\alpha_h}{d\alpha} \right)} = \frac{(4.5713)1.4456 - 7.06 E^{-5} + 0.75 \left(0.9 \frac{25.7}{149.6} \right)}{4.5713 + 0.75 \left(0.9 \frac{25.7}{149.6} \right)} \quad (12.11)$$

$$\Delta\alpha_{0_L} = \frac{-.9}{2\pi} \frac{dC_L}{d\delta_f} K_f \delta_e = \frac{.9}{(0.95)2\pi} (4.75)(1)(1) \delta_e = -0.716 \quad (12.12)$$

$$C_{L_h} = C_{L_{ah}} \left[\frac{d\alpha_h}{d\alpha} \alpha - \Delta\alpha_{0_L} \right] = 3.709 [0.625\alpha + 0.716] = 2.318\alpha + 2.656\delta_e \quad (12.13)$$

$$C_{m_g} = C_{L_\alpha} (\dot{X}_{cg} - \dot{X}_{ac_w}) + C_{m_w} + C_{m_{efuse}} + \eta_h \frac{S_{HT}}{S_w} C_{L_h} (\dot{X}_{ac_h} - \dot{X}_{cg}) = 4.5713(1.5374 - 1.4456) - 0.0 \quad (12.14)$$

$$C_{L_{total}} = C_{L_\alpha} \alpha + \eta_h \frac{S_{HT}}{S_w} C_{L_h} = 4.5713\alpha + 0.9 \frac{25.7}{149.6} 2.318\alpha + 2.656\delta_e = 4.92\alpha + 0.41\delta_e \quad (12.15)$$

$$C_L = \frac{W}{S} = \frac{11.06}{17.74} = 0.623 \quad (12.16)$$

$$C_{n_{\beta fuse}} = -1.3 \frac{Vol}{S_{ref} b_w} \frac{h}{w} = -1.3 \frac{293.96}{(149.6)33.5} \frac{4}{4} = -0.079 \quad (12.17)$$

$$C_{n_{\beta wing}} = C_L^2 \left(\frac{1}{4\pi AR} \right) = 0.623^2 \left(\frac{1}{4\pi 7.5} \right) = 0.0041 \quad (12.18)$$

$$\left(1 + \frac{d\sigma}{d\beta}\right) \frac{q_{VT}}{q} = 0.724 + \frac{3.06 S'_{VS}}{S_w} + 0.4 \frac{z_w}{d} + 0.009 AR = 0.724 + \frac{3.06(21)}{33.5} + 0.4 \frac{2}{4} + 0.009(7.5) \quad (12.19)$$

$$C_{n_{\beta VT}} = c_{VT} C_{L_{\alpha VT}} \left(1 + \frac{d\sigma}{d\beta}\right) \frac{q_{VT}}{q} = 0.04(2.7812)1.4319 = 0.1581 \quad (12.20)$$

$$C_{n_{\beta}} = C_{n_{\beta wing}} + C_{n_{\beta fuse}} + C_{n_{\beta VT}} = 0.0041 - 0.079 + 0.1581 = 0.086 \quad (12.21)$$

$$C_{I_{\beta r}} = -0.25 C_{L_{\alpha}} \Gamma \left(\frac{2(1+2\lambda)}{3(1+\lambda)}\right) = -0.25(4.5713)0.017 \left(\frac{2(1+2\lambda)}{3(1+\lambda)}\right) = -0.02 \quad (12.22)$$

$$C_{I_{\beta wing}} = C_{I_{\beta basic}} + C_{I_{\beta \Delta}} + C_{I_{\beta r}} = -0.05 + 0 - 0.02 = -0.07 \quad (12.23)$$

$$C_{I_{\beta VT}} = -C_{L_{\alpha VT}} \left(1 + \frac{d\sigma}{d\beta}\right) \frac{q_{VT}}{q} \frac{S_{VT}}{S_{ref}} \frac{z_v}{b_w} = (2.7812) \frac{15.4}{149.6} \frac{3.53}{33.5} = -0.0429 \quad (12.24)$$

$$C_{I_{\beta}} = C_{I_{\beta wing}} + C_{I_{\beta VT}} + C_{I_{\beta wf}} = -0.07 - 0.0434 - 0.0344 = -0.147 \quad (12.25)$$

$$T = D = q S_w (C_{D_0} + K C_L^2) = (3.97)267.8(0.0184 + 0.0515(0.614^2)) = 40.2 \quad (13.1)$$

$$L = W = q S_w C_L = 3.97(267.8)0.614 = 653.1 \quad (13.2)$$

$$V = \sqrt{\frac{2}{\rho} \frac{W}{C_L S}} = \sqrt{\frac{2}{0.002308(0.614)}} 6.02 = 92.2 \quad (13.3)$$

$$\frac{T}{W} = \frac{1}{L/D} = \frac{q C_{D_0}}{W/S} + \frac{W}{S} \frac{K}{q} = \frac{3.97(0.0184)}{6.02} + 6.02 \frac{0.0515}{3.97} = 0.13 \quad (13.4)$$

$$V_{min_T} = \sqrt{\frac{2}{\rho} \frac{W}{S} \sqrt{\frac{K}{C_{D_0}}}} = \sqrt{\frac{2}{0.002308} 6.02 \sqrt{\frac{0.0515}{0.0184}}} = 29.8 \quad (13.5)$$

$$C_{L_{min_T}} = \sqrt{\frac{C_{D_0}}{K}} = \sqrt{\frac{0.0184}{0.0515}} = 0.6 \quad (13.6)$$

$$D_{min_T} = q S_w (2 C_{D_0}) = 3.97(267.8)(2 * 0.0184) = 39.1 \quad (13.7)$$

$$P = DV = 40.2(92.2) = 22 \quad (13.8)$$

$$V_{min_P} = \sqrt{\frac{2}{\rho} \frac{W}{S} \sqrt{\frac{K}{3 C_{D_0}}}} = \sqrt{\frac{2}{0.002308} 6.02 \sqrt{\frac{0.0515}{3 * 0.0184}}} = 22.7 \quad (13.9)$$

$$C_{L_{min_P}} = \sqrt{\frac{3 C_{D_0}}{K}} = \sqrt{\frac{3 * 0.0184}{0.0515}} = 1.04 \quad (13.10)$$

$$D_{min_P} = q S_w (4 C_{D_0}) = (3.97)267.8(4 * 0.0184) = 78.3 \quad (13.11)$$

$$\phi = \frac{g\sqrt{N_e^2-1}}{V} 57.3 = \frac{32.2\sqrt{2^2-1}}{92.2} 57.3 = 10.6 \quad (13.12)$$

$$V_{v_{rate}} = \frac{550 \text{ bhp } \eta_P}{W} - \frac{DV}{W} = \frac{550(102)0.814}{1612.5} - \frac{40.2(92.2)}{1612.5} = 25.9 \quad (13.13)$$

$$V_{climb} = 1.2 \sqrt{\frac{2Wg}{\rho S C_{L_{stall}}}} = 1.2 \sqrt{\frac{2(1612.5)32.2}{0.002308(267.8)1.836}} = 64.0 \quad (13.14)$$

$$\gamma_{angle} = \sin^{-1}\left(\frac{0.9 V_{v_{rate}}}{V_{climb}}\right) = \sin^{-1}\left(\frac{0.9*25.9}{64.0}\right) = 21.4 \quad (13.15)$$

$$\frac{L}{D} = \frac{1}{\tan \gamma} = \frac{1}{\tan(21.4)} = 2.6 \quad (13.16)$$

$$\left(\frac{L}{D}\right)_{min} = \sqrt{\frac{3\pi A R e}{16 C_{D_0}}} = \sqrt{\frac{3\pi 7.5(0.825)}{16(0.0184)}} = 14.1 \quad (13.17)$$

$$V_{min_{sink}} = \sqrt{\frac{2}{\rho} \frac{W}{S} \sqrt{\frac{K}{3 C_{D_0}}}} = \sqrt{\frac{2}{0.002308} 6.02 \sqrt{\frac{0.0515}{3(0.0184)}}} = 22.8 \quad (13.18)$$

$$C_{L_{min_{sink}}} = \sqrt{\frac{3 C_{D_0}}{K}} = \sqrt{\frac{3(0.0184)}{0.0515}} = 1.04 \quad (13.19)$$

$$C_{D_{min_{sink}}} = \frac{C_{L_{min_{sink}}}}{\left(\frac{L}{D}\right)_{min}} = \frac{1.04}{14.1} = 0.74 \quad (13.20)$$

$$V_{glide} = \sqrt{\frac{W}{S} \frac{2}{\rho(C_L^3/C_D^2)}} = \sqrt{6.02 \frac{2}{0.0002308(1.04^3/0.74^2)}} = 1.6 \quad (13.21)$$

$$K_T = \frac{T}{W} - \mu_r = 0.566 - 0.04 = 0.562 \quad (13.22)$$

$$K_A = \frac{\rho}{2(W/S)} (\mu_r C_L - C_{D_0} - K C_L^2) = \frac{0.002308}{2(6.02)} (0.04(0.49) - 0.0184 - 0.0515(0.49^2)) = -z \quad (13.23)$$

$$D_G = \frac{1}{2g K_A} \ln\left(\frac{K_T + K_A V_f^2}{K_T + K_A V_i^2}\right) = \frac{1}{2(32.2) - 2.2 E^{-4}} \ln\left(\frac{0.562 \pm 2.2 E^{-4}(64^2)}{0.562 \pm 2.2 E^{-4}(0^2)}\right) = 174.7 \quad (13.24)$$

$$R_T = \frac{V_{TR}^2}{0.2g} = \frac{(1.15*53.3)^2}{0.2(32.2)} = 583.4 \quad (13.25)$$

$$h_{TR} = R_T (1 - \cos(\gamma_{climb})) = 583.4 (1 - \cos(21.4)) = 40.2 \quad (13.26)$$

$$D_{TR} = R_T \sin(\gamma_{climb}) = 583.4 \sin(21.4) = 212.9 \quad (13.27)$$

$$S_C = \frac{h_{obstacle} - h_{TR}}{\tan(\gamma_{climb})} = \frac{50 - 40.2}{\tan(21.4)} = 25 \quad (13.28)$$

$$D_i = D_G + D_R + D_{TR} + D_C = 174.7 + 53.3 + 212.9 + 25 = 465.9 \quad (13.29)$$

$$H_E = \frac{1.8 \left(4.86 W_{empty}^{0.777} V_{max}^{0.894} Q^{0.163} \right)}{2} = \frac{1.8 \left(4.86 (1140.7^{0.777}) (78.21^{0.894}) (50^{0.163}) \right)}{2} = 96,785 \quad (17.1)$$

$$H_T = \frac{1.8 \left(6.99 W_{empty}^{0.777} V_{max}^{0.696} Q^{0.263} \right)}{2} = \frac{1.8 \left(6.99 (1140.7^{0.777}) (78.21^{0.696}) (50^{0.263}) \right)}{2} = 74,410 \quad (17.2)$$

$$H_M = \frac{1.8 \left(7.37 W_{empty}^{0.82} V_{max}^{0.484} Q^{0.641} \right)}{2} = \frac{1.8 \left(7.37 (1140.7^{0.82}) (78.21^{0.484}) (50^{0.641}) \right)}{2} = 215,760 \quad (17.3)^{29}$$

$$H_Q = \frac{1.8(0.133 H_M)}{2} = \frac{1.8(1.33(215760))}{2} = 25,826 \quad (17.4)$$

$$C_{DS} = \frac{91.3 W_{empty}^{0.63} V_{max}^{1.3}}{2} = \frac{91.3 \left((1140.7^{0.63}) (78.21^{1.3}) \right)}{2} = 9,488,400 \quad (17.5)$$

$$C_{FT} = \frac{2498 W_{empty}^{0.325} V_{max}^{0.822} FTA^{1.21}}{2} = \frac{2498 \left((1140.7^{0.325}) (78.21^{0.822}) (6^{1.21}) \right)}{2} = 3,872,300 \quad (17.6)$$

$$C_{MM} = \frac{22.1 W_{empty}^{0.921} V_{max}^{0.621} Q^{0.799}}{2} = \frac{22.1 \left((1140.7^{0.921}) (78.21^{0.621}) (50^{0.799}) \right)}{2} = 2,467,200 \quad (17.7)$$

$$Cost = 115 H_E + 118 H_T + 98 H_M + 108 H_Q + C_{DS} + C_{FT} + C_{MM} + C_{Eng} Q + C_{Av} Q + C_{ES} Q = 115 \quad (17.8)$$